Computational histology image analysis of human cerebral cortex cytoarchitectonics

Štajduhar, Andrija

University of Zagreb

FACULTY OF ELECTRICAL ENGINEERING AND COMPUTING

Andrija Štajduhar

COMPUTATIONAL HISTOLOGY IMAGE ANALYSIS OF HUMAN CEREBRAL CORTEX CYTOARCHITECTONICS

DOCTORAL THESIS

Zagreb, 2019

University of Zagreb

FACULTY OF ELECTRICAL ENGINEERING AND COMPUTING

Andrija Štajduhar

COMPUTATIONAL HISTOLOGY IMAGE ANALYSIS OF HUMAN CEREBRAL CORTEX CYTOARCHITECTONICS

DOCTORAL THESIS

Supervisors:
Professor Sven Lončarić, PhD
Professor Miloš Judaš, MD, PhD

Zagreb, 2019

Sveučilište u Zagrebu
FAKULTET ELEKTROTEHNIKE I RAČUNARSTVA

Andrija Štajduhar

RAČUNALNA ANALIZA HISTOLOŠKIH SLIKA CITOARHITEKTONIKE LJUDSKE MOŽDANE KORE

DOKTORSKI RAD

Mentori:
prof. dr. sc. Sven Lončarić
prof. dr. sc. Miloš Judaš

Zagreb, 2019.

This dissertation was made at the University of Zagreb, Faculty of Electrical engineering and computing, Department of Electronic Systems and Information Processing in cooperation with School of Medicine, Croatian Institute for Brain Research and McGill University, Montreal Neurological Institute, Montreal, Canada.

Supervisors:
Professor Sven Lončarić, PhD
Professor Miloš Judaš, MD, PhD

The dissertation has: 120 pages

The dissertation number: _____

About the Supervisors

Sven Lončarić was born in Zagreb in 1961. He received Diploma of Engineering and Master of Science degrees in electrical engineering from University of Zagreb Faculty of Electrical Engineering and Computing (FER) in 1985 and 1989, respectively. He received Doctor of Philosophy (Ph.D.) degree in electrical engineering from University of Cincinnati, USA, in 1994. Since 2011, he has been a tenured full professor in electrical engineering and computer science at FER. He was researcher or project leader on a number of research projects in the area of image processing and analysis. From 2001-2003, he was an assistant professor at New Jersey Institute of Technology, USA. He has been the head of the Image Processing Laboratory at FER. He founded the Center for Computer Vision at University of Zagreb. Prof. Lončarić has been a co-director of the national Center of Research Excellence in Data Science and Cooperative Systems. He authored or co-authored more than 200 scientific publications. Prof. Lončarić is a senior member of IEEE and a member of Croatian Academy of Technical Sciences. He was the Chair of the IEEE Croatia Section. He founded and organized several international scientific conferences. He is an editor, a program committee member and reviewer for a number of scientific conferences and journals. He is a recipient of the University of Zagreb „Fran Bošnjaković“ Award, Croatian Academy of Engineering "Rikard Podhorsky" Award, FER Science Award, Fulbright stipend, and an IEEE Croatia Section Award.

Miloš Judaš was born in 1961 (Petrinja, Croatia). He graduated from School of Medicine, University of Zagreb in 1984, where he also received Doctor of Philosophy (Ph.D.) degree in 1996. He is currently employed at the University of Zagreb School of Medicine as full professor of neuroscience and anatomy, director of the Croatian Institute for Brain Research, and director of national Center of Excellence in Basic, Clinical and Translational Neuroscience. Since October 2014, he also serves as Vice-Rector for Science and International Cooperation at the University of Zagreb. Since 2008 he is member-collaborator of Croatian Academy of Sciences and Arts (Medical Sciences Class). Professor Judaš is internationally recognized developmental neuroscientist with steady publication output and extensive teaching and administrative experience in the academic community. He significantly contributed to development of neuroscience in Croatia through his involvement in the foundation of the Croatian Institute for Brain Research, the Croatian Society for Neuroscience, the first graduate course in neuroscience (for medical students), and the first Ph.D Study Program in Neuroscience. He has served as an invited speaker at many international meetings and schools, as well as an organizer or co-director of a number of international and domestic meetings and workshops. Research interests of prof. Judaš are in human neuroanatomy and human developmental neurobiology, developmental and evolutionary neurobiology of cognition, and language and history of neuroscience.

O mentorima

Sven Lončarić rođen je u Zagrebu 1961. godine. Diplomirao je i magistrirao u polju elektrotehnike na Fakultetu elektrotehnike i računarstva (FER) Sveučilišta u Zagreba, 1985. i 1989. godine. Doktorirao je u polju elektrotehnike na Sveučilištu u Cincinnatiju, SAD, 1994. godine. U zvanje redoviti profesor u trajnom zvanju u polju elektrotehnike i polju računarstva na FER-u izabran je 2011. godine. Bio je suradnik ili voditelj na brojnim istraživačkim i razvojnim projektima u području razvoja metoda za obradu i analizu slika i signala. Od 2001. do 2003. bio je Assistant Professor na Sveučilištu New Jersey Institute of Technology, SAD. Voditelj je istraživačkog laboratorija za obradu slike na FER-u. Osnivač je i voditelj Centra izvrsnosti za računalni vid na Sveučilištu u Zagrebu. Suvoditelj je nacionalnog Znanstvenog centra izvrsnosti za znanost o podatcima i kooperativne sustave. Sa svojim suradnicima publicirao je više od 200 znanstvenih i stručnih radova. Prof. Lončarić član je stručne udruge IEEE i Akademije tehničkih znanosti Hrvatske. Bio je predsjednik Hrvatske sekcije IEEE. Osnivač je i organizator više međunarodnih znanstvenih skupova i ljetnih škola. Bio je urednik, član uredničkih i programskih odbora i recenzent za više međunarodnih znanstvenih skupova i časopisa. Dobitnik je Nagrade „Fran Bošnjaković“ Sveučilišta u Zagrebu, Nagrade "Rikard Podhorky" Akademije tehničkih znanosti Hrvatske, Nagrade za znanost Fakulteta elektrotehnike i računarstva, Fulbrajtove stipendije i Nagrade Hrvatske sekcije IEEE.

Miloš Judaš rođen je 1961. u Petrinji, Republika Hrvatska. U Zagrebu je završio Klasičnu gimnaziju te Medicinski fakultet Sveučilišta u Zagrebu (1984.), na kojem je zaposlen od 1985. godine, a 2012. je izabran u redovitog profesora u trajnom zvanju za predmete Neuroznanost i Anatomija. Direktor je Hrvatskog instituta za istraživanje mozga i direktor Znanstvenog centra izvrsnosti za temeljnu, kliničku i translacijsku neuroznanost. Od 2014. je prorektor za znanost i međunarodnu suradnju Sveučilišta u Zagrebu. Od 2008. član je i suradnik Hrvatske akademije znanosti i umjetnosti. Profesor Judaš međunarodno je priznati znanstvenik u polju razvojne neuroznanosti sa trajnom aktivnošću kroj brojne publikacije u svjetskim časopisima te bogatim nastavnim i administrativnim iskustvom u znanstvenoj zajednici. Značajno je pridonijeo razvoju neuroznanosti u Hrvatskoj kroz uključenost u osnivanje Hrvatskog instituta za istraživanje mozga, Hrvatskog društva za neuroznanost, te prvog poslijediplomskog studija neuroznanosti. Održao je brojna pozvana predavanja na međunarodnim skupovima i školama te je organizator mnogih međunarodnih i domaćih znanstvenih skupova i radionica. Znanstveni interes prof. Judaša su ljudska neuroanatomija i ljudska razvojna neurobiologija, razvojna i evolucijska neurobiologija kognicije, pozadina razvoja jezika te povijest neuroznanosti.

Acknowledgement

The realization of this dissertation would not have been possible without unconditional support of my family. I owe my greatest gratitude to my dad, mom and brother. Thank you for always giving me love and attention and supporting my goals and decisions, encouraging me to develop myself in the direction that makes me happy and fulfilled.

I would like to thank my mentors, prof. Miloš Judaš and prof. Sven Lončarić for their guidance in many aspects of my professional development. Many thanks to prof. Ivica Kostović and prof. Alan C. Evans for widening my career path with valuable guidance and helping me achieve scientific maturity through international collaboration.

I am thankful to my scientific family where we all support and learn from each other, trying to become better in our individual and joint work. I have never regretted the path that I have chosen for realization of myself and my dreams, in great part because of the people I met and became friends with. Thanks to my scientific brothers and sisters from the Croatian Institute for Brain Research and the Montreal Neurological Institute for many moments spent in working together and the adventures we have been through together. Thank you Dora, Vinka, Iris, Mihaela, Pero, Tena, Domagoj, Terezija, Sara, Ema, Seun, Jonathan, Konrad, Andrew, Trisanna, Jennifer, John and Greg. Thank you Goran for helping me find my way in the neuroscience. Thank you Tomislav for inspiring me in achieving scientific excellence. Special thanks to Claude for all the fish. Also, many thanks to Andrej, Mario, Amela, Jelena, Miran, Miro, Andrija and all others whose life paths crossed with mine. I am grateful for being your friend.

Abstract

The structure of the cerebral cortex is defined by organization and distribution of neurons in the tissue. Today, most investigations in brain cytoarchitectonics are not automatized and require significant involvement of the researcher, which is very time consuming and may introduce significant bias. This type of analysis may not be accurate enough or reveal enough information about the structure of the tissue. Brain tissue forms complex structures whose organization and distribution may be reliably revealed only using systematic computational approach.

The goal of this dissertation is development of novel computational methods for automatic and objective analysis of histological images of human brain suitable for advanced and fast analysis of brain cytoarchitectonics and laminar structure. The methods were developed aiming for a completely data-driven approach, with as little assumptions about the data as possible. Quantitative analysis of neuronal distribution and exploration of underlying principles of variation that facilitate parcellation of cortical layers resulted in novel framework and methodology for cellular-level investigations of brain tissue.

Keywords: brain cytoarchitecture, partial differential equations, digital image processing, machine learning

Računalna analiza histoloških slika citoarhitektonike ljudske moždane kore

Razumijevanje ljudskog mozga izazivalo je interes znanstvenika kroz čitavu povijest, a danas predstavlja jedan od najvećih izazova suvremene znanosti. Sve brojnija istraživanja koja se provode s ciljem pružanja uvida u strukturu, organizaciju i funkciju mozga ukazuju na njihov zdravstveni i ekonomski značaj u suvremenom društvu, ali i u razvoju računalnih metoda koje su inspirirane funkcijom mozga, poput umjetnih neuronskih mreža i drugih metoda umjetne inteligencije.

Moderna istraživanja u neuroznanosti započela su tijekom ranog 20. stoljeća otkrićima koja su omogućila naprednije i detaljnije proučavanje strukture mozga, nedugo nakon pojave prvog mikroskopa. Najvažnije od njih predstavljaju različite histološke metode bojanja tkiva koje, između ostaloga, omogućavaju prikaz pojedinih stanica u mozgu. Znanstvenici su ubrzo došli do zaključka kako se središnji živčani sustav sastoji od mnogobrojnih neurona, osnovnih funkcionalnih jedinki povezanih u mrežu te raspodijeljenih diljem mozga prema različitim organizacijskim uzorcima. Uskoro se pojavljuju i prve citoarhitektonske mape ljudske moždane kore u kojima su opisane suptine promjene u organizaciji, gustoći i veličini neurona. I danas se smatra da upravo te promjene definiraju organizacijske cjeline mozga te su podloga specifičnih funkcija različitih dijelova mozga. Neuroni moždane kore raspodijeljeni su u nekoliko slojeva, paralelno s naboranom površinom mozga, odnosno prateći girifikaciju. Takva organizacija naziva se *laminarna* struktura, s različitim veličinama i gustoćom neurona specifičnim za svaki od slojeva. Heterogenosti u staničnoj organizaciji moždane kore koje čine podlogu funkcije istražuju se detaljnim proučavanjem i opisivanjem stanične raspodijele u mozgu, nazivane *citoarhitektura* ili *citoarhitektonika*.

Od njihovog nastanka, prve mape ljudske moždane kore činile su okvir unutar kojeg su nastala brojna istraživanja te unutar kojeg su se rezultati tumačili. One i danas, više od stoljeća nakon njihovog nastanka, predstavljaju temelj suvremene funkcionalne neuronanatomije te imaju važnu ulogu u našem razumijevanju mozga. Međutim, za njihov nastanak koristili su se grubi alati dostupni u to doba, poput mikroskopa ili rukom crtanih ilustracija neurona, što je uzrok nekoliko manjkavosti tih ranih istraživanja. Primjerice, originalni preparati mozga nisu više pogodni za istraživanje, stoga se mjerenja ne mogu ponoviti danas dostupnim alatima. Rukom crtane mape tkiva mogu odstupati od stvarnog rasporeda stanica u mozgu zbog pristranosti istraživača. One također zanemaruju individualne razlike među uzorcima različitih mozgova. Upravo su neodređeni i nestandardizirani kriteriji suptilnih promjena u tkivu mozga prema kojem se istraživači vode kako bi označili različita područja mozga potakli brojne rasprave u znanstvenoj zajednici. Riješenje ovog izazova upravo su jasno određene smjernice i definirani kriteriji koji su jednako primjenjivi i ponovljivi na svim ispitivanim uzorcima. Ova spoznaja potakla je interes prema detaljnijim istraživanjima koja su postajala sve sofisticiranija,

praćena značajnim tehnološkim napretkom. Vrijednost kvantitativnih obilježja za procjenu citoarhitektonskih kriterija u razumijevanju zdrave i patološke organizacije mozga odavno je cijenjena. Kvantitativne studije također su važne za prepoznavanje homolognih područja između vrsta i usporedbu znanstvenih pronalazaka u mozgu primata i ljudskom mozgu. Prvi pokušaj kvantitativne procjene gustoće neurona objavljen je sredinom dvadesetog stoljeća, a slijedilo je nekoliko radova koji su ponudili različite pristupe u idućim desetljećima. Gustoće stanica i stope promjena procjenjuju se ekstrapolacijom iz mjerenja koje se temelje na ručnim prebranjanjem neuronskih populacija u nekoliko površinom malih, nasumično odabranih dijelova tkiva. No ovakve metode temeljene na ručnom brojanju zahtijevaju veliku količinu vremena istraživača, što isključuje preciznu i objektivnu analizu različitih područja mozga.

Napredak u kvantitativnim tehnikama za analizu laminarne strukture bila je upotreba denzitometrije, metode koja je uvela uzorkovanje optičke gustoće duž poprečnih linija preko slojeva cijelom širinom korteksa. Ovom računalno potpomognutom metodom utvrđuju se promjene neuronske gustoće stvaranjem profila koji odražavaju uzorke kortikalne laminacije. U isto vrijeme razvija se i ideja upotrebe objektivnih mjera kortikalnih područja za njihovu identifikaciju, analogne konceptu otiska prsta. Međutim, metode koje koriste pristup optičke gustoće vrlo su osjetljive na šum i artefakte staničnog bojanja koje koristi u pripremi tkiva, što može uzrokovati značajan otklon od stvarnih iznosa mjera karakteristika tkiva. Daljnji napredak u profiliranju laminarne strukture postignut je uvođenjem mjera gustoća neurona susjednih područja duž profila koje se dobivaju segmentiranjem elemenata slike, prilikom kojeg se označavaju neuroni u staničnom matriksu. Susjedni dijelovi u profilu mogu biti predstavljeni vektorima svojih svojstava, koji se mogu uspoređivati među različitim dijelovima korteksa. Ovakvi detaljniji i precizniji opisi tkiva doveli su do razvoja apstraktnih matematičkih značajki izvedenih iz profila gustoće, poput različitih statističkih usporedbi. No te značajke može ponekad biti teško tumačiti u biološkom i anatomskom smislu.

U svjetlu značajnih napredaka u tehnologiji i znanju stečenom krajem stoljeća, nedostaci ranih arhitektonskih studija rađenih korištenjem klasičnih metoda postali su izraženiji, a počinje se i preispitivati njihova uporaba za anatomske studije. Glavni nedostaci odnose se na subjektivne kriterije istraživača prilikom ranijih mjerenja, a koje je danas vrlo teško, čak i nemoguće reproducirati. Prikazivanje trodimenzionalne strukture mozga u dvodimenzionalnom kontekstu također predstavlja nedostatak, kao i ograničena mogućnost da se metode primjenjuju na većem broju uzoraka zbog sporosti ručnog obrađivanja preparata, posljedica čega je mali broj dostupnih analiziranih uzoraka, čime se zanemaruje istraživanje varijabilnosti strukture mozga između više uzoraka. Uvođenjem digitalizacije i računala u područje mikroskopije te snimanja ultravisoke razlučivosti i naprednih metoda obrade tkiva, istraživanja u ovom području postigla su ogroman napredak. Međutim, postoje mnogi otvoreni izazovi koji zahtijevaju napore znanstvenika iz više disciplina, od neuroznanosti do računarstva.

Koristeći napredak u računalnom vidu i odnedavno dostupnim velikim količinama podataka iz svjetskih histoloških zbirki, po prvi puta je moguće detaljno i objektivno analizirati strukturnu organizaciju cijelog mozga i razviti redefiniranu citoarhitektonsku mapu u dosad neviđenim detaljima. Istraživanja u ovom području vode razvitku metoda računanja i automatske obrade velikih količina histoloških podataka, što će omogućiti vjerodostojnije i pouzdanije računalne modele mozga. Važno pitanje koji valja razmotiriti prilikom razvoja automatizirane analize slika ljudskog mozga, ili biomedicinskih slika općenito, je u kojoj mjeri bi automatizirani sustavi trebali reproducirati znanstvenika. Ovo je pitanje postaje sve relevantnije, budući da su nedavni rezultati u metodama analize slike temeljeni na dubokom učenju postali sposobni nadmašiti ljude u određenim zadacima. Ljudski vidni sustav koristi model svijeta koji je naučen tijekom godina života kako bi bolje objasnio vidni ulaz, povezujući promatrane signale slike s prethodnim vidnim iskustvima. Međutim, to ponekad može dovesti do pristranosti, budući da ovaj sustav teži podupiranju unaprijed stvorenih ideja, štomože rezultirati time da dva promatrača različito objašnjavaju iste pojave, ovisno o vlastitim osobnim iskustvima. Također, neke teško uočljive, ali značajne razlike u uspoređivanju novih podataka s prethodnim opažanjima mogu biti propuštene zbog sličnih, ali ipak različitih slika. Time se smanjuje objektivnost analiza, kao i njihova ponovljivost i osjetljivost u opažanju važnih karakteristika slike. S druge strane, sustavi računalnog vida pristupaju i obrađuju elemente slike koji nisu vidljivi ljudskom oku, mogu obraditi svaku sliku na isti način te omogućiti djelomičnu ili potpunu automatizaciju procesa. Istraživanje ograničenja u ljudskom radu uvelike će koristiti budućem razvoju metoda obrade i analize histoloških slika, dovodeći u pitanje klasičnu upotrebu ručnog označavanja kao polazišta za ocjenjivanje učinkovitosti automatiziranih metoda.

Istraživanje računalnih metoda i automatizacije u suvremenim istraživanjima citorearhitektonike moždane kore koje danas znanstvenici uglavnom obavljaju ručno središte su istraživanja ove disertacije. Iako su već predložene brojne metode računalna analize moždanog tkiva kao rezultat inkrementalnog napretka tijekom godina u ovom polju, još uvijek postoje mnoga neodgovorena pitanja, a metode treba poboljšati u smislu njihove primjenjivosti i učinkovitosti.

Osnovni preduvjet u klasičnim i računalnim citoarhitektonskim istraživanjima je lokalizacija i segmentacija stanica, dva slična, ali različita pojma koji se smatraju osnovom automatske analize slike. Rezultat detekcije odnosno lokalizacije stanica su njihove koordinate, a rezultat segmentacije je opcrtavanje granica i određivanje površina stanica. Ti se pojmovi često mogu zamjenjivati, jer jedan zadatak često uključuje i drugi. Oni omogućuju različite kvantitativne analize koje uključuju mjerenja morfologije stanica kao što su veličina, oblik, izduženost i slično. No slikovni podaci mogu varirati na mnogo načina, kao što su podaci dobiveni snimkama iz različitih mikroskopa, vrste staničnog bojanja, gustoća stanica, struktura i organizacija u različitim tipovima tkiva. Također, podaci mogu biti vrlo složeni, sadrže slikovne artefakte i šum te ih je vrlo često teško prikupljati. Posebice neuroni mogu činiti nepravilne formacije, imati

različite veličine tijela nepravilno oblike, a pritom biti oslikani pomoću staničnog bojenja koje proizvodi gotovo potpuno sive slike, sprečavajući time primjenu metoda temeljene na varijacijama boja na slici. Stanice se mogu nalaziti i u nakupinama te se djelomično preklapati, što je posebno problematično za mnoge automatizirane metode. Stoga je teško dobiti robustnu i točnu detekciju i segmentaciju unatoč tome što su predložena mnoga različita rješenja.

Prema literaturi objavljenoj od 1960. godine do danas, može se zaključiti da se većina metoda detekcije i segmentacije stanica temelji na nekoliko osnovnih pristupa temeljenih uglavnom na segmentaciji slike prema intenzitetu, detekciji rubova, matematičkoj morfologiji. Često se primjenjuju i metode poput deformabilnih modela i izrastanja regija, a u posljednje vrijeme sve se više koriste metode temeljene na učenju, primjerice duboke neuronske mreže. Zanimljivo je promatrati kako se tijekom godina razvijalo korištenje različitih pristupa segmentacije stanica. Korištenje nekih od početnih metoda zbog njihovih ograničenja polako se smanjivalo i otvaralo mjesta novim metodama. No, mnoge se još i danas koriste, uglavnom kao jedan od elemenata u pristupima koji upotrebljavaju više od jedne osnovne metode. Iako nijedan od pristupa ne daje rezultate koji bi u potpunosti zadovoljili mnoge izazove analize histoloških slika, oni se još uvijek u određenoj mjeri koriste. Kao posljedica toga, nedavno predložene metode nisu utemeljene na jednom konceptu, nego su kombinacija i prilagodba starih. Rezultat toga je divergencija područja u smislu da se za svaki problem segmentacije stanica razvijaju posebne metode. Međutim, sve veći broj radova u posljednjem desetljeću sugerira da razvijene metode još uvijek ne rješavaju problem na zadovoljavajući način te da je potrebno razviti preciznije i robusnije metode.

Kod automatske segmentacije kortikalnih slojeva, koja nema dugu povijest kao stanična analiza, noviji radovi značajno su pridonijeli području. Profiliranje duž širine korteksa okomito na kortikalne slojeve ostaje središnja ideja u automatskim metodama za kvantifikaciju promjena u laminarnoj strukturi. Zapravo, sve poznate kvantitativne metode do 2005. godine koriste profile gustoće, a taj pristup i dalje dominira u automatiziranom pristupu, uz neke napretke, primjerice upotrebom prvih metoda automatskog brojanja neurona, korištenjem statističkog testiranja za razlikovanje područja mozga te strojnog učenja. Međutim, metode koje se temelje na profilima ne koriste informacije o distribuciji i organizaciji na staničnoj razini, uključujući svojstva pojedinačnih stanica. One koriste značajke tkiva, poput varijacija u intenzitetu slike ili postotku staničnih tijela koja pokrivaju unaprijed određena područja. Tek posljednjih godina pojavljuju se prvi radovi koji koriste detaljnije značajke tkiva, automatizirane metode i strojno učenje. Nedavno je predstavljen pristup koji integrira značajke stanica s analizom laminarne strukture u korteksu miša. Autori razvijaju nekoliko značajki automatski segmentiranih neurona i na temelju varijacija u raspodjeli stanica razlikuju se između različitih slojeva korteksa, ponovno koriste profile duž korteksa. Prvi pristup koji ne koristi metodu profiliranja pojavio se 2018. godine, u kojem autori baziraju svoju analizu kortikalnih slojeva mišjeg mozga na

kombiniranju nenadziranog i nadziranog učenja. Lokalizacija i nekoliko značajki neurona izvedeni su automatskom metodom. U kombinaciji s analizom teksture tkiva korištene su različite kombinacije tih značajki u hijerarhijskom grupiranju. Trendovi u analizi laminarne strukture ukazuju na činjenicu da metode postaju sve više automatizirane, detaljnije, neovisnije o istraživačima koji ih koriste, upotrebljavaju velike količine podataka visoke rezolucije i razvijaju različite neurobiološke značajke koje se koriste kao ulazni podaci u metodama strojnog učenja.

Cilj istraživanja u ovoj disertaciji je razvoj računarskih metoda za automatsku i objektivnu analizu histoloških slika ljudskog mozga pogodnih za naprednu i brzu analizu citoarhitekture mozga i laminarne strukture. Razvijen je integrirani pristup koji povezuje kvantitativnu analizu distribucija neurona s istraživanjima temeljnih načela varijacije koja uzrokuju raznovrsnost kortikalnih slojeva. Metode su razvijene pristupom potpuno temeljenim na podacima, uz što manje pretpostavki ili zaključaka o samim podacima. Istraživanje je usmjereno prema dvije glavne metode, automatsku detekciju neurona u histološkim preparatima i automatsku segmentaciju slojeva moždane kore. Ostale teme uključuju prikupljanje histoloških preparata i ručnih označavanja, analizu varijabilnosti označavanja, razvoj krakteristika neurona i njihovu primjenu u modelima strojnog učenja, analizu dobivenih modela. Disertacija je raspodijeljena u šest poglavlja kroz koje se opisuje i gradi istraživanje, od početnih razmatranja o podacima, motivacije i definiciji problema do konačnog modela automatske segmentacije slojeva temeljenog na značajkama neurona.

U prvom poglavlju prikazan je kontekst istraživanja u kojem se navode ciljevi istraživanja, s naglaskom na izazove u kvantitativnim metodama za detekciju i segmentaciju slojeva u laminarnoj strukturi mozga, što je glavni fokus istraživanja ove disertacije. Nakon uvodnog uvoda i navođenja važnih povijesnih pronalazaka, slijedi pregled suvremenih istraživanja u obradi i analizi histoloških slike. U ovom pregledu uspoređuje se uspješnost različitih metoda primjenjivanih na probleme u pokušajima automatizacije procesa analize histoloških preparata, ali i obradi digitalne slike općenito. Navode se metode za detekciju stanica koje se razmatraju i u širem kontekstu detekcije objekata na slici. U nastavku je dan prikaz metoda za segmentaciju slojeva moždane kore, u kojem se tek odnedavno koriste automatske metode te se razmatraju različiti pristupi ovom problemu. Na kraju prvog poglavlja navode se ciljevi disertacije i kratak pregled svakog od poglavlja.

Drugo poglavlje sadrži detalje o podacima korištenim u ovom doktorskom istraživanju i jedinstvenoj bazi ručno označenih neurona i kortikalnih slojeva dobivenih tijekom ovog istraživanja. Prikazane su osnovne informacije o digitalizaciji histoloških slika te pojedini koraci koji se koriste prilikom dobivanja preparata, od izrade histoloških preparata do dobivanja konačne digitalne slike preparata. Opisan je i postupak dobivanja ručnih označavanja lokacija neurona i podjele slojeva moždane kore, a koji će biti korišteni za razvoj metoda u idućim poglavljima. Kako bi se mogle usporediti i interindividualne razlike, tri stručnjaka u području neuroanatomije

i citoarhitektonike ručno su označili navedene strukture koristeći računalne programe posebno razvijene kao dio ovog doktorskog istraživanja, a u svrhu lakšeg i točnijeg označavanja.

U trećem poglavlju opisana je nova metoda za automatsku detekciju neurona na histološkim slikama ljudskog mozga. Ova metoda temelj je istraživanja ove disertacije, na kojoj počivaju i iz koje se grade ostale metode i rezultati. Automatizacija procesa označavanja neurona značajno ubrzava ovaj zadatak, a budući da se na jednom preparatu mogu nalaziti i stotine tisuća neurona, zbog dugotrajnosti ručnog prebrajanja često se obrađuju samo dijelovi preparata, a o ukupnom broju neurona zaključuje se na temelju tih mjerenja, što može dovesti do značajnog otklona od stvarnog broja neurona (i do 20%). Usto, istraživači mogu različito interpretirati radi li se o neuronu ili ne, što je pokazano usporedbom ručnih označavanja triju stručnjaka, pri čemu se oni međusobno slažu u prosječno samo 86% pronađenih neurona. U eksperimentu gdje je s vremenskim odmakom isti stručnjak ponovio označavanje na istom skupu slika slaganje je iznosilo 81%. Ovakva nekonzistentnost predstavlja značajan izazov istraživanjima koje se temelje na ručnom prebrajanju, dovodeći u pitanje pouzdanost dobivenih rezultata. Pokazano je kako se dobiveni rezultati dobiveni automatskom metodom opisanom u ovom poglavlju slažu s rezultatima ručnih označavanja stručnjaka u gotovo jednakoj mjeri u kojoj se oni međusobno slažu, čineći time rad metode ekvivalentan radu stručnjaka. No, automatska metoda detektira metode uvijek jednako, dajući konzistentne podatke na svim preparatima i to u vrlo kratkom vremenu. To je postignuto modeliranjem upijanja boje u tkivo tijekom izrade histološkog preparata. Parcijalna diferencijalna jednadžba (PDJ) korištena za modeliranje varijacija intenzitete histološke slike temeljni je element metode za automatsku detekciju neurona razvijene u ovom poglavlju, a koja nadmašuje rezultate suvremenih metoda za istu namjenu. Opisana je primjena PDJ-a u diskretnom kontekstu digitalne slike te su prikazana neka od važnih teorijskih svojstava. Prednost ove metode je uspješno razdvajanje neurona koji se dodiruju ili preklapaju, što inače predstavlja poteškoće drugim metodama. Također, za razvoj ove metode nije potrebna velika količina podataka, kao što je primjer kod mnogih popularnih suvremenih metoda u ovom području temeljenih na dubokom učenju. Pokazuje se kako upotreba specifičnog znanja o području rezultira uspješnijom metodom. Konačno, prikazana je primjena automatske metode na cijelom histološkom preparatu te razvijena mapa gustoće. Pritom se jasno vide citoarhiteknoske razlike u gustoći neurona kroz slojeve moždane kore, a što će biti temelj razvoja metode za automatsku segmentaciju slojeva u petom poglavlju.

Prelazak iz dvodimenzionalnog u trodimenzionalni konteks detekcije neurona prikazan je u četvrtom poglavlju. Treća prostorna dimenzija izvodi se korištenjem histoloških preparata digitaliziranih u više optičkih ravnina duž z-osi. Pojedini neuroni prate se kroz dubinu različitih razina preparata te se njihova dubina određuje na temelju oštrine slike, mjerenjem varijacija diskretne derivacije, odnosno Laplaceovog operatora. Prikazano je i razmatranje o razlikama između konfokalne i svjetlosne mikroskopije te metode za obradu i analizu takvih slika. Rezul-

tat ovog dijela istraživanja je metoda za vjerniji prikaz trodimenzionalnog rasporeda neurona unutar jednog histološkog preparata te kontinuiranog rasporeda neurona u spajanju više uzastopnih preparata. Još jedan važan rezultata istraživanja u ovom poglavlju je precizna segmentacija tijela pojedinih neurona, temeljena na njihovoj prethodnoj detekciji, a s kojom čini temelj za razvoj detaljnije karakterizacije neurona i metoda u idućem poglavlju.

Peto poglavlje objedinjuje znanstvena postignuća ove disertacije kroz razvoj novog istraživačkog okvira i metodologije za analizu laminarne strukture i klasifikacije neurona prema njihovom položaju unutar slojeva mozga. Prikazuje istraživanje varijacija brojnih citoarhitektonskih karakteristika koje uzrokuju podijelu mozga u slojevitu strukturu. Izvedeno je opsežno istraživanje i primjena suvremenih algoritama grupiranja temeljenih na gustoći neurona. Iako niti jedan od njih nije dao jasnu podjelu prema slojevima, ova analiza pružila je bolju intuiciju o podacima za daljnje istraživanje, utvrđujući da je polumjer od $100-300\mu$m oko svakog neurona optimalan za utvrđivanje njegovih karakteristika. U tom polumjeru obično je sadržano oko $250-500$ neurona. U ovom istraživanju, pred polumjerom prednost je dana broju neurona, budući da se poznavajući taj broj mogu izračunati učinkovite strukture podataka koje olakšavaju i ubrzavaju daljnje računanje. Također, zadani polumjer može se drugačije tumačiti pri različitim povećanjima. Uz lokacije i osnovne značajke neurona, poput njegove površine, karakteristika oblika i samih vrijednosti piksela, oblikovane su složenije značajke poput promjera i oblika konveksne ljuske zadanog broja susjednih neurona, različitih mjera iz populacijske raznolikosti vrsta, mjera raspršenosti rasporeda stabala i naselja i druge. Izvedeno je oko 400 različitih značajki neurona, koji su se zatim koristili za predviđanje pripadnosti neurona slojevima u moždanoj kori koristeći modele stojnog učenja. Konkretno, za nadzirano učenje koristili su se podaci koje su označili tri stručnjaka, a kao model odabrani su ansambli stabala odlučivanja, budući da za učenje ne trebaju velike količini podataka, njihova primjena nije računalno zahtijevna te se rezultati mogu lako analizirati i tumačiti. Kao najboljim pokazao se model dobiven kombinacijom triju ansambala, po jedan naučen na podacima svakog od stručnjaka. Pristup putem segmentaciji slojeva moždane kore putem strojnog učenja na razini individualnih neurona daje doprinos s dva značajna aspekta: (i) pružajući mogućnost klasificiranja neurona unutar slojevi te strukture mozga, razlikujući time područja kortikalnih slojeva i (ii) analiza i interpretacija modela daje uvid u važne značajke neurona i njihove lokalne strukture. Ovaj pristup objedinjuje nekoliko rezultata iz disertacije korištenjem širokog skupa kvantitativnih značajki neurona i njihove okoline, pronađenih u literaturi i razvijenih u ovom doktorskom istraživanju. U razvoju ove metodologije, poseban je naglasak stavljen na interpretaciju modela i analizu značajki neurona koje dovode do podjele moždane kore u slojeve. One se mogu analizirati na razini cijelog modela, ali i na individualnoj razini za svaki neuron. Primjerice, može se ustanoviti koje su značajke imale najveći doprinos tome da se pojedini neuron svrsta u određeni sloj.

Šesto poglavlje zaključuje disertaciju te navodi glavne znanstvene doprinose. Glavni istraživački doprinosi su: (1) računalna metoda za automatsku detekciju neurona na histološkim slikama ljudskog mozga, (2) računalna metoda za segmentaciju kortikalnih slojeva na histološkim slikama ljudskog mozga, (3) javno dostupna baza originalnih i od strane eksperata anotiranih histoloških slika te postupak za ispitivanje metoda detekcije neurona i segmentacije kortikalnih slojeva te (4) računalna metoda za određivanje treće prostorne dimenzije neurona u histološkim slikama dobivenim svjetlosnom mikroskopijom. Poglavlje završava kratkim razmatranjem budućih istraživačkih smjernica.

Ključne riječi: Citoarhitektonika, parcijalne diferencijalne jednadžbe, obrada digitalne slike, strojno učenje

Contents

Chapter 1

Introduction

Understanding the brain and how it works has certainly been one of the grandest challenges of modern science. Even though scientist have made profound discoveries, the brain still remains one of nature's most mysterious creations.

Modern neuroscience began with the discoveries made at the very beginning of the last century by works of Camillo Golgi who enabled more detailed and sophisticated studies of brain using at that time recently developed microscope. Ramon y Cajal [1] used the developed technique and introduced the neuron doctrine in which he hypothesized that the brain was made up of a network of neurons as individual functionals, connected and organized in different patterns across the cortex. Shortly after, detailed maps of cortical areas that described variations in density, distribution or typical size of neurons within specific layers of human cortex were developed, most famous being those made by Brodmann [2] and von Economo [3]. Over the years, these works provided framework within which many discoveries were made, interpreted and communicated. Today, it is thought that variations in neuronal distribution in the brain and their density determine function, with many evidences linking architectonic variation and brain function [4], [5]. These variations define several distinct layers of the cortex that are arranged parallel to the brain's folded surface. The structure of these layers, known as *laminar structure*, also varies, as well as distribution and size of neurons found within the layers. Based on these variations, we distinguish a series of spatially discrete areas of the brain. The subtleties in this fine structure of the brain underlying it's function can be characterized in great detail by studying the organization of cells across the cortex, which is usually known as *cytoarchitecture* or *cytoarchitectonics*.

Almost a century after the first cytoarchitectonic maps of human brain were developed, these works are still a foundation on which modern functional neuroanatomy is based and play an important role in our understanding of the brain. However, these early discoveries were made by hand using drawings and crude apparatus available at that time and have several limitations. The original specimens are no longer in condition to be analyzed, so the measurements cannot

be repeated using the modern tools available today. Manual drawings of tissue observed under the microscope may possess large deviations from the original due to the observer-dependent variations. In addition, they neglect the inter-subject differences. Undefined criteria for determining subtle changes of the brain structure between the areas have spurred many questions among independent investigators of cortical structure in the last century [6]. A solution to this problem is only a clearly stated definitions which may independently be reproduced, verified and refined among the scientific community. This has driven the interest towards more detailed investigations, which were becoming increasingly sophisticated through the use of significant technological advancements.

The value of quantitative characteristics for evaluating architectonic criteria in understanding healthy and pathological brain organization has long been appreciated [3], [7]. Quantitative studies are also important for identifying homologue areas between species and transferring conclusions from subhuman to human brains [8]. First attempt in quantitative estimation of neuron densities was done by Abercrombie [9] and was followed by several works that offered different approaches in the decades after [10], [11], [12], [13], [14], [15], [16]. Cell densities and rates of changes are usually extrapolated from analyses based on manual counts of neuron populations in randomly chosen, sparse portions on the tissue. The methods based on manual cell counting require great amount of time of investigator involved, which precludes detailed and objective large-scale analysis of brain areas.

A step forward in quantitative techniques for the analysis of laminar structure was the use of densitometry [17], which introduced sampling of optical density along transverse lines across the layers spanning the full width of the cortex. The lines created in this computer-aided method represent a profile of changing neuronal density, reflecting the pattern of cortical lamination. Authors also present the idea that an objective measures of cortical regions, analogue to the concept of fingerprint, could be developed for identification of distinct cortical areas. The very natural concept of sampling across the layers was also proposed independently by two other groups [18], [19]. However, the methods using the optical density approach are very sensitive to staining artefacts commonly found in preparation of tissue for examination under microscope and may be heavily biased by uneven staining or illumination. An advancement in laminar profiling was made by introduction of areal densities which are obtained by thresholding the image and segmenting image elements, thus extracting neurons from the cortical matrix. Blocks of adjacent profiles may be represented by feature vectors, which can be compared between areas of the cortex. This has led to development of abstract mathematical features derived from density profiles, like the mean, standard deviation, skewness, kurtosis and other. These features, however, may be difficult to interpret in terms of biological and anatomical perspective [20].

In the light of significant advancements in technology and knowledge made by turn of the century, drawbacks of the early architectonic studies using the classical methods became more

expressed and sometimes critical for practical use as references for anatomical studies. Main disadvantages concern (i) subjective, observer-dependent criteria and measurements that are very hard, if impossible to reproduce, (ii) presentation of findings in two-dimensional context, while the brain is a three-dimensional structure, (iii) limited data processing capabilities hinder the application of methods on larger number of samples, thus neglecting the variability in the brain structure between individual samples. With the introduction of ultrahigh-resolution imaging, advanced tissue processing methods, and especially the digitization and introduction of computers, research in this field has achieved enormous advances. However, there are many open challenges that call for effort of scientists from multiple disciplines, from neuroscience to computer science.

Using advances in machine vision and recently available large amounts of data like, for instance, from the BigBrain project [21], we are for the first time able to deeply, objectively and consistently analyze structural organization across the whole brain and develop a redefined cytoarchitectonic map of the brain in as yet unseen detail. Results from investigations in this field will provide capacity to computationally and automatically process large amounts of histological data, allowing for more realistic and reliable models.

One important aspect to consider in the analysis of images of human brain, or biomedical images in general, is to what extent should automated systems recreate the work of human investigators. This question has become increasingly relevant since recent results in image analysis methods based on deep learning have become able to outperform humans in certain tasks [22], [23]. Human visual system employs model of the world learned over years of one's life to better explain visual input, associating observed image signals with previous visual experiences. However, this may sometime introduce bias as this system tends to support preconceived ideas, which, in turn, may result in two observers explaining the same phenomena differently, depending on their own personal experiences. Also, some subtle but significant differences in comparing new data with previous observations may be missed due to similarly looking yet distinct images. This lowers the objectivity of analyses, as well as reproducibility and sensitivity. Computer vision systems, in contrast, can give access to underlying image contents that are not visible, process every image equally and provide partial or complete automation of the process [24]. A research into limitations of human performance will greatly benefit future computational image analyses, calling in question the classical use of 'gold standard' as a baseline for evaluating performance of automated methods.

Investigations in computer-based methods and automation of tasks currently mostly done manually by human investigators involved in modern study of cerebral cortex cytoarchitectonics are the central point of this thesis. Although there are numerous methods being proposed for computational analysis of brain tissue as a result of incremental advances in the field over the years, there are still many unanswered questions, and the methods need to be improved in terms

of applicability and performance. In the following subsection an overview of classical image processing and analysis methods is given, in the broader context of general tissue analysis at the cellular level, but relevant to the context of analysis of brain cytoarchitectonics.

1.1 State-of-the-art

Computer-aided analysis of cellular organization dates to the mid-20th century when first systems for automating classification of cells and enabling mass screening for cervical cancer were developed. The systems applied thresholding-based decision rules to serialize one-dimensional microscopic line scans of the cell specimen [25]. The first example of automated processing of counting of cells was in the 1960s when the two-dimensional images were processed for purpose of differential counting of white blood cells (leukocytes), according to their classes which were based on simple colorimetric and morphological measurement [26]. Systems for automatic counting became widely accessible and used in hospitals, labs and other medical facilities around mid-1970s and included multiple computers working together to parallelize the task of analyzing the images. At that time the first computer assisted microscopes were developed for tracing and analysis of neuronal cells [27]. In the 1990s computers became powerful enough that image processing and computer vision became very influential in the field of microscopy. Being such a new approach, it is no wonder that most of the relevant literature was written after the year 2000. Published cell analysis methods have already been the basis of numerous studies that involved cell counting, identification of cell shapes and types, quantification of cell migration and interaction, cellular sociology and intracellular structures.

Nowadays, advanced systems used in microscopy research produce large images with many details in amounts like never before. The abundance, heterogeneity, dimensionality and complexity of such data makes it impossible for the professionals to process them and analyze manually. Computational techniques have therefore become of key importance in further research.

A critical prerequisite in both classical and computer-aided cytoarchitectonic investigations is cell detection and segmentation, usually considered as the basis of automated image analysis [28]. These are two similar but distinct concepts. In cell detection/localization, the output are x, y-coordinates of the cells, while in cell segmentation borders or areas of the cells are given. These concepts may often be used interchangeably, since one often involves the other. They provide various quantitative analysis that include measurements of cell morphology such as size, shape, elongation and similar. However, image data can vary in many ways, such as data from different microscopes, staining, cell densities, structure and organization found in different tissue and cell types. Also, the data can be very complex, contain artifacts and noise, and also not easy to acquire. Especially neurons may form irregular formations, have different cell size,

and be visualized using stains that produce almost grayscale images, preventing the application of methods that use color variation to identify objects of interest. The cells may be clumped together in clusters and partially overlap, which is especially problematic for many automated methods. Therefore, it is difficult to obtain robust and accurate detection/segmentation and many different solutions have been proposed. Looking through the literature published on the subject since 1960 suggests that the majority of cell detection and segmentation methods are based on a few basic approaches. A review of these follows, considering some of the common methods used in plethora of challenges in analysis of different cell structures, but staying in the context of those relevant for analysis of neuron distribution.

Surely one of the first things that seem natural, it is no wonder that intensity thresholding was the first but still predominant approach in cell segmentation. Assumption behind this approach is that cells have significantly and consistently different intensities than the background. In cases when the intensity changes gradually over the image, adaptive thresholding may be required. The threshold itself is often selected automatically, based on statistical analysis of the local or global image intensities [29]. In practice, however, thresholding alone is not enough to yield a good segmentation result due to the many imperfections the image may have, such as noise and overlapping cells. But the idea of different intensities between the cells and the background is still the reason thresholding methods are used as a part of the segmentation pipeline in some segmentation processes [30].

Besides differing from the background by intensity, cells also possess rather uniform intensity derived features. Those features can be detected using linear image filtering. For example, blob detectors such as Laplacian of Gaussian [31] may be used for images at low magnification, where cells resemble small compact particles. We can observe cells in more detail at higher magnification, were they appear as larger regions. Sometimes it is assumed that their shapes are invariant, and a filter template may be developed to use this property. Edge detection using first or second order partial differentiation filters is also often used [32], [33]. Similarly, like thresholding methods, feature detection methods may be of use but do not produce definitive cell outlines and are rather used as a part of the segmentation procedure.

Being a theory and technique based on set theory, lattice theory, topology, and random functions, mathematical morphology can be employed as well on graphs, surface meshes, solids, and many other spatial structures [34]. It regards an image in a more abstract sense, thereby offering prolific set of results for use in image processing. Due to their nonlinearity, operators based on mathematical morphology such as erosion, dilation, opening and closing offer numerous ways of analyzing and processing geometrical and topological properties of objects in images. These operators are often used in cell segmentation, with more complicated operators being constructed by combining basic ones, for instance, the watershed technique has its foundation in mathematical morphology operators. A morphology-based cell segmentation was proposed

in [35]. It is suitable for images in which cell boundaries are easy to extract. A distinction has to be made between binary morphology, which is often used as a post processing step, for example to polish coarse segmentation, and grayscale morphology which is mostly used as a preprocessing step as a way of manipulating and preparing image structures before segmentation [36]. Some other works employed morphological filters on Pap smear images [37], mitotic cell detection [38] or white blood cell detection [39]. Image morphology is usually one of the first steps in the processing pipeline, and is combined with other methods to produce final results.

Methods based on region growing approach use the assumption that pixels within a single region have similar intensities. Comparing the intensities of neighboring pixels, based on some similarity criterion, one can determine if the pixel belongs to the cluster of neighboring pixels. The suitable choice of seed points is important, as is the choice of similarity criterion. Regions are then grown from these points using the chosen criterion, until the whole image is divided in labeled regions. Unseeded region growing methods exist, and do not require explicit seeds [40], [41]. A single pixel which corresponds to the first region is chosen. During growing of that region, all pixels that do not match the requirements of similarity criterion compared with the pixels in that region are added to another new region and grown as the first region. For instance, in watershed transform [42], image is viewed as a landscape being filled with water from local minima, and segmented using lines where catchment basins meet. Watershed transform may sometimes over-segment the image because of image intensity variations. Marker-controlled watershed is often used to overcome this problem [43], [44].

The increasingly important role in cell segmentation have methods that fit a deformable model to the data. Deformable models offer an attractive approach to tackling such problems, because they can represent the complex shapes and shape variability of cell structures and are often used in medical image analysis [45]. Deformable models overcome many of the limitations of traditional low level image processing techniques, by providing compact and analytical representations of object shape, by incorporating anatomic knowledge, and by providing interactive capabilities. At first initialized at coarse scale, a deformable model is iteratively evolved to minimize a predefined energy functional which typically consists of shape based (e.g. elliptical) terms and terms that are formulated from *a priori* knowledge about structures on the image data to constrain the results. The choice of terms usually depends on practical implementations [46]. Authors in [47] used properties of fitted ellipsoids to distinguish neurons from other image elements. Deformable models are, however, very sensitive to noise which may obstruct proper evolution of the model and result in objects not being properly delineated [45].

Recent methods increasingly use supervised learning techniques to segment and detect cells. In pixel-wise classification, the class of each pixel in the image is determined by a learned model with a certain criterion. In [48] used supervised learning to detect nuclei in images of lymphoma, and in [49] authors used bag of local Bayesian classifiers with mixture of other

classifiers. In most cases, pixel-based approach is usually unable to separate touching cells and requires additional steps. Superpixel classification separates image into regions which are then used as an input to a classifier. Multi-class support vector machine (SVM) was used in [50] with additional step of splitting overlapping cells [51]. In [52], authors use alternating decision tree (ADT) [53] to select the best superpixels for cell nucleus segmentation. The superpixel approach is usually much faster than pixel-based. However, its performance highly depends of creation of superpixels which sometimes may not properly delineate cell boundaries. Random forests were used for cell detection in [54], and a high-throughput method based on feed-forward artificial neural network is presented in [55]. These methods achieve an accuracy of approximately 90%, as do most of learning-based methods for problems related to neuron detection. Today very popular deep learning methods were used in several recent works [56], [57], [58]. Downside of this approach is the need for a large amount of manually annotated data [59]. This poses a fundamental problem for methods based on supervised learning. Again, this brings back the question of whether annotations made by investigators should be considered as a ground truth and to which extent [24], [60], [59].

Observing how the usage of various approaches to cell segmentation has evolved during the years is very interesting. We can see that thresholding methods, being the simplest and most intuitive, were the first approach, but due to limitations of their usage slowly diminished and other methods emerged. However, it is still being used, mostly as a part of the pipeline in approaches that use more than one method. It was soon realized that differential features of the image (e.g. edges of objects) could also be easily computed and used for segmentation. The field of mathematical morphology was starting to develop about the same time and basic operators from this field were seeing their first use in late 1970s. They would soon be followed by mentioned methods of region accumulation, first use of which we observe in mid-1980s. The first deformable model fitting approaches were introduced in cell segmentation at the beginning of 1990s. Since then, the whole variety of approaches to cell segmentation was used, from support vector machines, dynamic programming, tensor voting schemes, various artificial neural networks and other. We can make several observations that follow literature analysis on cell segmentation. Most approaches were originally developed with some other purpose or application in another field (robotics, material science) and were later adopted for cell segmentation. This is remarkable, since the cell image analysis is a unique field, which should develop new ideas and approaches. Even though these new approaches are introduced every once in a while, it seems that the old ones are never fully abandoned and replaced, but rather kept as a part of a multi-stage segmentation process.

Although none of the approaches provides results that would completely satisfy many challenges in cellular image analysis, they seem to still be useful to some extent. Consequently, recently proposed methods are not based on a single concept but are rather a combination of old

ones, adapted and fitted to work together in a better way. The result of this is that it seems that the field is not converging to a single method but is rather diverging in the sense that by now for every cell segmentation problem there are different methods being developed. However, an increasing number of publications in the last decade suggests that the methods developed are still not grasping the problem in the satisfactory way, and more powerful and robust methods for cell segmentation have to be developed.

In automatic cortical layer segmentation, which does not have a long history as the cellular analysis, recent works have brought significant contributions to the field. Profiling across the width of the cortex perpendicularly to cortical layers remains the central idea in automatic methods for quantification of the changes in laminar pattern. In fact, all known quantitative methods up to 2005. use density line profiles [61], and this approach continues to be dominate in algorithm-based approach. Expansions built upon it have been made, for instance by using automated neuron counting to obtain information about changing cellular density [62], [63], developing tissue feature vectors and using statistical testing to distinguish brain areas [64], or by using machine learning approach [65]. Especially the Zilles' group has done most of the work in the subject and has been involved since the beginning of the development of automated approach [66], [67], [68], [69]. It is important to mention that in their work [61], the same group has made a significant contribution by expanding the cytoarchitectural considerations of profiling and introduced receptoachitectural and myeloarchitectural views. However, the works based on profiles usually do not employ information about the distribution and organization at cellular-level, including the properties of individual cells. They are rather concerned with tissue features on a coarser scale, like variations in in image intensity or percentage of cellular bodies that cover a predefined areas in a mesh. Traverses across the cortex, perpendicular to the layers, measure the changes in gray level index (GLI), which is often obtained either by smoothing the image or measuring averages in pixel densities in small image frames. GLI-based approach does not take into account the variation in individual cell density and size. For instance, regions of many smaller cells will be characterized similarly to regions of sparser but larger cells. Authors in [61] use *cluster analysis* to separate adjacent brain areas by identifying regions with homogeneous properties of these traverses. An interesting approach that integrates cell features with laminar structure analysis in mouse cortex was recently presented in [70] and [71]. Authors develop several features of automatically segmented neurons and based on variations in cell distribution distinguish between different layers of the cortex, using again the profiles across the cortex. The first approach which does not use the profiling method appeared in 2018 [72], where authors base their analysis of cortical layers of 2-photon images of mouse brain on combining unsupervised and supervised learning. Neurons were automatically detected and measures of individual neurons were made. Combined with texture analysis of the tissue, various combinations of these features were used in hierarchical clustering. The

trend in analysis of laminar structure points to the fact that the methods are becoming more automatized, more detailed, more observer-independent, use large amounts of recently available high resolution data and develop various neurobiological features to use as inputs to machine learning methods.

As early as 1966. researchers claimed that "automation of the acquisition and interpretation of data in microscopy has been a focus of biomedical research for almost a decade" and believed that "many facets of the problem appear to be well within the grasp of present day technology", which led them to a conclusion that "modern large capacity, high speed data facilities at last provide the ability to manipulate the hitherto unmanageable quantities of optical information contained within all but the simplest images" [26]. It may seem surprising, but the researchers have still not dealt with the problem in a way from which a widely used and recognized method would appear. Considerations from previously reviewed methods indicate that no satisfactory results for automatic neuron segmentation and counting, or segmentation of cortical layers, exist. It is also noticeable that even recent techniques that employ very sophisticated methods like machine learning or deep learning do not achieve very high accuracy.

1.2 Thesis objectives

Brain tissue forms complex structures whose organization and distribution may be reliably revealed only using systematic computational approach. Today some analyses may be done using available image analysis software, for example Adobe Photoshop, ImageJ [73], and others, but most analysis in histology is not automatized and remains semiquantitative with great involvement of the investigator performing the analysis. The amounts of certain cell types or cell densities may be described as low, medium or high, or visually estimated as approximate of total population in intervals $< 25\%$, $25 - 50\%$ or $> 50\%$. This type of analysis may not be accurate enough or reveal enough information about the structure of the tissue. Automatic methods are still struggling to provide satisfactory results. Most methods are highly depending on setting the right parameters which are often hard to interpret and are obtained by empirical methods and systematic testing.

The objective of this research is development of computational methods for automatic and objective analysis of histological images of human brain suitable for advanced and fast analysis of brain cytoarchitecture and laminar structure. An integrated approach was developed, which combines quantitative analysis of neuronal distributions with exploration of underlying principles of variation that facilitate parcellation of cortical layers. The methods were developed aiming for a completely data-driven approach, with as little assumptions about the data as possible.

For the purpose of realization of basic goals of this doctoral research, results of the con-

ducted investigations shed light on the following questions:

1. Is it possible to model the method of neuronal staining and develop an image analysis method that can enable faster, more accurate, and more reliable localization of neurons, and that is completely automated and observer-independent?
2. Can the information from the properties of individual neurons like their body size, orientation, class or density distribution be used for developing more complex image features that may lead to segmentation of larger structures like cortical layers and areas?
3. To which extent are human investigators able to similarly recognize cytoarchitectural elements, or what is the amount of inter-rater variability?

1.3 Structure of the thesis

This thesis is structured through six chapters. In this, Chapter 1, the context of the research is given within which objectives of the research are stated, with emphasis on challenges in quantitative methods for neuron detection and segmentation of layers in laminar structure of the brain, which is the main focus of research in this doctoral thesis. After the initial introduction and mention of some historical findings, outline of state-of-the-art of research conducted in histological image processing and analysis is given.

Chapter 2 provides details about the data used in this doctoral research and the unique database of manually labeled neurons and cortical layers produced as the result of this research. Background information about histological imaging is given and steps used in producing such an image are described. Further, details about image datasets of neurons and layers are presented, as well as procedures and specialized software developed for obtaining the manual labels provided by neuroanatomists.

In Chapter 3, a new method for automatic detection of neurons in histological sections of the human brain cortex is presented. Details of image acquisition and processing is described, as well as performance analysis of three investigators who conducted manual localization of neurons in the histological images. A partial differential equation (PDE) which was used to model the variations in histological image contrast is the key element in this approach. Application of the PDE in the discrete context of digital images is described with some of its theoretical properties. A performance of the automatic method is given, which confirms that the results of the method are indistinguishable from those of human investigators'. Finally, the developed method is applied on whole histological sections and density map on data from BigBrain [21] is developed.

A movement from two-dimensional to three-dimensional neuron localization is presented in Chapter 4. Third spatial dimension is inferred from histological sections digitized in multiple planes along the z-axis. Individual neurons are tracked throughout the depth of the whole image

stack and placed at the appropriate z-level in the stack based on variations in image sharpness. Differences between confocal and bright-field microscopy imaging and methods to process such images are discussed.

Chapter 5 presented a novel framework for analysis of laminar structure of the cortex and classification of neurons according to their position within the laminar structure of the brain. From the location and basic measures of neurons, more complex features were developed for use in machine learning models. Tree ensembles, as today's one of the most powerful and interpretable models, were used on data manually labeled by three human experts. This approach synthesizes several results from this thesis in a new approach that aims to describe variations in laminar structure through substantial and elaborate set of quantitative measurements both used in the literature and developed in this thesis. Analysis of ability of human investigators to manually delineate boundaries in laminar structure is given.

In the final, Chapter 6, the conclusion of the thesis is given, with reflections on the achieved contributions and possible guidelines for future research.

Chapter 2

Framework for Development and Validation of Neuron Detection and Cortical Layer Segmentation

Since the establishment of cell theory in early 19th century, microscopy has had an important role in life sciences. Scientists made many discoveries observing and studying tissues and cells, fundamental building units of life. In this thesis, we are interested in the tissue of the human brain cortex and a specific type of cells - the neurons. In this chapter we present background information about histology and give more details about the brain organization and visualization of its cytoarchitecture using histological methods.

Histology, or also *microanatomy*, is the study of the microscopic structure of tissues and cells as well as structural and functional relationships between individual components. Histological studies are conducted by obtaining the tissue and preparing it for examination under the microscope. Histology has a key role in biomedical sciences, providing insight into both biochemical and molecular processes on one side, and pathological processes and their effect on the other. The study of diseased tissue is known as *histopathology*, and is an important tool for determining precise diagnosis of tissue processes in clinical practice.

Modern histology and histopathology studies have been significantly advanced by the introduction of computational methods, including image processing methods, experimental design, statistics, modeling and other. This has led to current emergence of research fields like computational histology or computational pathology [59] that provide automatized pipelines for processing of histological data.

2.1 Histology and imaging

Images of brain histology are not easily acquired, requiring several steps in tissue processing in obtaining the brain and preparing it for inspection under microscope or digitization using specialized scanners. Here we give a short outline of these steps, important for understanding the nature of the data we are working with in this doctoral research.

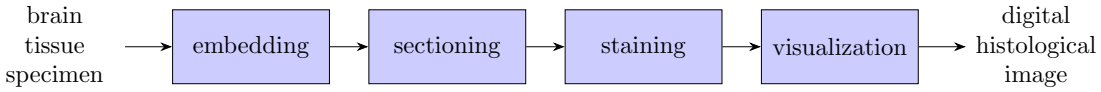

Figure 2.1: Pipeline of the process of obtaining digital histological image.

2.1.1 Specimen preparation

The very first step in histological study is the preparation of the obtained tissue. In brain histology, specimens are usually collected *post mortem*. The whole brain is extracted from the skull and prepared for sectioning using various chemicals. Separate parts are then cut into blocks and a tissue of interest is preserved using chemical fixatives. These blocks may be embedded into paraffin or frozen before they are further sectioned, or cut into very thin slices using precise tools like microtomes, which operate like a deli slicer. These tools may produce sections much thinner than a human hair. Lateral resolution, or thickness, of such sections of neural tissue may be as low as $20-30$nm [74]. However, sections are usually cut about $1-50\mu$m thin, and some older celloidin specimens up to 100μm [75].

Sections of brain tissue inherently have very little variation in colors/shades and are nearly invisible under a light microscope. To enhance inherently small visual contrast in such sections and highlight features of interest they are treated with various stains or dyes. Today, there exist many types of stains used for different purposes of histological research. One of the common method is NeuN (Neuronal Nuclei) [76], an immunohistochemistry method which indicates the neuronal cell bodies in histological preparations. Sections used in this doctoral research are mainly stained by this method. NeuN protein is nuclear, RNA-binding protein which regulates alternative splicing in neurons and is specifically expressed in all neurons with the exception of cerebellar Purkinje cells and Golgi cells, olfactory Mitral cells, retinal photo-receptors and gamma motor neurons [77], [78]. Therefore it allows for clearly visualization of the neurons and their distribution across the whole section of the brain, providing sufficient contrast between the cells and the background, which was the reason we used it in this research.

After staining, the thin sections are mounted on a glass slide and ready for examination under the microscope. This is a sensitive manual step where filigree precision is required, as

inadequate handling of thin slices may lead to tissue tearing or folding, which in turn produces artefacts and misinterpretations of structures in final visual representation and analysis of the slide.

2.1.2 Bright-field and confocal imaging

Most of today's histological slides are examined using bright-field (non-confocal) imaging, because of the compatibility with the histological staining methods used in slide preparation. In these methods, a histological slide being examined is homogeneously illuminated with the background light and captured through the lens of a microscope. Stained neurons absorb the light and are shown as areas of dark contrast on a brighter background. This microscopy modality is also referred to as trans-illumination or transmitted light microscopy [79]. This terminology is often closely used with the terms whole slide imaging (WSI), or sometimes wide-field microscopy because of the whole slide being illuminated (Fig. 2.2). The limitation of this modality for 3D analysis of cellular locations is the presence of background signal from out-of-focus structures throughout the slide. To determine an accurate 3D depth of a neuron in the tissue, a researcher relies on subtle adjustments in focusing using finely-tuned focusing wheels while observing the individual neurons under the lens of a microscope, which is very slow and time consuming.

In confocal imaging, a tissue section is stained using fluorescent dyes that emit light under excitation by laser units located within the confocal microscope. The emitted light is captured using a light-sensitive camera and the image is formed. Using precisely focused laser beams, which are spatially filtered through a pinhole aperture, it is possible to obtain a signal from a single focal plane, hence the name *confocal*. By creating z-series through the depth of the tissue it is possible to reconstruct cells in the tissue. Confocal imaging produces tomography-style cellular imaging data that provide richer information about 3D neuronal structures, with less noise from background and out-of-focus structures. There are successful methods for cell tracking and reconstruction that consider the context of neuron imaging in 3D using confocal or other similar imaging modalities [81, 82, 83]. However, due to the nature of fluorescent dyes, confocal preparations suffer from photobleaching and photodamage and are viable only for a limited amount of time. Also, they are not appropriate for whole slide imaging as the image capturing field is very narrow, but are rather used in detailed analysis of smaller structures like dendritic spines and axonal arborization.

In this doctoral research, we focused our investigation to bright-field microscopy. In chapter 4 we explore in more detail the possibilities of 3D context in bright-field images and present a method for inferring the depth of neurons found in such histological sections of the brain, digitized at high resolution in multiple planes along the slide thickness, the z-axis.

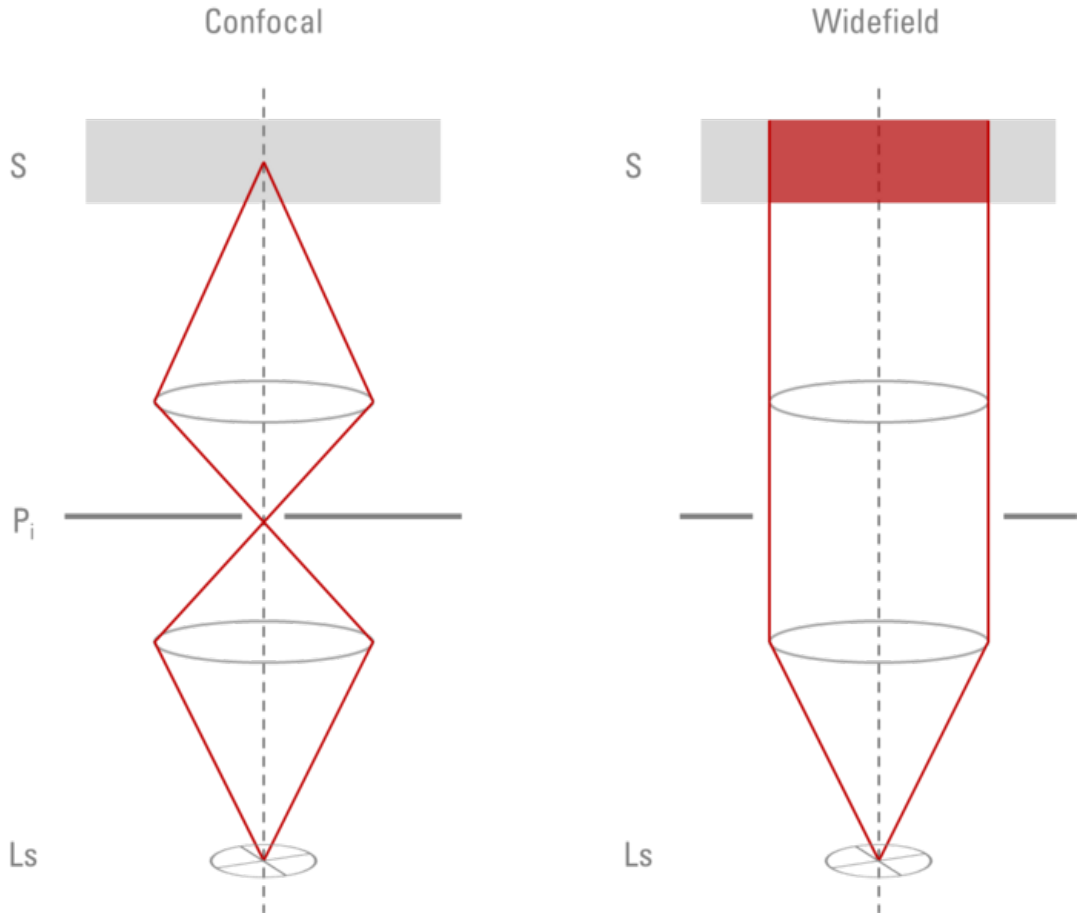

Figure 2.2: Confocal and wide-field microscopy. In confocal imaging, light from the source (Ls) is focused through a pinhole (Pi) and subsequently into the sample (S) resulting in a relatively small volume being observed. In wide-field imaging, histological slide being examined is homogeneously illuminated with the background light. Image reproduced from [80].

2.1.3 Digital histological images

Final step in obtaining digital images in histology is the use of specializes, high-resolution scanners in which glass slides are placed and the image is acquired using the microscope built in the scanner. Digitizing histological sections allows for easier examination, panning, storage and sharing of such images. But above all the greatest endowment of the field is achieved by the possibility to process and analyze histological images using vast amount of modern computing capacities, both from technical and theoretical aspects. Today's whole-slide scanners provide rapid digitization of slides in very high resolution. For instance, it is common to obtain digital images at $40\times$ magnification with about 0.25μm/pixel resolution. This yields files several gigabytes or tens of gigabytes in size, but which are still more convenient to handle than physical glass slides which may be lost or broken, and which fade with time. Digitized images are also often used by neuroanatomists with aid of computer-assisted methods which make manual quantitative analysis a lot easier. Locations of neurons or borders between cortical layers obtained from such manual labeling may be saved and overlayed over the original image.

2.1.4 Sources of variability

There are three main sources of variability in histological image processing and analysis of histological data. *Biological* or *anatomical variability* is a result of normal variability in brain organization among the individuals and in different areas of the brain. The second source is *technical variability*, which is a result of the ways sections are handled and digitized, resulting in slightly different appearance between the slides or even in different areas of the same histological slide. *Inter-observer variability* comes from different interpretation of cytoarchitectural elements present in the histological image examined by neuroanatomists. This is perhaps the most challenging obstacle in development of automatic methods in digital histology, as it puts into question the validity of ground truth used in most learning based methods, as discussed in section 1.1. In this doctoral thesis we explore and measure inter- and intra-observer variability using manually labeled images. We have acquired and developed our methods on different histological slides, parts of which were labeled by three experts in histology and human brain cytoarchitecture which provided locations of neurons and delineated borders between cortical layers.

2.2 Manually labeled histological images

Focus of this thesis is cortical cytoarchitectonics, whose key elements are neurons and their laminar distribution. To reveal cellular organization in the tissue, neuronal staining is used to highlight cells in the tissue. However, we did not find adequate database of manually labeled neurons or manually delineated cortical layers on such images. Therefore we developed our own which was used for development of methods in this doctoral research, and which is also made freely available to the scientific community to study and use, and develop and compare other methods suitable for analysis of brain cytoarchitectonics. Histological slides were obtained from Zagreb Brain Collection[84] at Croatian Institute for Brain Research (CIBR), where they were also digitized using Hamamatsu Nanozoomer 2.0 (Hamamatsu Photonics, Japan) scanner, at 40x magnification, which corresponds to 0.226μm/pixel resolution. This scanner produces images several gigabytes large in proprietary NDPI format (more in [85] and [86]). To extract and convert images to conventional formats we used NDPITools software [87].

For creating manually labeled datasets, in this doctoral research we included experts from CIBR and Montreal Neurological Institute (MNI). The experts who performed manual labeling of neurons and delineation of cortical layers have years of experience in neuroanatomy, cytoarchitecture and histological methods. For easier and faster neuron labeling, a specialized software was developed. As mentioned earlier, we used histological preparations dyed with NeuN stain, a neuronal marker that indicates neuron bodies in the tissue. For both neuron detection and layer segmentation method we used images obtained from thinner (10μm) and thicker

(20μm) histological sections to investigate the performance of both the automatic methods and human experts, across all cortical layers.

2.2.1 Software developed for manual labeling

For easier acquisition of manually annotated locations of neurons, a specialized software was developed, which provided efficient and intuitive interface for raters. This software, named *NeuronSelect* and developed in C#, provided capacity to label locations of neurons and later store, load or modify them. The interface, shown in Fig 2.3, also allows for assigning classes to individual neurons, whether to distinguish between correctly/incorrectly labeled ones, or for selecting between neuron classes in anatomical sense.

Figure 2.3: An interface for manual localization of neurons. This interface is a part of the *NeuronSelect* software developed as a support for easier manual labeling and storage of neuron locations and their classes.

For faster manual classification of neurons, another program was developed which enables raters to focus on individual neurons and label them according to their classes, or to identify image patches that were incorrectly recognized as neurons in the histological image. The program named *Neuron labeler* provides a simple and intuitive interface for the raters, who are able to select between four classes: pyramidal, non-pyramidal, uncertain/unknown and non-neuron. Labels created this was can be saved and also loaded into the program, so the rater performing the manual classification can easily pause and continue the task when preferred. After selecting an appropriate class for the neuron shown, the program automatically switches to next image patch. Neurons shown in images used in our experiments were first automatically detected us-

ing the method described in 3, after which a smaller image patch 128×128 pixels in size was cropped from the larger histological image. This software is also freely available as a part of the framework for development of evaluation of automatic methods on our histological data.

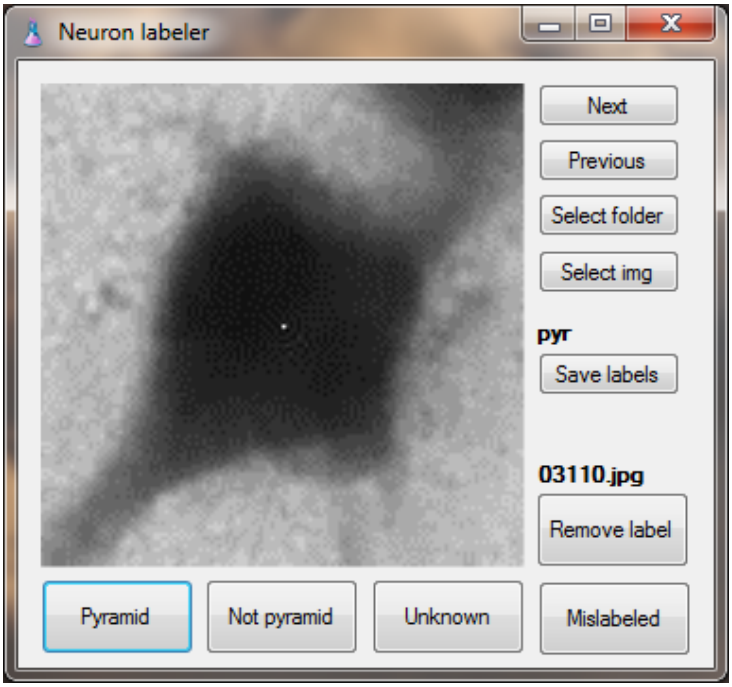

Figure 2.4: Manual classification of neurons was done using software we developed for that purpose. It provides a simple and intuitive interface through which experts can focus on individual neurons and label them according to their classes, or to identify image patches that were incorrectly recognized as neurons in the histological image.

2.2.2 Database of manually labeled neurons

To obtain more reliable results and to better understand the process of manual labeling, we obtained labels for neuron locations on histological images from three raters. Throughout this thesis, we will consistently refer to them as Rater 1 (R_1), Rater 2 (R_2) and Rater 3 (R_3). Rater 1 was given a repeated dataset for measurement of intra-rater variability. This rater also assessed the performance of output of the automatic method in chapter 3.

Data overview and variability assessment

Database of manually labeled neurons is divided in three parts, according to the purpose and acquisition procedure: (I) thin tissue neurons, (II) thick tissue neurons and (III) repeated measurement. An important observation to be made here regarding tissue sectioning is that long apical shafts of neurons are visible, indicating that the section has been cut at reasonably perpendicular angle to allow studying anatomical changes through the layers without introducing

undesirable effects of oblique slicing. The apical dendrites are especially observable for thin tissue (Fig. 2.6), and slightly less but still apparent for thick tissue (Fig. 2.8).

To assess the variability between the raters, a method was developed that uses locations of neurons provided by the raters. Since raters, hovering the mouse pointer over histological image shown on the screen, did not click on the same pixel for each neurons, combining their results is not straightforward. Moreover, not only did they not click on the same pixel, it was often the case that manual labels were found even outside dark area of the neuron body. Using spatial information from label coordinates the method creates clusters based on closeness of the locations indicated by the raters. The same approach was used for measuring the performance of the automatic method developed in Ch. 3. Neuron coordinates from our automatic method's output were added as fourth rater, and compared against human raters. Results of this analysis are shown in Table 3.1. The method for comparison of raters, as well as comparison of raters with an automatic method are a part of the neuron detection database and one of the results of this doctoral research.

(I) Thin tissue neurons. We have extracted 10 images from across all cortical layers of human adult orbitofrontal cortex, which were then labeled by the three raters. These images contained approximately 600 neurons. However, raters counted different numbers of neurons, and sometimes did not agree on what is recognized as a neuron. The inter-rater variability overview is shown in Fig 2.5 and an example of thin tissue section on Fig. 2.6.

Rater 1	Rater 2	Rater 3	
+			34 (5,0%)
	+		16 (2,4%)
		+	23 (3,4%)
+	+		14 (2,1%)
+		+	21 (3,1%)
	+	+	25 (3,7%)
+	+	+	543 (80,3%)
623	598	601	

(a)

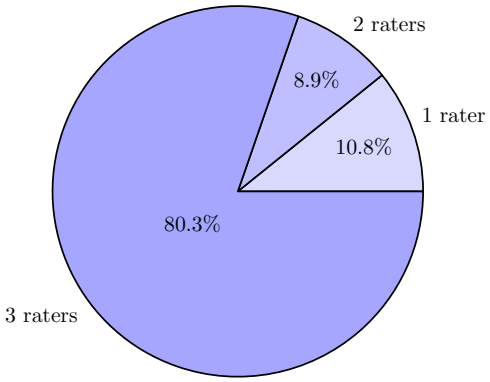

(b)

Figure 2.5: Inter-rater variability for thin sections.

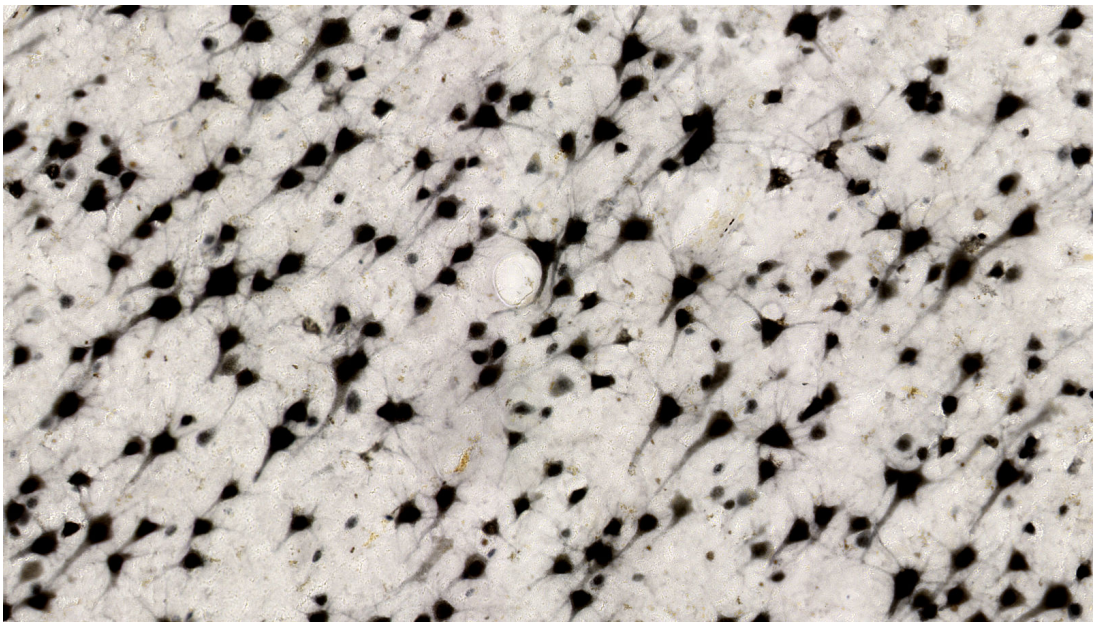

Figure 2.6: Example of digital histological image of tissue sliced at 10μm (thin section).

(II) Thick tissue neurons. Like for the thin sections, we extracted 10 images that included all cortical layers the cortex, which were again labeled by the three raters. These images contained more neurons than thin section, approximately 3000. Due to greater density and more overlapping neurons, there are more cases which were labeled differently among the raters. Inter-rater variability overview for images of thick tissue is shown in Fig 2.7.

Rater 1	Rater 2	Rater 3	
+			279 (7,8%)
	+		253 (7,1%)
		+	159 (4,4%)
+	+		135 (3,8%)
+		+	151 (4,2%)
	+	+	297 (8,3%)
+	+	+	2303 (64,4%)
3030	2988	2748	

(a)

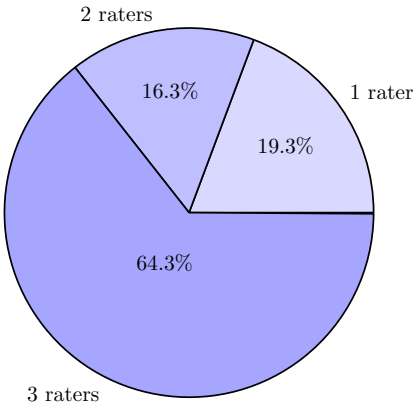

(b)

Figure 2.7: Inter-rater variability for thick sections.

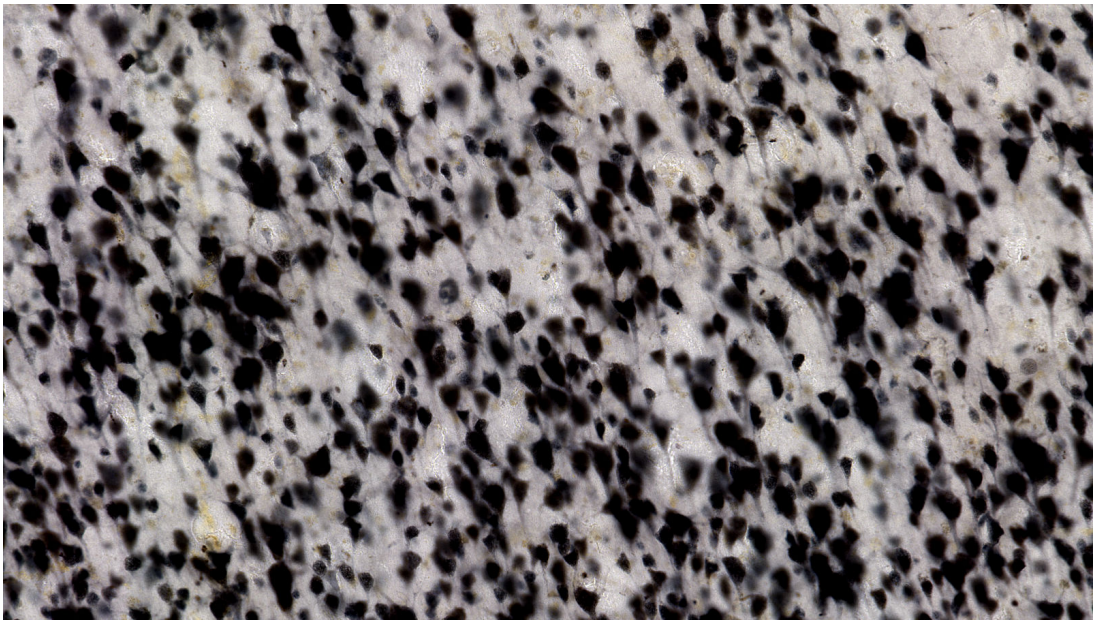

Figure 2.8: Example of digital histological image of tissue sliced at 20μm (thick section).

(III) Repeated labeling - intra-rater variability. We chose 10 images that were manually labeled by Rater 1, and the same dataset was given to the rater after a six month time interval. As expected, the rater did not labeled all neurons the same in both trials. In second labeling Rater 1 agreed with himself in only $81,41\%$ cases. Total number of neurons counted also differed - Rater 1 counted 602 in first and 588 neurons in second trial. An example of intra-rater variability in manual labeling of histological images is shown in Fig. 2.9.

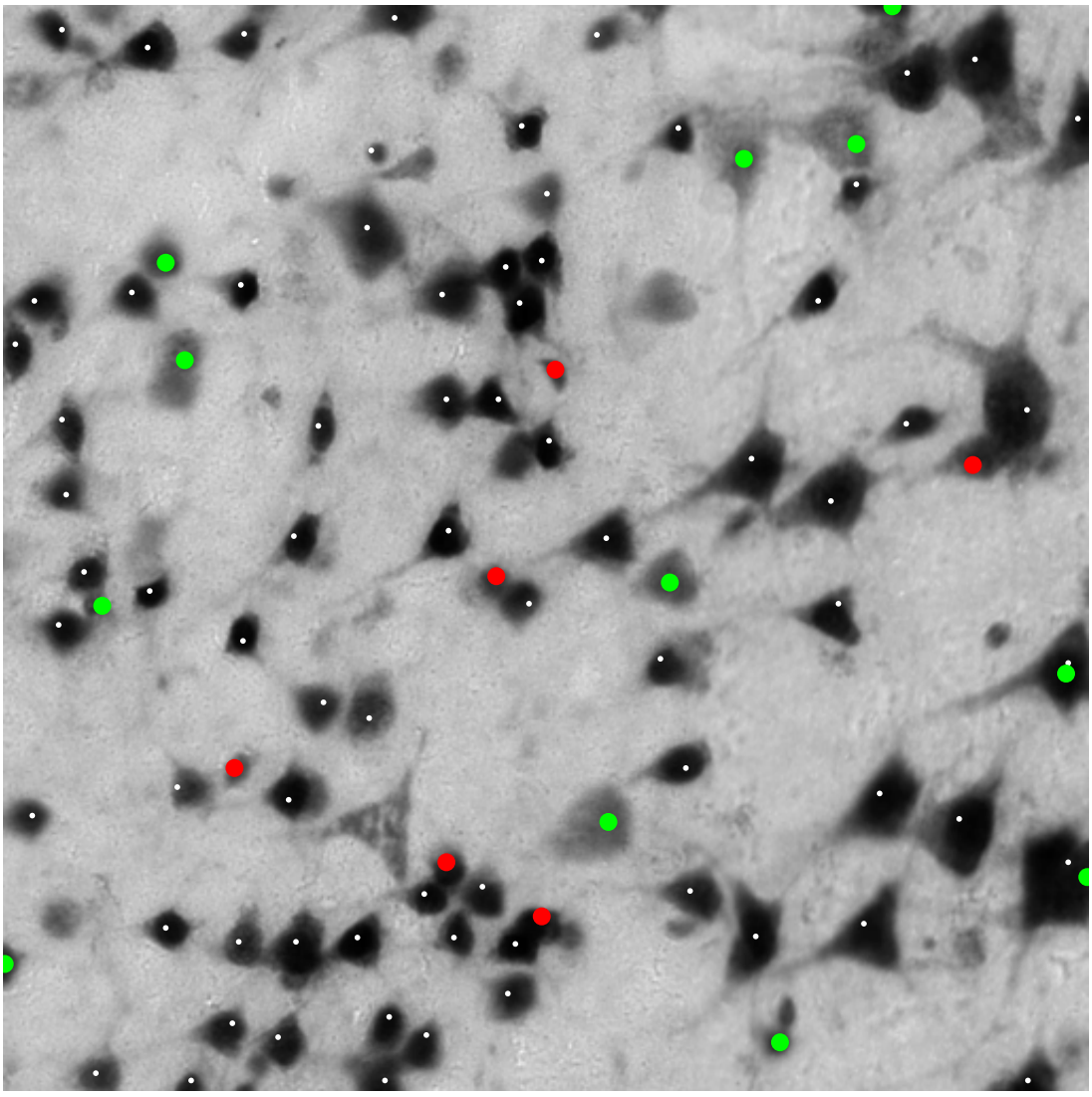

Figure 2.9: Example of intra-rater variability between two trials of manual labeling. The same rater labeled some neurons only in first (red), and some only in second (green) trial of manual labeling. White points indicate neurons labeled in both trials.

2.2.3 Database of manually labeled cortical layers

Similarly as for database of manually labeled neurons, the database of manually labeled cortical layers is divided in two parts, according to tissue thickness: (I) thin tissue preparations and (II) thick tissue preparations. On both, the cortical layers were manually segmented by three experts, who delineated borders between the layers. The delineations as well as experts' inter-rater agreement is shown below. The agreement was measured as percentage of overlapping regions, or intersection over union for all three raters and between each pair of raters. One can observe significant disagreement between the raters, which is not unexpected. The area of layers II and IV have particularly low average overlap. However, these layers anatomically have smaller area than others, so differences in delineation of their boundaries have stronger impact in lower rater agreement than in other layers.

(I) Thin tissue cortical layers. Manual delineations of cortical layers by the three raters for thin tissue section are shown in the Fig. 2.10. Their agreement is quantitatively measured as percentage of overlap of regions for each layer they segmented, as shown in Table 2.1. The sectioned tissue was part of adult *gyrus rectus*, and total area of the manually labeled image was 24,15mm^2.

Table 2.1: Overlapping of cortical layers obtained from manual layer segmentation by three experts (thin section).

	Overlap (%) between the raters				
Layer	All 3	R1&R2	R1&R3	R2&R3	Average
I	89,52	92,17	92,92	93,56	92,88
II	27,86	67,35	36,41	31,68	45,15
III	62,87	84,74	71,48	66,76	74,33
IV	8,60	11,78	55,26	20,30	29,11
V	41,62	63,25	61,05	46,36	56,89
VI	63,84	69,06	84,66	68,66	74,13

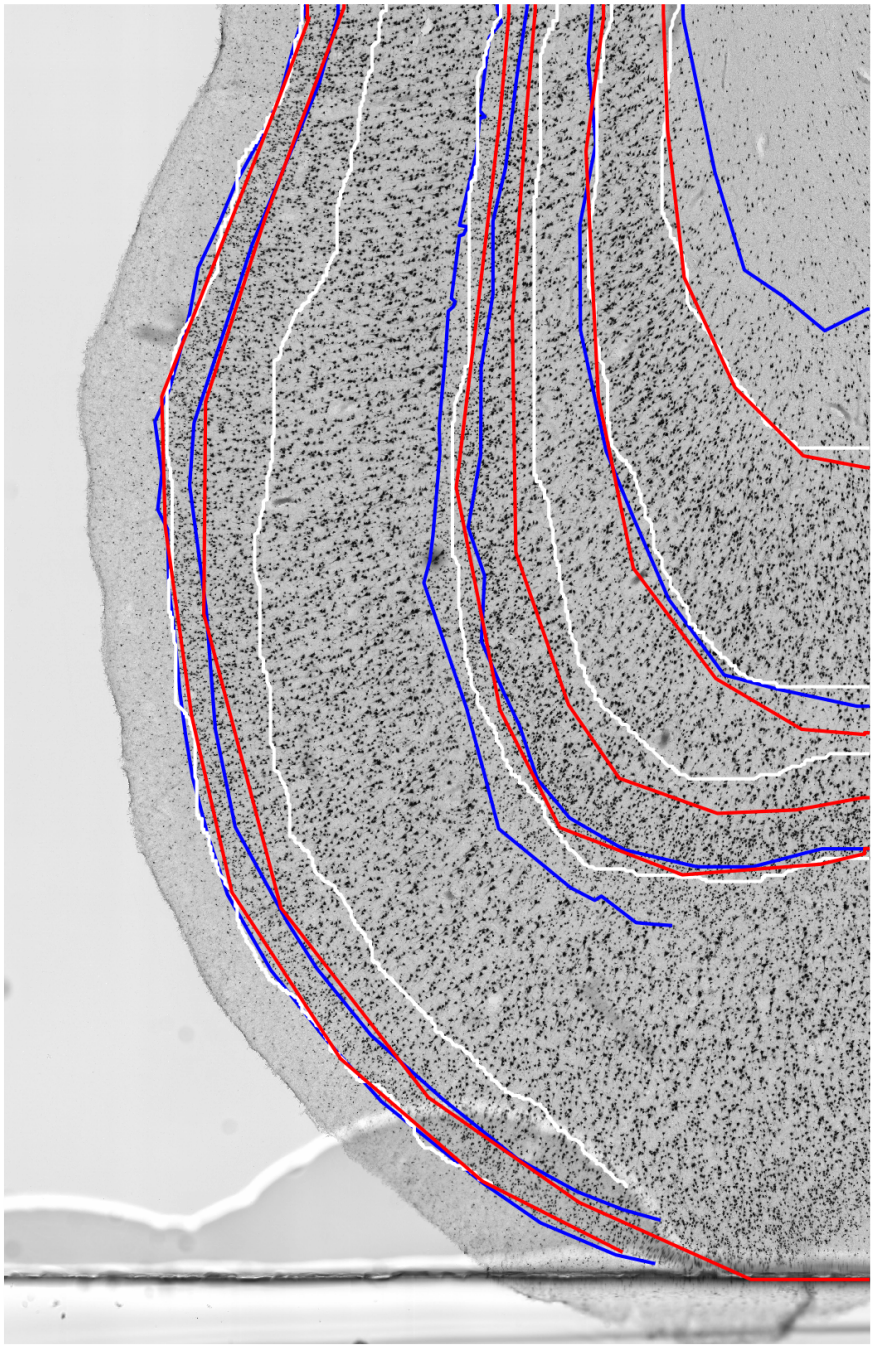

Figure 2.10: Manual labels of cortical layers by three experts (thin section).

(II) Thick tissue cortical layers. Manual delineations for thin tissue section are shown in the Fig. 2.11. The agreement is quantitatively measured the same as for the thin section, as percentage of overlap of regions for each layer they segmented, and shown in Table 2.2. This tissue was part of adult *motor cortex*, with total area of 7,4mm^2.

Table 2.2: Overlapping of cortical layers obtained from manual layer segmentation by three experts (thick section).

	Overlap (%) between the raters				
Layer	All 3	R1&R2	R1&R3	R2&R3	Average
I	89,58	92,52	94,65	91,62	92,93
II	29,77	62,27	44,36	32,21	46,28
III	63,55	90,86	69,80	63,67	74,78
IV	24,58	57,85	44,20	26,13	42,73
V	79,31	89,36	84,80	83,12	85,76
VI	56,78	59,68	69,54	78,04	69,09

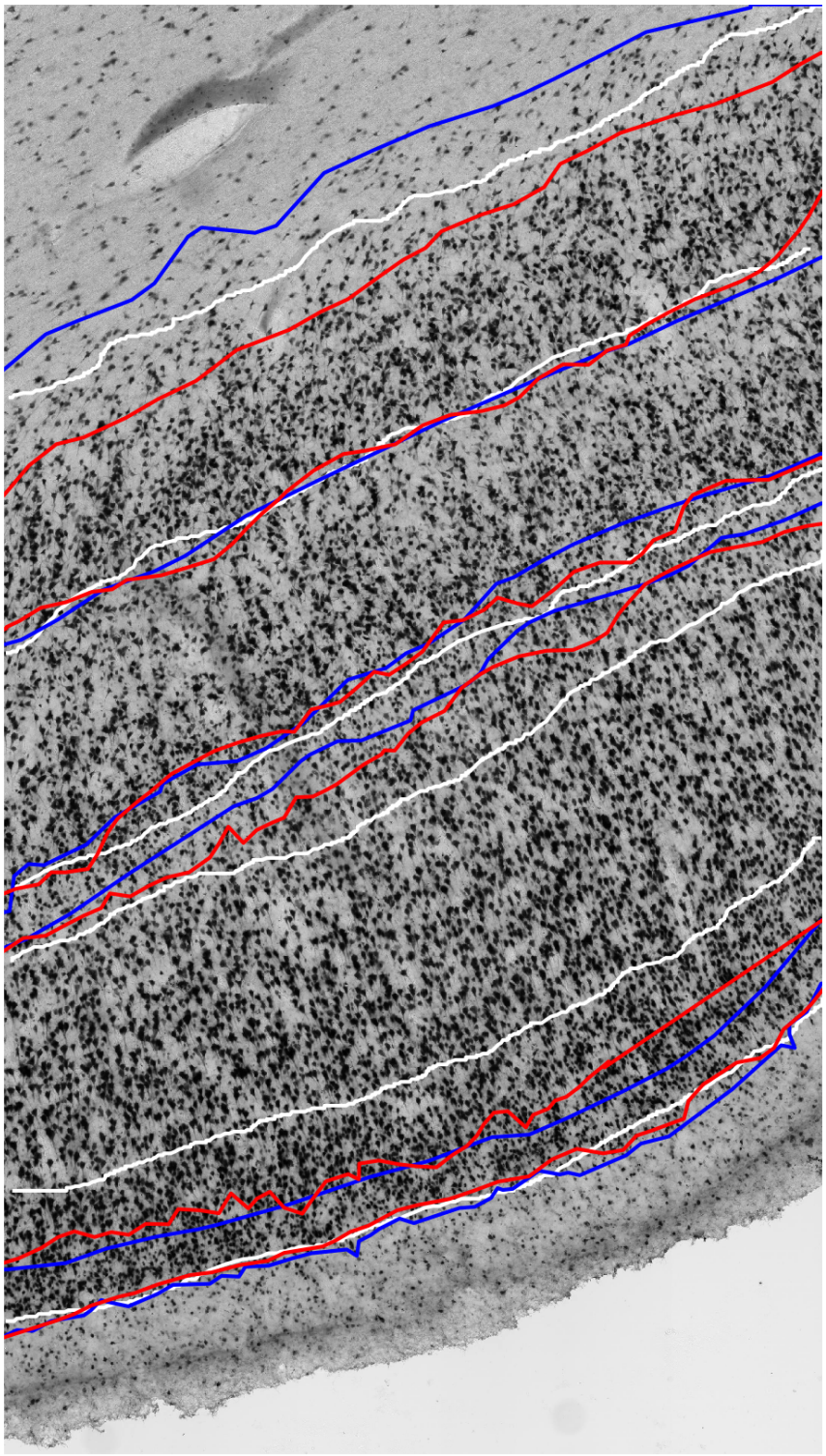

Figure 2.11: Manual labels of cortical layers by three experts (thick section).

Chapter 3

Automatic Detection of Neurons in NeuN-stained Histological Images of Human Brain

This chapter describes a method for automatic detection of neurons in NeuN-stained histological images of human brain [88] that was developed as a part of this doctoral research. The anisotropic diffusion is modeled using a partial differential equation (PDE) and is applied to high resolution microscopy images of the brain in order to detect neurons. We also present a novel approach for PDE-model parameter optimization. Due to the issue of inter-observer variability, three human experts have manually annotated neurons in the image dataset on which the proposed method was trained. We show that proposed method's performance is equal to that of human experts. Moreover, the proposed automatic method provides consistent and reproducible results on all sections and is much faster than human raters or other automatic methods. Additionally, the proposed method's output was verified by a human expert and has correctly distinguished over 95% of neurons in the test images.

3.1 Neuron Quantification

Many neurological and psychiatric diseases cause changes in the number and density of neurons in the brain. These changes are often subtle and can only be proven by quantification [14, 15, 16]. Currently, neuron counting is done manually based on sparse sampling methods such as stereology [89], [90], during which only a small sample of neurons is marked and counted, and the total number is estimated with large errors. This approach has several shortcomings. The process of manual counting is tedious, repetitive, uses a vast amount of time and requires expertise in the field of neuroanatomy and stereology. The fact that there are more than 10^5 neurons in an average section makes the process of precise counting of each neuron

infeasible. Also, researchers doing the counting may have strong biases in recognition of neurons which results in inter- but also intraobserver variability, putting in question validity of the number of counted neurons. Statistical methods for approximation of total number of neurons base the projections on manual counts of small areas which may yield large errors, despite many stereological procedures applied to overcome this issues [91]. The density values are usually reported with accuracy of about 10% [92], but may vary significantly more. For instance, density values reported for primary visual area range from $40,000$ to $80,000$ neurons per mm^3, suggesting to a presence of strong bias in measurements, and differences between some automated methods are reported to be up to 20% [83].

Automatic detection of neurons in histological sections would allow for an objective classification on a large scale, free of human bias, and provide an equivalent analysis on all available preparations. Precise and fast neuron identification across whole sections would enable researchers to identify subtle changes in density between neuron populations in cortical layers and functional subunits, gain better insight in neuron organization and distribution, small network and column formation, delineation of brain area boundaries, and comparison of various pathologies. It would thus significantly improve and speed up quantitative studies in histology.

3.1.1 Histological Imaging

Histological staining is a method used to visualize cells and examine cellular and structural layout of tissue. In this technique, the tissue of interest is preserved using chemical fixatives and sectioned, i.e. cut into very thin sections. Uncolored, these sections inherently have very little variation in colors/shades, so they are treated with various stains to increase the contrast in the tissue. The stained tissue is then mounted on a glass slide and prepared for examination under a classical microscope or to be digitized using a histological scanner.

Some of the most commonly used methods for staining are Nissl method, a classical staining for the cells in brain tissue, and NeuN, an immunohistochemical method which indicates neuronal cell bodies in histological preparations. An example of a histological image is shown in Fig. 3.1.

Both techniques have their advantages and drawbacks. Nissl method is more affordable but stains all cells in the brain tissue, while NeuN method only stains neurons. In our considerations, we decided that the case in which only neurons are visible is more appropriate for the purpose of neuron quantification. After preparation and slicing of the tissue, one may choose to stain only a number of sections with NeuN and use them for neuron quantification and have the other sections stained with more classical staining for other purposes. A work that shows comparison of the two methods is presented in [93].

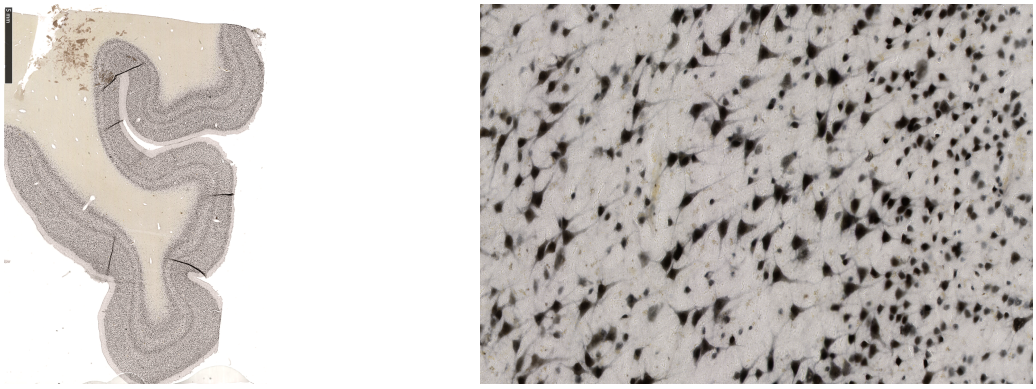

(a) Histological section (b) Magnified (40x) portion with visible individual neurons

Figure 3.1: Example of NeuN-stained histological section under different magnifications. Image on the right hand side is obtained under 40x magnification which corresponds to 0.226μm/pixel resolution.

3.1.2 Related work

Although methods for automatic identification and counting of non-neuronal cells might be successful and in widespread use [94], they are usually based on very basic concepts which are appropriate for detection of regularly shaped (mostly oval-like) objects with distinguishable background, like in [95]. However, as mentioned in chapter 1, cells in brain tissue may form complex, irregular formations where cells are clumped close to one another – these can easily be miscounted as one cell even by a human investigator, which is probably the reason for a lack of accuracy and speed in current automated methods for this task.

It is remarkable that, to the best knowledge of the authors, the first paper published with the focus on automatic neuron segmentation [47] appeared in 2008, and was followed by two papers [83, 96] a year later. We mention and provide a brief outline of some of these related methods.

In [47], the authors introduced an algorithm whose purpose is to obtain coordinates of individual neurons in digitized images of Nissl-stained preparations of the cerebral cortex of the Rhesus monkey. Their approach combined image segmentation and machine learning methods, namely active contour segmentation seeded with use of watershed method for detection of outlines of potential neuron cell bodies and a multilayer perceptron (MLP) containing a single, 4-node hidden layer. The MLP was used to distinguish between neurons and non-neurons based on features derived from the segmentation, such as segment area, optical density, contour gyration and similar. The authors state that their method positively identifies $86 \pm 5\%$ neurons with $15 \pm 8\%$ error (mean $\pm$ SD) on a range of Nissl-stained images at 10x magnification.

In the second article [96], the authors propose a novel multi-layer shape analysis of blobs that are candidates for being identified as neurons. Although not significantly improving in accuracy ($87 \pm 6\%$ positively identified neurons) over the first method, the main segmentation idea is multilevel thresholding and analysis of the obtained level structure for separating neurons

that are closely located. Some shape descriptors for distinguishing neuron bodies from other structures are also used.

We can observe that these methods are not very reliable in terms of accuracy. Probably the biggest challenge are closely located or overlapping neurons that are often identified as a single neuron cell, and shapes too different from predefined oval-like contours that are not being identified as neurons. Present noise and speckles may also cause problems for deformable models [45]. Besides inaccuracy being the obvious shortcoming, the methods suffer from high computational cost - as authors state, it takes days to process a single, medium size section.

Authors in [83] report over 90% detection accuracy on NeuN images of rat cortex using three-step image processing pipeline that includes significant image pre-processing, morphological filtering and finally model-based filtering, with many sub-steps. The last two steps are essential for splitting of closely located neurons, indicating the importance of overcoming this issue in neuron detection. Although more precise than the first two methods, this approach is relatively more computationally expensive - its analysis time is about one fourth of that of the manual effort, thus still taking days or even more than a week, depending on a section size, to process a whole section, with some manual work still included.

3.2 Automatic method for neuron detection

Our aim was to develop a procedure for automatic identification of all neurons visible in the tissue, distinguish neurons from noise and artifacts and separate closely located neurons, doing so in significantly shorter time than humans.

3.2.1 Dataset

For the development and testing of our method, we used histological sections of the adult human prefrontal cortex, stained with NeuN immunohistochemistry method, from the Zagreb Brain Collection [84]. Preparations were digitized using Hamamatsu Nanozoomer 2.0 scanner using a single optical plane at 40x magnification, corresponding to 0.226μm/pixel resolution. Images were acquired using bright-field imaging, a method where a histological slice being examined is homogeneously illuminated with background light and the the image is captured through the lens of the scanner. Here, we do not experience unbalanced illumination across the image as it is the case in, for example, confocal imaging, where the light is emitted from laser-excited cells stained with fluorescent dyes. Because of the size and the special image format of scans produced by the scanner (.ndpi), we exported smaller TIFF tiles using NDPITools software [87], and processed them separately. Tiles had overlapping pixels to account for border effects. We concluded that images of a slightly lower in-plane resolution also yielded satisfying

results. Therefore, we subsampled the original scans by a factor of 2, and used the images at 0.452μm/pixel resolution. This enabled greater processing speed and lower memory load. Further subsampling would result in slight loss of the method's performance. In our experiments we used 10μm thick sections. As shown in section 3.3, it is not easy to measure efficiency of the method because there is no absolute mutual agreement between the experts on what is to be identified as neuron. Some neuron bodies that have low color intensity are considered to be in the tissue of adjacent section, and are not to be counted among the neurons of current section. There is also disagreement between the researchers doing manual counting on some neurons of smaller body size.

Therefore, our goal is to develop a model that agrees with the human experts in the similar fashion as they agree between themselves, i.e. does not differ in neuron identification from human experts more than they mutually differ from each other.

In this task, we are faced with two main challenges - recognize neuron bodies and separate closely located ones. In literature, we usually find two approaches, cell segmentation, for example by thresholding and blob analysis, and cell localization, which means finding a single pixel that represents cell center or *nucleus*, as we do in our approach. One could do this by looking for local minima on the image and identify each that is darker than some predetermined intensity as a neuron center. This indeed very basic idea is fundamental in our approach, especially given the fact that the neurons are most commonly darker in their center due to the dye uptake during staining. However, a single neuron may have many local image intensity minima (noise) that would in this way be identified as multiple neurons. One could process the located minima in a way that those located closely to each other may be combined into a single one. Unfortunately, this approach would often also merge some small neurons; the distance between local minima that may appear in a single neuron might be greater than a few smaller closely located neurons combined.

Although these extra minima are not present due to the noise added during the image acquisition, but are rather inherent by the nature of neuron representation on the stained preparation, we steered our approach inspired by denoising techniques in image processing. Visualizing images of neurons as functions of two variables in 3D (see Fig.3.6), the third dimension being image gray intensity, it seems that cone-like structures of neuronal bodies should be smoothed in some way. For that purpose, we decided to approach the problem of finding neuron cells from a new perspective, one that is not usually seen in literature on this subject, but that seems more natural and is fit for the specific purpose of detecting neurons on a histological preparation. The idea is to capture the diffusive nature of this staining, i.e. dye uptake in the neurons which occurs mostly in the neuron center, since here, NeuN is a neuronal antigen that binds mostly in the neuron nuclei. Therefore, we investigated methods that are inspired by diffusion process and are described by partial differential equations that govern such processes in nature. Some

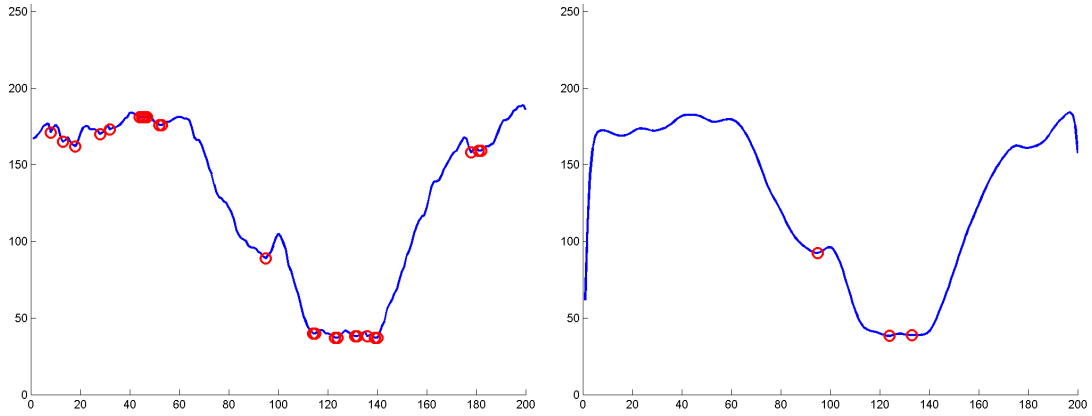

(a) (b)

Figure 3.2: Image gray intensity minima removed by diffusion.

of the methods we considered were shock filtering [97], L0 gradient minimization [98], global image smoothing based on weighted least squares [99], bilateral filtering [100]. Our approach avoids exhaustive preprocessing, complicated pipelines and multiple steps in tissue image processing, such as compensation for artifacts and speckles, noise reduction, background removal and similar, commonly seen in various approaches for cell detection [47, 83, 95, 96].

3.2.2 PDE model

Partial differential equations (PDEs) introduce a new approach to digital image processing. Extensive mathematical results relying on strong theoretical foundations are available and provide stable numerical schemes. Some ad hoc filters that were developed in image processing were later justified by PDE theory [32, 33], which continued to produce new, more efficient filters for various purposes based on studied mathematical properties of these filters. Here, we briefly introduce application of PDEs in the discrete image context.

One well known denoising technique is filtering with a Gaussian kernel with purpose to remove noise and smooth the image. As it can be shown, it is equivalent to applying the heat equation

$$u_t(x,t) = \nabla^2 u(x,t) \tag{3.1}$$

to the image, in terms of its discrete, two-dimensional domain with initial condition being $u_0(x,0) = f(x)$, $x = (x_1,x_2)$ where f is the original image. This is due to the fact that the function

$$\Phi(x,t) = \frac{1}{(4\pi t)^{n/2}} e^{-\frac{|x|^2}{4t}}, x \in \mathbb{R}^n, t > 0 \tag{3.2}$$

is the *fundamental* solution of (3.1). We see that it is the Gaussian function used to construct frames that are convolved with the image. Convolution of initial condition added to (3.1) with

fundamental solution

$$u(x,t) = \int_{\mathbb{R}^n} \Phi(x-y,t)g(y)\,dy = \frac{1}{(4\pi t)^{n/2}} \int_{\mathbb{R}^n} e^{-\frac{|x-y|^2}{4t}} g(y)\,dy\, x \in \mathbb{R}^n, t > 0 \tag{3.3}$$

yields the analytic solution of the appropriate initial problem [101].

Our aim was to exploit properties of PDE based models to *smooth* the extra minima that are present in the neuronal bodies. In the two-dimensional case of processing an image, we use the initial problem

$$\begin{cases} u_t = u_{xx} + u_{yy}, & \Omega \times \langle 0, T \rangle \\ u = I & \Omega \times \{t = 0\} \end{cases} \tag{3.4}$$

with $I = I(x,y)$ representing the image intensity we consider image and Ω being the image domain. We assume Dirichlet boundary condition as we do in our considerations of PDE application on images.

However, this model does not yield the desired results. The image intensities are diffused before the extra minima are removed and during the process neurons with lighter intensities are fused with the image background, due to dissipation of their pixel value intensity, and closely located ones are merged into a single blob. This directs us to modify our approach in a way that we maintain the smoothing effect but preserve contours of neuronal bodies. We wish diffusion to have effect in the regions of neuronal bodies but not to fuse intensities over the neuron edges. Anisotropic diffusion provided satisfying results.

3.2.3 Anisotropic diffusion filtering

We write the equation (3.1) in its divergence form,

$$u_t(x,t) = \nabla^2 u(x,t) = \text{div}\,(\nabla u(x,t)), \tag{3.5}$$

and insert diffusion control function inside the divergence, as authors did for denoising purpose in [102].We obtain

$$\begin{cases} u_t(x,t) = \text{div}\,(g(x,t)\nabla u(x,t)), & \Omega \times \langle 0, T \rangle \\ u(x,0) = I(x) & \Omega \times \{t = 0\} \end{cases} \tag{3.6}$$

known as the Perona-Malik model with usual choice of diffusion function $g(x,t)$ as a monotonically decreasing function of the image gradient magnitude $g(x,t) = f(|\nabla u(x,t)|)$ that inhibits the diffusion effect in image areas with large gradient. This equation has been extensively studied (see, for example [103] and references therein), and important and valuable theoretical

results are available. Most commonly, two diffusion functions are used,

$$g_1(x,t) = \exp\left(-\left(\frac{|\nabla u(x,t)|}{\lambda}\right)^2\right), \tag{3.7}$$

or

$$g_2(x,t) = \frac{1}{1+\left(\frac{|\nabla u(x,t)|}{\lambda}\right)^2}. \tag{3.8}$$

Here, *diffusion constant* or the *flow constant* λ It is a scaling parameter that depends on range of image pixel values. To clarify its effect on the behaviour of the diffusion, we define a flow function

$$\Theta((x,t)) = g((x,t)) \cdot \nabla u(x,t), \tag{3.9}$$

using which we can rewrite 3.6 as

$$u_t(x,t) = \text{div}\,(\Theta(x,t)) \tag{3.10}$$

We will use the Θ function in developing the discretization scheme in the next subsection. Two flow functions that correspond to functions 3.7 and 3.8 are plotted in Fig 3.3. Regarding the function g used in our method, we chose function 3.7 as it favors edge preservation over smoothing, which is imortant for distinguishing between closely located neurons with only a small variation of image intensity between them. It is necessary for the method to be sensitive to such edges which have lower gradient magnitude, and inhibit diffusion effects in those areas.

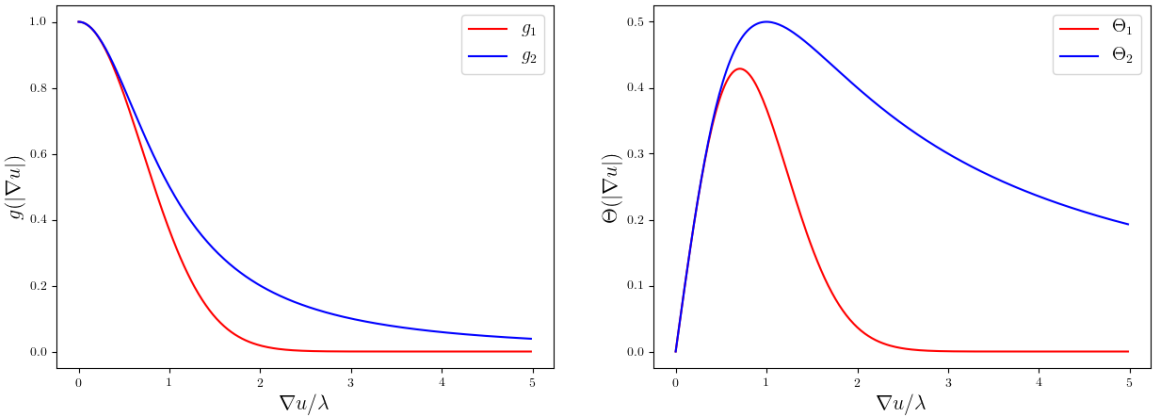

Figure 3.3: Left: Diffusion functions commonly chosen in Perona-Malik equation, plotted as functions of image gradient. Right: Flow functions that correspond to diffusion functions, plotted as functions of image gradient. Maximum flow is generated as the gradient ∇u becomes approximately equal to λ.

One can observe that the maximum flow is generated as the gradient ∇u becomes approximately equal to λ. It tends to decrease to zero when the gradient is moving away from λ, halting

the diffusion at locations of high gradients and in the very homogeneous areas. A proper choice of diffusion constant λ thus has significant impact on the effect of applying the diffusion to the image. The procedure for choosing λ is discussed in subsection 3.2.5.

3.2.4 Discretization and stability analysis

After the analytic considerations, in order to apply the diffusion process governed by 3.6 on the image, the equation is solved numerically through the development of a numerical scheme. The goal is to interpret the continuous initial problem in discreet terms of 2D image. Spatial domain Ω is discretized into a rectangular mesh whose nodes are separated by unit distance in both spatial dimensions, and who correspond to image pixels. This allows the use a 2D image as an initial condition of the PDE 3.6. The equation is then solved iteratively on the discreet domain, with intensity change in one step is defined as the sum of the flow contributions from neighboring node intensities, determined by the flow function $\Theta(x,t)$.

Let us first derive the 1D discretization which will then be generalized to the 2D case. In one dimension, Eq. 3.6 reduces to

$$\frac{\partial}{\partial t}u(x,t) = \frac{\partial}{\partial x}\left(g(x,t)\frac{\partial}{\partial x}u(x,t)\right). \tag{3.11}$$

By taking discreet derivatives of spatial variable we obtain

$$\begin{aligned}\frac{\partial}{\partial t}u(x,t) &\approx \frac{\partial}{\partial x}\left(g(x,t)\frac{1}{\Delta x}\left(u(x+\frac{\Delta x}{2},t)-u(x-\frac{\Delta x}{2},t)\right)\right)\\ &\approx \frac{1}{(\Delta x)^2}\left(g(x+\frac{\Delta x}{2},t)(u(x+\Delta x,t)-u(x,t))-g(x-\frac{\Delta x}{2},t)(u(x,t)-u(x-\Delta x,t))\right)\\ &= \Theta_{\text{right}}+\Theta_{\text{left}} \mid \Delta x = 1\end{aligned} \tag{3.12}$$

Here, the last step is a consequence of

$$g(x,t) = f(|\nabla u(x,t)|) \approx f(\frac{1}{\Delta x}\left|u(x+\frac{\Delta x}{2},t)-u(x-\frac{\Delta x}{2},t)\right|), \tag{3.13}$$

from which is

$$g(x+\frac{\Delta x}{2},t) \approx f(\frac{1}{\Delta x}|u(x+\Delta x,t)-u(x,t)| \tag{3.14}$$

and

$$g(x-\frac{\Delta x}{2},t) \approx f(\frac{1}{\Delta x}|u(x,t)-u(x-\Delta x,t)|. \tag{3.15}$$

In each iteration of this scheme, the values of nodes are updated according to the *flow* contributed from its neighbors 3.12. Visual representation of the flow contribution from two neighboring nodes is shown in Fig. 3.5. By discretizing the time variable

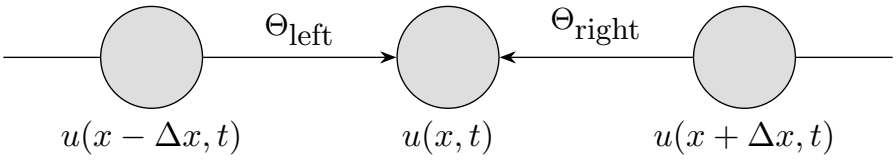

Figure 3.4: Flow contribution from neighboring nodes for one-dimensional case.

$$\frac{\partial}{\partial t}u(x,t) \approx \frac{u(x,t+\Delta t)-u(x,t)}{\Delta t}, \tag{3.16}$$

and using Eq. 3.12 we obtain the final 1D diffusion scheme

$$u(x,t+\Delta t) \approx u(x,t) + \Delta t \left(\Theta_{\text{right}} + \Theta_{\text{left}}\right). \tag{3.17}$$

The ideas from the development of one-dimensional diffusion can easily be carried to the two-dimensional case. Adding an additional spatial variable to 3.11, we write

$$\frac{\partial}{\partial t}u(x,y,t) = \frac{\partial}{\partial x}\left(g(x,y,t)\frac{\partial}{\partial x}u(x,y,t)\right) + \frac{\partial}{\partial y}\left(g(x,y,t)\frac{\partial}{\partial y}u(x,y,t)\right), \tag{3.18}$$

and as in 3.12 have

$$\begin{aligned}
\frac{\partial}{\partial t}u(x,y,t) &\approx \frac{\partial}{\partial x}\left[g(x,y,t)\frac{1}{\Delta x}\left(u(x+\frac{\Delta x}{2},y,t)-u(x-\frac{\Delta x}{2},y,t)\right)\right] + \\
&+ \frac{\partial}{\partial y}\left[g(x,y,t)\frac{1}{\Delta y}\left(u(x,y+\frac{\Delta y}{2},t)-u(x,y-\frac{\Delta y}{2},t)\right)\right] \\
&\approx \frac{1}{(\Delta x)^2}\Big[g(x+\frac{\Delta x}{2},y,t)(u(x+\Delta x,y,t)-u(x,y,t)) \\
&\quad - g(x-\frac{\Delta x}{2},y,t)(u(x,y,t)-u(x-\Delta x,y,t))\Big] + \\
&+ \frac{1}{(\Delta y)^2}\Big[g(x,y+\frac{\Delta y}{2},t)(u(x+\Delta x,y,t)-u(x,y,t)) \\
&\quad - g(x,y-\frac{\Delta y}{2},t)(u(x,y,t)-u(x-\Delta x,y,t))\Big] \\
&= \Theta_{\text{east}} + \Theta_{\text{west}} + \Theta_{\text{north}} + \Theta_{\text{south}} \mid \Delta x = \Delta y = 1
\end{aligned} \tag{3.19}$$

From this, and using time discretization as in 3.17, the two-dimensional iterative scheme is obtained.

$$u(x,y,t+\Delta t) \approx u(x,y,t) + \Delta t \left(\Theta_{\text{e}} + \Theta_{\text{w}} + \Theta_{\text{n}} + \Theta_{\text{s}}\right). \tag{3.20}$$

Again, we visualize the contributions from neighboring nodes in Fig 3.5. For using eight neighbors of each node, i.e. using the flow from diagonal neighbors, one must account for lager relative distance Δd between these nodes and the central node. By this, we obtain the final

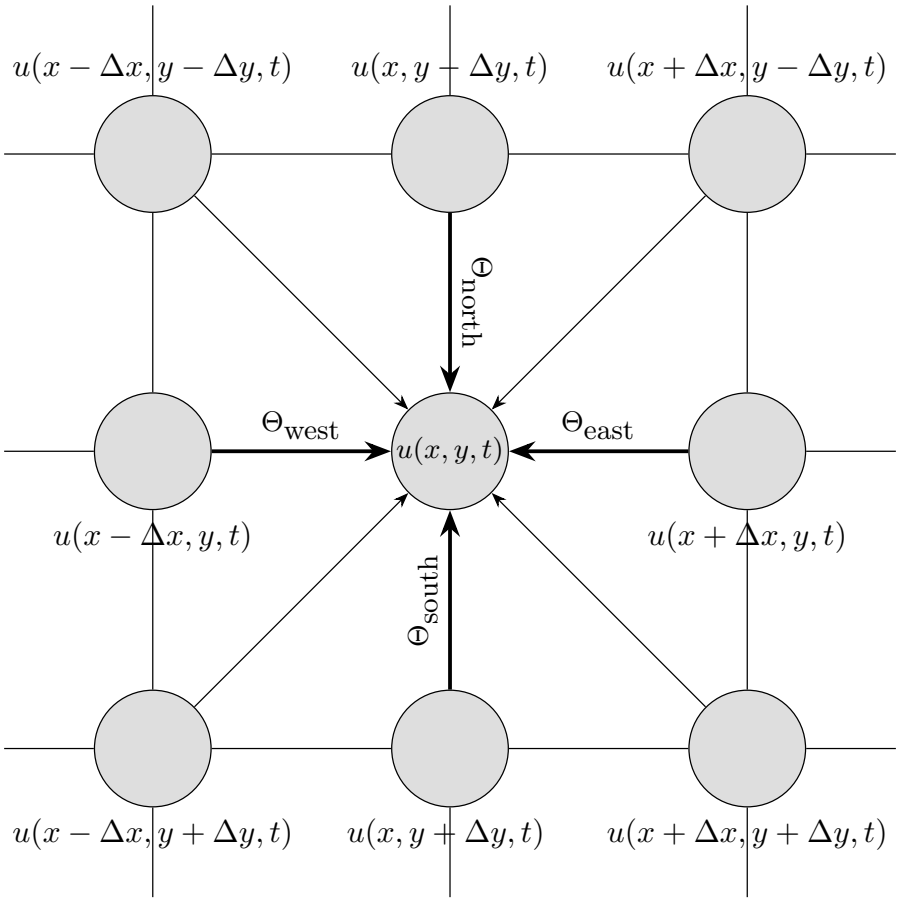

Figure 3.5: Flow contribution from neighboring nodes for two-dimensional case.

scheme used in our method.

$$\begin{aligned} u(x,y,t+\Delta t) &\approx u(x,y,t) + \Delta t \Big[\Theta_{\text{e}} + \Theta_{\text{w}} + \Theta_{\text{n}} + \Theta_{\text{s}} + \\ &+ \frac{1}{(\Delta d)^2}(\Theta_{\text{ne}}(\Delta d) + \Theta_{\text{nw}}(\Delta d) + \Theta_{\text{se}}(\Delta d) + \Theta_{\text{sw}}(\Delta d))\Big] \\ &\approx u(x,y,t) + \Delta t \Big[\Theta_{\text{e}} + \Theta_{\text{w}} + \Theta_{\text{n}} + \Theta_{\text{s}} + \\ &+ \frac{1}{2}(\Theta_{\text{ne}}(\sqrt{2}) + \Theta_{\text{nw}}(\sqrt{2}) + \Theta_{\text{se}}(\sqrt{2}) + \Theta_{\text{sw}}(\sqrt{2}))\Big]. \end{aligned} \tag{3.21}$$

In Eq. 3.6, the diffusivity control function g introduces nonlinearity. However, with its values being between 0 and 1, it does not introduce additional restrictions on the choice of time step Δt for numerical stability in the explicit finite differences discretization scheme we used. There is no lower bound of Δt, but too small value would result in many iterative steps needed to evolve the process. Therefore it is beneficial to know the upper bound. Taking $\Delta x = \Delta y = h$ for discrete derivatives, we show here that for an 8-neighbor scheme, maximum time integration constant is $\Delta t/h^2 = 1/7$ for unit node distance [104]. Using superscript indices for neighboring nodes of the central node u^0 and omitting spatial variables for brevity, we write the discrete

formulation of the diffusion process:

$$\begin{aligned} u(t+\Delta t) &\approx u(t) + \Delta t u_t \\ &= u^0 + \Delta t \sum_{i=1}^{n} g^i (u^i - u^0) \\ &= u^0 \left(1 - \Delta t \sum_{i=1}^{n} g^i\right) + \Delta t \sum_{i=1}^{n} g^i u^i \end{aligned} \tag{3.22}$$

For numerical stability, the weight of the central node must be larger than or equal to the weights of the neighboring nodes [105]:

$$\begin{aligned} 1 - \Delta t \sum_{i=1}^{n} c^i &\geq \Delta t \max(c^i) = \Delta t c \\ \Delta t \left(c + \Delta t \sum_{i=1}^{n}\right) &\leq 1 \\ \Delta t &\leq \frac{1}{c + \sum_{i=1}^{n} c^i} \end{aligned} \tag{3.23}$$

Letting λ to infinity results in maximum blurring and diffusion coefficients equal to one, independent of gradient value

$$\Delta t \leq \frac{1}{1+n},\ c^i = 1,\ i \in \{1, \ldots, n\} \tag{3.24}$$

Equation 3.24 assumes 4 neighbors of u^0 are used. The distance of diagonal nodes from u^0 must be taken into account if we use all adjacent nodes as in Eq. 3.21, which is done by adding a distance factor

$$\Delta t \leq \frac{1}{1 + \sum_{i=1}^{n} \frac{1}{(\Delta d^i)^2}} \tag{3.25}$$

where Δd^i is the distance between the central node u_0 and the node u^i. Diagonal nodes have $\Delta d = \sqrt{2}$ while nearest neighbors have $\Delta d = 1$. For better isotropy, in our method we chose the 8-neighbors variant for which maximum Δt is $1/7$.

For the total time of the integration T in the final neuron detection model, we chose 12 iterations in the discretization process, after the parameter optimization described in section 3.3, resulting in $T = N \times \Delta t = 12 \times 1/7 \times h^2 \approx 1.71h^2$. Again, by letting the scaling factor λ to infinity, we obtain $g = 1$, thus removing the nonlinearity and reducing the Eq. 3.6 to its linear form. We can now relate T to the full width at half maximum (fwhm) for linear case. Using

$$\text{fwhm} = 4\sqrt{T \ln 2}, \tag{3.26}$$

we obtain fwhm $= 4.36h$, which is about one fifth of the diameter of an average neuron, and almost half of the diameter of a smallest interneurons in our images. To use the method on images of another resolution, one should account for the difference in pixel size to preserve the same diffusion properties. Using the Eq. 3.26, we establish relation between number of iteration steps needed in processing of images of different resolution. For a constant fwhm, from Eq. 3.26 one obtains

$$h_1^2 N_1 = h_2^2 N_2, \tag{3.27}$$

h_i being the distance between integration nodes in discretization mesh and N_i being the number of iterations. For example, in images of half the resolution, one should perform one fourth of the number of iterations.

It can be shown that Eq. 3.6 behaves both like a usual diffusion forward, but also backward in time, especially along the high-contrast edges [106]. Backward diffusion is well-known to be highly sensitive to perturbations in the initial data, so one could expect some instabilities in discretization scheme of this is forward-backward parabolic type equation. However, practical implementations of the Perona-Malik equation work satisfactorily, and are not very unstable. Essentially, the only instability observed in numerical schemes is the stair-casing effect, where a smooth step edge develops into piecewise linear segments separated by jumps. More details on this can be found in [107]. Fortunately, this does not influence local minima, so is of no concern to us. The effect of applying the diffusion process on a portion the image containing neurons is shown in Fig. 3.6.

It was shown in [102] that one of the properties of this equation is non-introduction of new extrema, known as minimum-maximum principle. If a point in the processed image is a local minimum at some point in time, it was previously a local minimum in the original image as well. Nevertheless, the equation will eliminate minima that do not differ much in pixel value from pixels in their surrounding or are global in some small vicinity in short time. It will keep minima with larger vicinity for a longer time, which is in our case exactly the desired property. Image noise and fluctuations in pixel values in neurons that come from uneven dye uptake and during image acquisition is smoothed and eliminated, while single local minima per neuron remain and are preserved from being fused together. The implementation and application of the model on the images was done in Python.

3.2.5 Method outline

We use the model to acquire a single local minimum per neuronal body. However, some minima remain in the image outside the neuronal bodies so from the PDE model we obtain *candidates* for neuron locations, some of which must be ruled out by other means.

We first perform selection of candidate points based on their grayscale intensity, level of

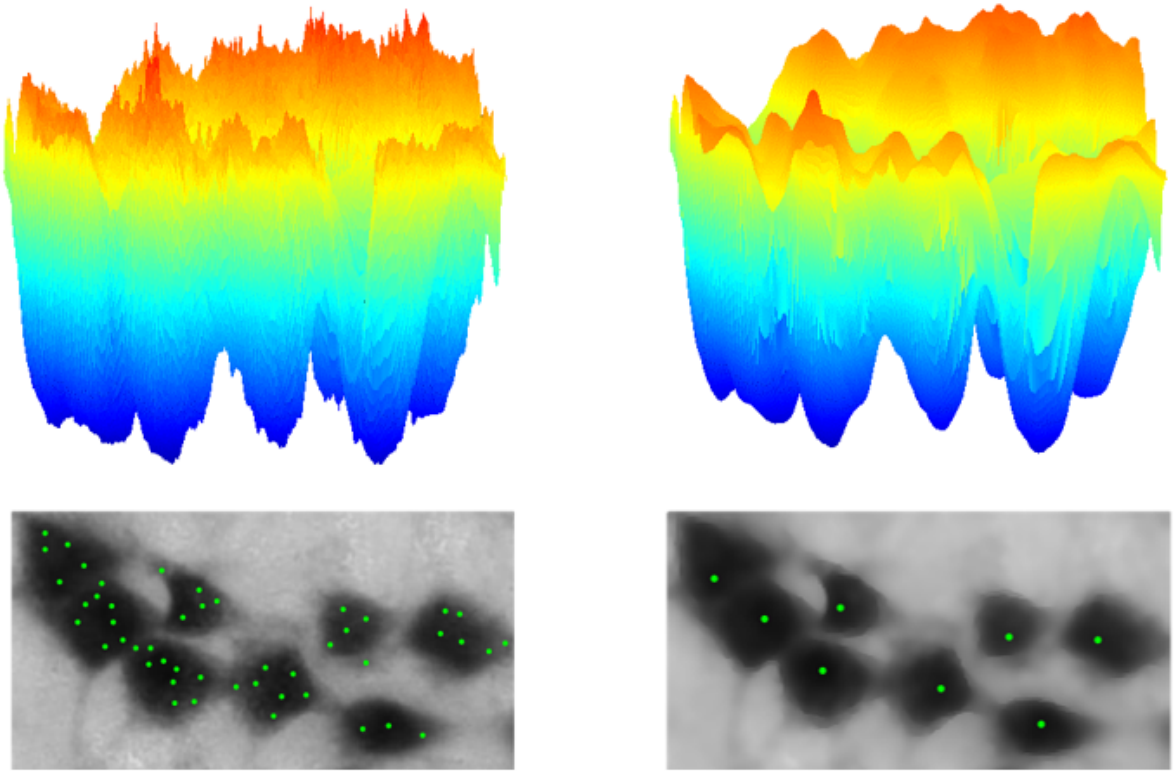

Figure 3.6: Result of processing a histological image patch using Perona-Malik model. On the left-hand side is the original data with visible large local signal variation, resulting in multiple image intensity minima per neuron. After applying the diffusion model, the data is smoother with less local variation, and a single local minima per neuron remains, as shown on the right hand side. *Jet* color map used for better visualization of 2D grayscale data in 3D.

which was derived from the data that was manually labeled by human experts. If a candidate point is brighter than a predefined threshold, it means that it is a point outside a neuron, but is rather being part of the background. Another example are image regions that are a part of a neuron whose main body is located in the next section and is not to be counted among neurons in the current one. Since image may contain noise and artifacts, small but dark objects are possible to appear. To detect minima that are located in such areas we performed image thresholding at above mentioned intensity level. A local minimum that is located in a blob whose area is smaller than the minimum neuron size is also excluded.

There are four parameters used in this method – gray intensity threshold and minimum cell size were derived from measurements made on manually labeled data. Diffusion scaling constant ($\lambda = 11$, for $h = 1$ and image grayscale range $[0, 255]$) in function g and number of iterations ($N = 12$) in numerical scheme were obtained by optimization described in Section 3.3.

3.3 Experimental results and analysis

As mentioned earlier, it is not always clear whether an object in the image should be considered a neuron or not, which is reflected by the presence of variability in manual labeling between the experts. We measured the agreement between two manual labeling results on the same data by dividing the number of neurons in the image that both raters labeled as neurons with number of neurons labeled in total by any rater. In other words, we divided the number of neurons in the intersection with number of neurons in the union of the two raters' labeling output (Jaccard index),

$$J(i,j) = \frac{|i \cap j|}{|i \cup j|} \tag{3.28}$$

The agreement was measured by analysis of dataset that was independently manually labeled by three experts. This dataset consisted of 10 histological images containing over 550 neurons. Those identified by all three experts made 80.33%, identified by two made 8.88%, and those identified by only a single expert made 10.80% of total number of neurons. This results in average pairwise mutual agreement between the raters of $86.88 \pm 0.77\%$. Going through the literature, this amount of error seems reasonable, although is slightly less than the agreement obtained in [59]. In our experiments we also noticed the experts' high inconsistency on the same dataset. In an experiment with repeated data, an expert achieved agreement as low as 81.41%, indicating high intraobserver variability. Overall intra classification error found in [59] was 21.2% for binary classification of malignant cells in the tissue. Consequently, such variations in manual labeling pose a fundamental problem for learning-based methods. Instead of having classical labels, one could replace individual labels of objects of interest with n-dimensional vector $\bar{y} = \{y^1, \ldots, y^n\}$, where n is the number of raters who labeled the object. It is an open question, how should we formulate a classifier $\Phi(X, \bar{Y})$ from the feature matrix X and labels matrix $\bar{Y}$.

Taking all this into account, and that there is no true baseline that we can rely on, we sought to reproduce the work of raters, which meant creating a method whose performance would be indistinguishable from that of humans, as it seems that it is the best way to tackle this task. The method should nevertheless be consistent in terms of giving the same result for the same input and much faster than humans.

To compare performance between rater, kappa statistics is often used. However in this case, the non-existence of true negatives prevents us from using it. Every image element that was not labeled as a neuron by any expert would represent an agreement between the raters, leading to an artificially large agreement on true negatives. Therefore, in diffusion parameter optimization (diffusion scaling constant λ and number of iterations steps N) for the proposed method, a ratio of average agreement between the experts and average agreement of experts with the method

was used to measure how similar the method's performance is to humans',

$$\widehat{J}(E,m) := \frac{\sum\limits_{i,j\in E,\, i\neq j} J(i,j)}{\sum\limits_{i\in E} J(i,m)} \tag{3.29}$$

where $E = \{e_1, e_2, e_3\}$ represents experts and m represents the method's output. In searching through the λ, N parameter space, the best obtained value was $\widehat{J}(E,m) = 0.9784$, which indicates a high similarity in the method's performance with human performance. The diffusion process constants obtained were $\lambda = 11$ and $N = 12$. We have also measured the agreement ratio $\widehat{J}$ for each human rater, exchanging its place with the automatic method in 3.29. For each rater we obtain values that are very close to 1 (Table 3.1), once again confirming that the method's performance is closely the same as that of humans.

Table 3.1: Inter-rater agreement measured by $\widehat{J}$, the ratio of average agreement between three raters and between three raters and one singled-out rater, as defined in 3.29.

Singled-out rater	Agreement ratio $\widehat{J}$	Diff. from mean
e_1	1.0311	0.0309
e_2	1.1032	0.0129
e_3	0.9783	−0.0219
m	0.9784	−0.0218

$\widehat{J}$ ratio mean = 1.00025, std. dev. = 0.022814

Our method is much faster than human raters, and faster than methods found in literature [83], [47], [96]. Unparallelized, the method processed a cortical area of 1mm^2 in about 40 seconds on a computer with Intel i7 8-core processor and 16GB of working memory. Considering the total number of neurons counted on all images, the average number reported by three experts is 547.33 ± 11.14, while the method counted 552 neurons which is about 5 neurons or 0.91% more.

Table 3.2: Approximate comparison with other relevant methods. We observe that our method has improved accuracy, while the execution time is significantly shorter.

Method	Cortex type	Image resolution	Accuracy	Time
Inglis [96]	Rh. monkey	10×, 1.5μm/px	$86 \pm 5\%$	Several days
Sciarraba [47]	Human	40×, 0.26μm/px	$87 \pm 6\%$	2 Days
Oberleander [83]	Rat	40×, 0.26μm/px	$\sim 90\%$	Several days
Our method [88]	Human	40×, 0.26μm/px	95.41%	Few hours

After developing the method and obtaining the model parameters we tested our method by

producing the automatically obtained locations. Correctness of these locations was then evaluated by the most experienced expert. We chose a new set of images totaling ≈ 660 neurons. The expert who examined the automatically found neurons labeled them as correctly or incorrectly identified and labeled all neurons that were not identified by our method, which allowed for a classical performance estimation. Overall, the method achieved high accuracy (0.9541), sensitivity (0.9674), specificity (0.9858) and F1-score (0.9765). Fig. 3.7 shows automatically obtained locations using the developed method on whole histological section.

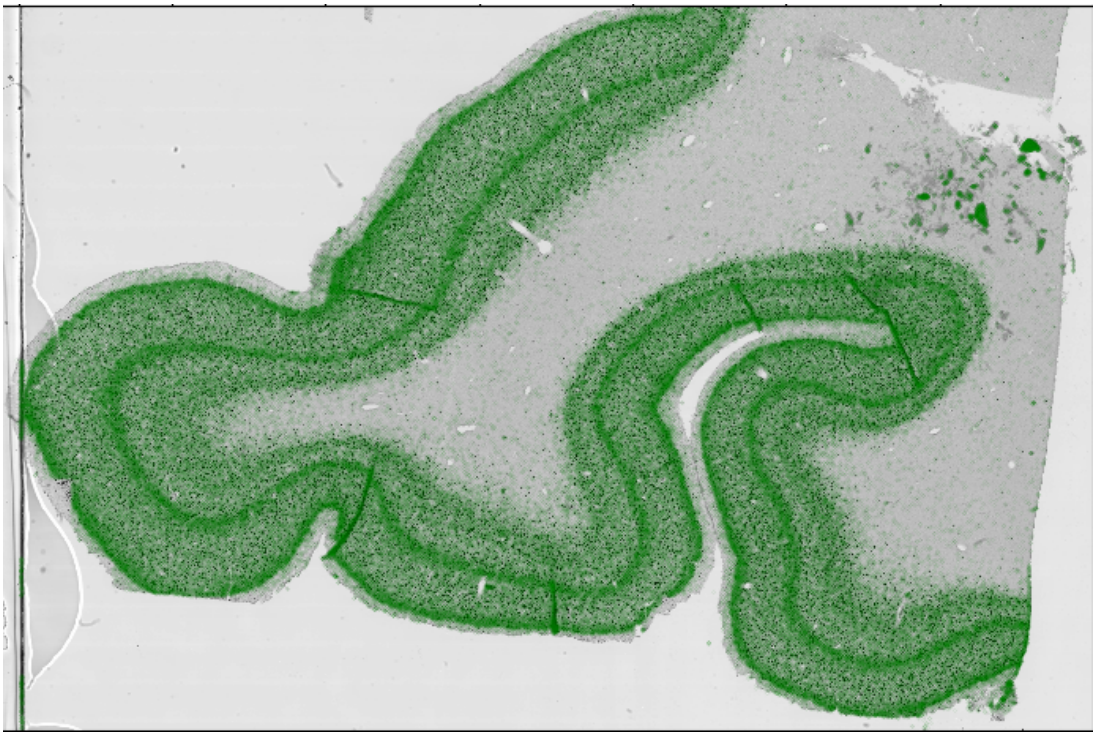

Figure 3.7: Whole histological section of human orbitofrontal cortex overlayed with locations of all neurons found by our method. Variations in cell densities reveal laminar differentiation of cortical layers.

3.3.1 Comparison with ImageJ particle analysis toolkit

Detection of neurons may be brought in relation with more general task of cell or particle detection. In image processing community, such tasks are often performed using ImageJ [73], an extensible open source program which is designed for processing and analysis of scientific multidimensional images. This program is one of the most commonly used for various analysis in biomedical imaging. For our data, best $\widehat{J}$ value obtained using particle analysis method in ImageJ is 0.9482. This method has counted 617 neurons on our test data, which is an overestimation of 13.35%. Through analysis of its performance on our dataset using particle analysis toolkit, we highlight common challenges for methods used for automatic detection of neurons and other cells.

The main challenge for this approach is separating closely located and overlapping neurons.

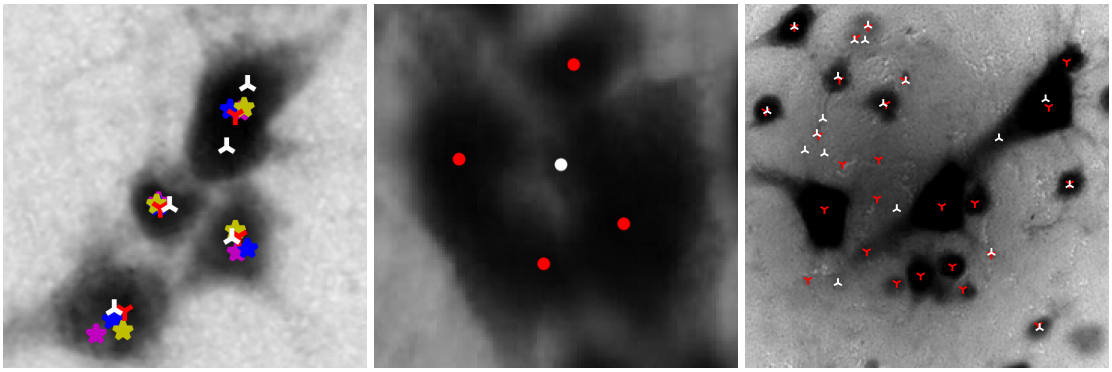

(a) (b) (c)

Figure 3.8: Common challenges for automatic methods. The performance of ImageJ particle analysis pipeline applied for neuron detection (white) is compared to our method (red). Stars represent manual labels of three experts. (3.8a): ImageJ's distance maps often oversegment neurons who's binary mask in not convex, like on the neuron at the top right. 3.8b: Neurons grouped together in oval-like, convex groups are recognized as a single neuron. 3.8c: Performance of automatic methods in overly-stained regions.

In ImageJ particle analysis, as well as in many other related approaches, the first step is obtaining a binary image by intensity thresholding, followed by separation of objects using watershed transform. The pixels below threshold (those that belong to neuron bodies), are then replaced with grayscale pixels of an intensity proportional to their distance from background pixels. By this, a Euclidean distance map (EDM) of the neuron areas is obtained. From this the centers of the neurons are calculated. These are the ultimate eroded points of each neuron, meaning that they are equidistant from edge of a neuron. These points are then dilated until they touch another neuron pixel. This meeting point is where a watershed line is drawn that separates neurons. However, as presented in Fig. 3.8, there are shortcomings to this approach. The distance maps often oversegment neurons whose binary mask in not convex 3.8a. Also, neurons grouped together in oval-like, convex groups are recognized as a single neuron 3.8b. Another problem are staining artefacts in which larger area of a tissue appears darker with lower gray intensity. Usually the whole area is segmented as a single, convex object, and is recognized as a single neuron, even though there may be several neurons distributed in this area, as in 3.8c.

3.3.2 Relation to other automated methods for neuron detection

In Table 3.3 we summarize experimental results of our method and other methods for automatic neuron detection found in literature and discussed in subsection 3.1.2.

In [47] authors used histological sections scanned at 0.264μm/px resolution in 80×34 patches of 1292×968 pixels, with total section area of $200\mu\text{m}^2$. Authors state that it takes 2 days to process one such slide using an AMD Dual Core processor (2.2 GHz). The method's performance was verified on 7 images, each of them containing approximately 150 neurons.

Method	Cortex type	Image resolution	Accuracy	Time
Inglis [96]	Rh. monkey	10×, 1.5μm/px	$86 \pm 5\%$	Several days
Sciarraba [47]	Human	40×, 0.26μm/px	$87 \pm 6\%$	2 Days
Oberleander [83]	Rat	40×, 0.26μm/px	$\sim 90\%$	Several days
Our method	Human	40×, 0.26μm/px	95.41%	Few hours

Table 3.3: Relation with other relevant methods. We observe that our method has improved accuracy, while the execution time is significantly shorter.

Authors in [96] developed their method using 17 image patches 512×512 pixels in size, scanned at 1.5μm/px resolution having ≈150 neurons per image. Authors compare their method to a human-assisted method that samples 10 neurons per second and state that their method offers a speed-up by a factor of 3.5× using 20 Intel P4 processors (up to 3.4 GHz). In [83] authors used different microscope magnifications (40×, 63×), and various imaging (confocal, two-photon, widefield) and staining (NeuN, GAD67, Ca2+) techniques. Their approach is based on three-step pipeline where only the first step depends on input data type. The first two steps correspond to ImageJ pipeline described in section 3.3.1. For widefield NeuN-stained neurons, performance was tested on ≈300 manually labeled neurons. Time needed to process one image stack (0.056mm^2) containing approximately 300 neurons was 1 hour on AMD Dual Core processor (2.2 GHz).

3.4 Application on BigBrain data

After development and evaluation, we applied our method on the data from the BigBrain project [21], a freely accessible high-resolution 3D digital atlas of the human brain. These sections were cut at 20μm thickness and stained with Merker cell-body stain, which stains all the cells, not only neurons as has been the case in our data. Therefore, in experiments with BigBrain data we consider the detection and density of all cells. To detect all visible cells, we used the method on sections from primary visual cortex digitized at 1μm/px resolution. Due to the change in image scanning resolution, we had to adapt method parameters. BigBrain resolution is twice the resolution of the data the method was developed on. Therefore, from 3.27 ollows that the number of steps is 3 for the diffusion with same FWHM for this data. The images were saved in MINC format [108], which keeps image data in `unsigned int16` with range $0 - 65535$. To account for larger absolute differences in image pixel values, we multiplied the original λ used in our `unsigned int8` images with 256.

Although precise evaluation of the cell detection accuracy for whole sections is not feasible, visual inspection showed satisfying results. After the procedure, we calculated a density map

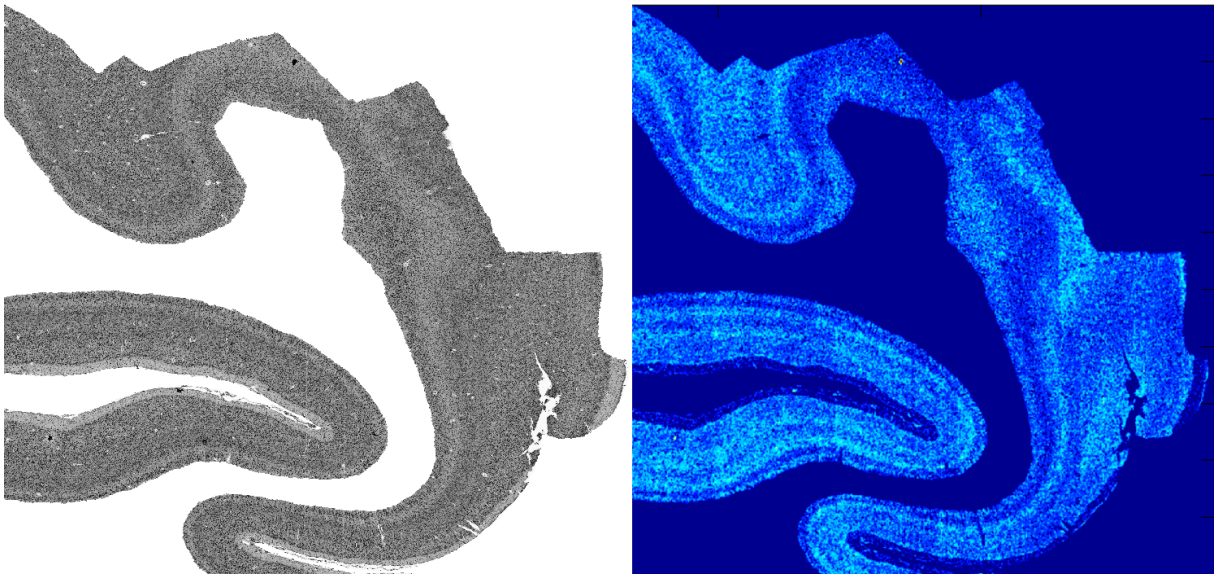

Figure 3.9: Application of the method on the BigBrain data. Left: Image of manually segmented gray matter of primary visual cortex. Right: Cell density map obtained using the developed method. Visually darker regions in the histological image coincide with cell density.

of identified cells, which is shown on the right-hand side of the Fig. 3.9. Each pixel on the map represents number of cells found in a single frame of the mesh overlaid on the original image. Size of the mesh frames was 27×27 pixels, which corresponds to an area of $729\mu\text{m}^2$. Resulting image was also slightly blurred to account for granularity and for better visual perception. The obtained cell density map clearly reveals and highlights cortical layers and points to correspondence between cell density and optical image intensity.

However, in our experiments we noticed the presence of sharp changes in density of detected neurons, which did not seem to be the result of normal anatomical changes in density but rather an artefact in processing of the histological slide. Zooming in on the location of the sharp transition, it was noticed that there is a sudden change in image sharpness along the x-axis of the digitized image. An example of one such change is show in the Fig. 3.10. One can observe that the image is blurred and objects seem out of focus on the left hand side, while the object on the right hand side are sharper, with stronger variations in pixel intensity and with clear boundaries. This resulted in more cells being detected on the right hand side than on the left and in turn produced sharp changes in density of detected cells along the x-axis. Our automatic method diffuses the image to remove local variations in pixel intensity and produce smooth transitions between the neurons and the background. But in this case, the image is already blurred and performing further diffusion may cause image elements to fuse with the background to the point where they can no longer be identified as cells, and closely located cells cannot be separated, which results in underestimation of their true number.

To further explore this anomalous transitions, we quantified the image sharpness using a classical approach in microscopy by measuring the variation of image Laplacian [109], the same

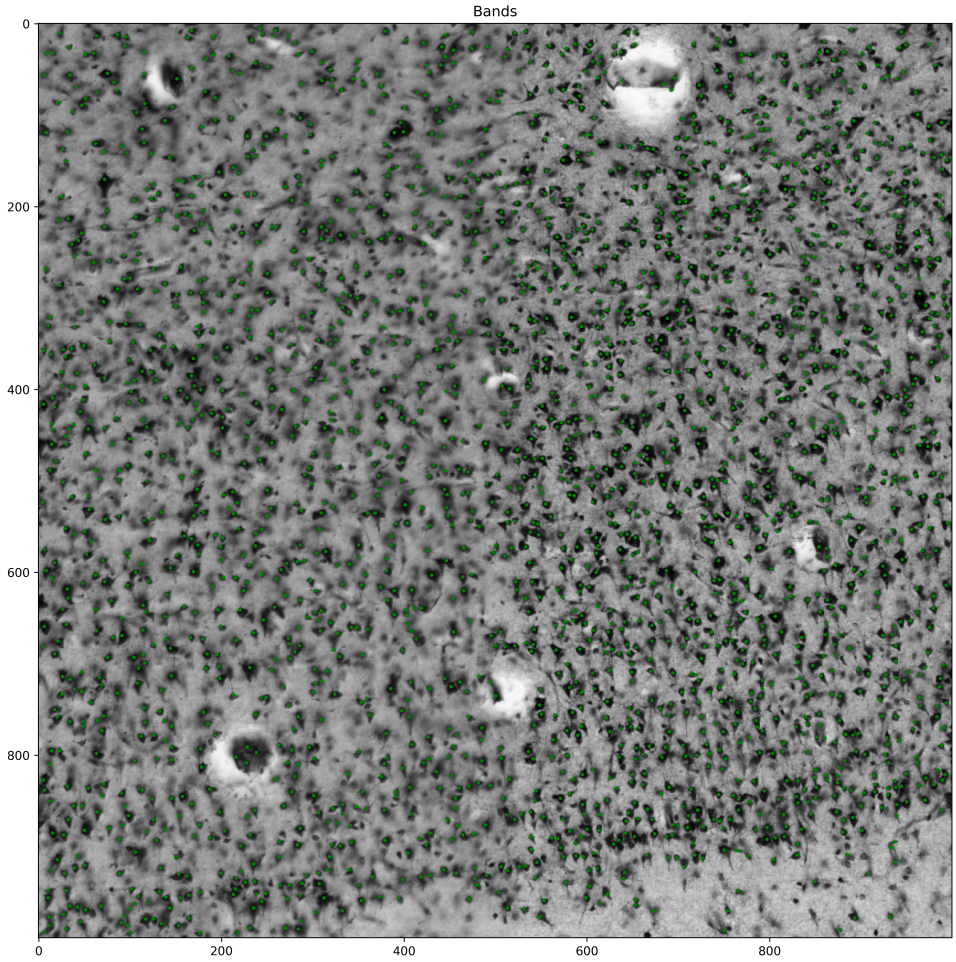

Figure 3.10: Change in image sharpness due to the uneven focusing during the scanning procedure resulted in abrupt change in density of detected cells in adjacent regions along the x-axis of the image.

measure we used in Ch. 4 for estimation of level of focusing for individual neurons. Using this measure we develop a sharpness map that gives better insight in changes of focus for the whole histological section and conclude that the uneven sharpness across the whole digitized section is a result of focusing issue during the acquisition. One of the reasons for this may be that due to the preparation being scanned at an angle, the scanner adapted the focusing automatically while traversing over the glass slide. Since this changes in choosing the focal plane during the image acquisition are done in discreet steps, parts of the image may go out of focus before the scanner adapts, which results in parts of the image being blurred. This becomes apparent when we visualize the sharpness map of the whole section. The sharpness mapping was obtained by computing the variance of Laplacian for image patches of size 50×50. An example of strong

and smooth variations in image sharpness are shown in Fig. 3.11 and 3.12.

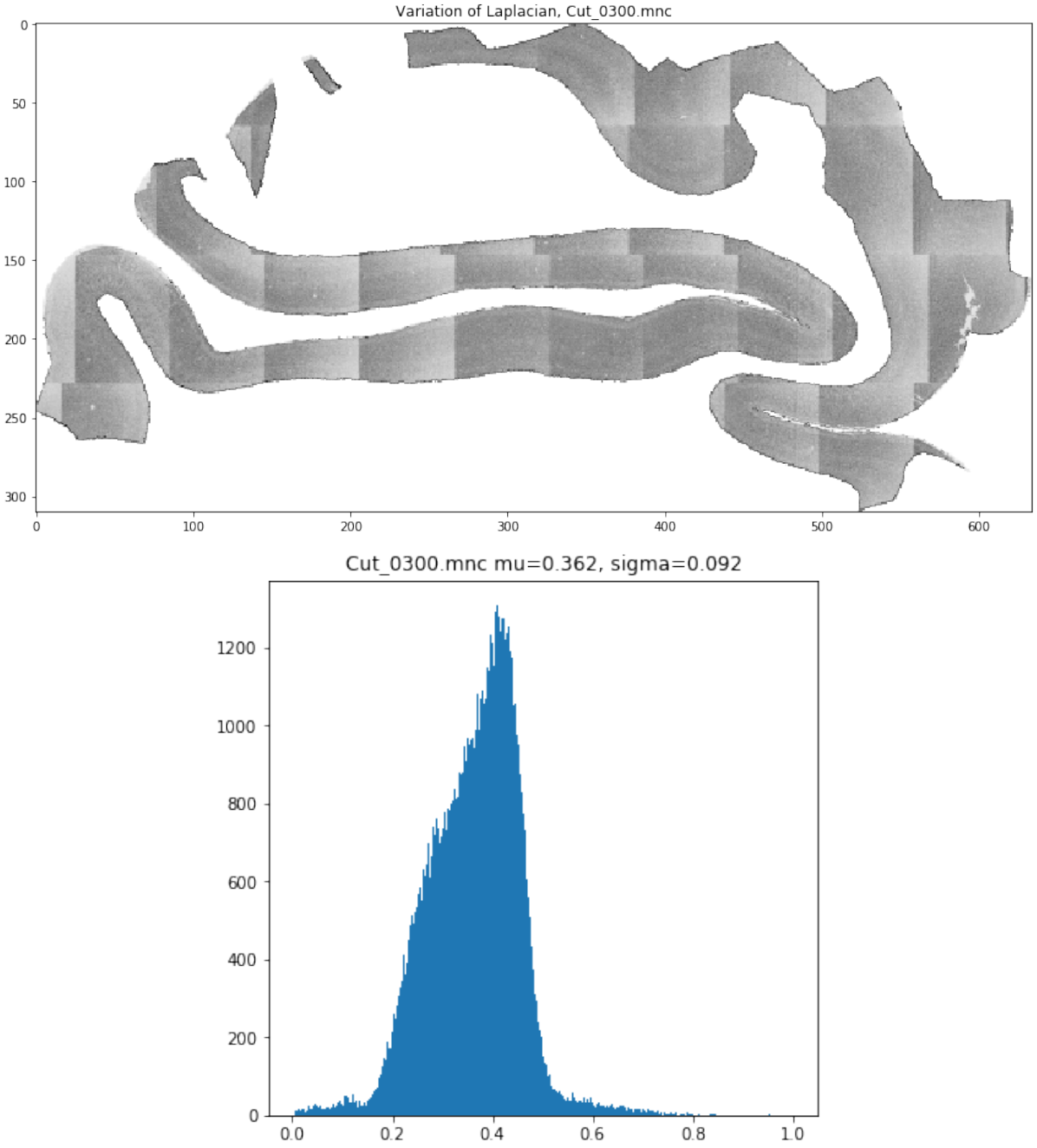

Figure 3.11: Sharpness map of digitized histological sections with jumps in image sharpness, due to changes in focusing during the image acquisition.

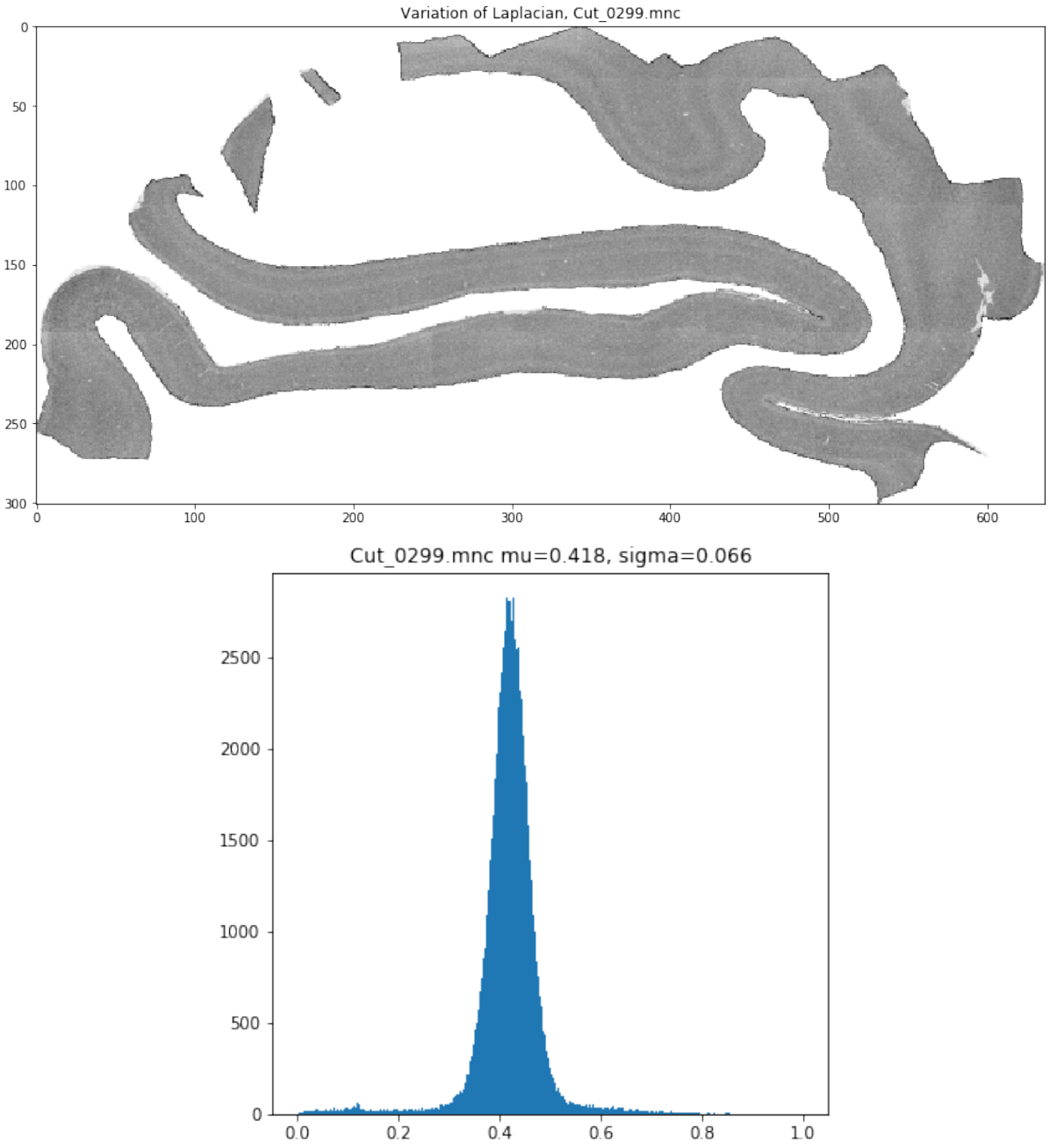

Figure 3.12: Sharpness map of digitized histological section with mostly homogeneous sharpness. Focusing during the image acquisition did not change, which resulted in approximately similar image sharpness across the whole section.

3.5 Conclusion

In this chapter, we have described a fast and accurate method for neuron detection based on anisotropic diffusion model with an histological image as a initial condition to appropriate partial differential equation (PDE). In our experiments, we studied the extent of inter-observer variability on the same dataset. The proposed method has proven to reproduce the work of human experts almost equally and consistently on repeated data. It is also much faster than humans and other proposed automated methods, being able to process whole sections in matter of hours or even less, instead of days. We have demonstrated the use of the proposed method by creating a cell density map of a whole slice of human cortex. We discussed details some details Application of this method significantly speeds up quantitative studies and provides highly reliable and reproducible results, free of human bias. Given the locations of neurons one could also develop precise measurements of density, distinguish between different neuron populations and observe distribution, size and shape of neurons and further obtain other tissue features across whole tissue sections.

Chapter 4

3D Localization of Neurons in Bright-Field Histological Images

In this chapter, we examine the use of multi-level scanning of bright-field images of histological preparations along the z-axis to explore its 3D context. We propose an automatic determination of neuron locations in three dimensions by combining the in-plane neuronal depth information from adjacent 2D planes obtained at different z-levels into full 3D neuronal localization. This chapter is mostly based on our work published in [110].

4.1 Introduction

Technological advances in the past several decades have empowered scientists in life sciences to analyze data in hitherto unseen detail. Whole slide digital imaging enables (i) the digitization of histological preparations of various types, and (ii) provides the capacity to store, share and analyze tissue specimens with the same level of detail as one would observe under the lens of a microscope [111]. However, as is most often the case, objects whose nature is three-dimensional are captured by a camera that produces a series of two-dimensional images.

The 3D context provides a more detailed and realistic insight in cellular organization and is therefore more anatomically meaningful. This is especially relevant for studies in which several consecutive sections are registered to produce a 3D volume. For instance, if the sections are cut with a 20μm thickness but scanned at 1μm in-plane resolution, we benefit from the higher scanning resolution only in the horizontal plane, while the 3D resolution remains limited by the section thickness. By accurately positioning the cells within the section in 3D, one can better approach an isotropic 3D resolution and obtain realistic and continuous distribution of cells across the volume. Such analysis may more accurately reveal subtle changes in cellular organization, columnar formation and underlying tissue cytoarchitectonics.

4.2 Neuron imaging in 3D

To visualize cells in the tissue and examine its cellular layout, a histological preparation is made, as described in more detail in chapter 2. The tissue of interest is cut into thin sections and treated with various stains to enhance inherently small visual contrast in such sections and highlight features of interest. The stained tissue is then mounted on a glass slide and ready for examination under the microscope, to be digitized using a histological scanner, or to be stored for future examination.

In conventional microscopy, we distinguish two main modalities, confocal and wide-field imaging. The former offers better insight into 3D structure, but is however limited to small tissue patches. The latter offers whole-slide imaging, but at the cost of reduced information about the 3D structure. Vast collections of histological sections that were stained in traditional methods are not suitable for inspection under confocal microscopes. Histological slides produced in large scale histological database, such as the BigBrain [21], are usually produced using a bright-field imaging modality. In this chapter we present a method that leverages the use of multilevel image acquisition that produces images of histological sections at multiple optical levels. We derive spatial data based on changing sharpness of objects that are tracked along the z-axis of the section stack. This procedure resembles the above-mentioned traditional manual approach used by anatomists to track neurons along the z-axis by adjusting the microscope's focus.

4.3 Inferring the third spatial dimension

Our aim was to develop a procedure that, based on given locations of neurons in 2D, adds another coordinate to each neuron location, placing it within the 3D space of the histological slide. This section details the procedures we performed as well as the nature of the images used.

4.3.1 Dataset

We used histological sections of an adult human brain that were stained using NeuN, a common immunohistochemistry method that is used for labelling neurons in the brain tissue. Samples were obtained from the Zagreb Brain Collection [84] and scanned using the Hamamatsu Nanozoomer 2.0 scanner (Hamamatsu Photonics, Japan), using multiple optical planes. An example of a neuron at different focal planes is shown on Fig. 4.1. Images were acquired from a section of 10μm thickness using 11 optical planes with 1μm step at 40x magnification, which corresponds to 0.226μm/pixel resolution. The NDPI files produced by the scanner were several gigabytes in size, making the whole slide processing infeasible. Therefore, we extracted smaller image patches using open source software NDPITools [87] for each optical plane, created im-

age stacks and processed them separately. Initial locations of individual cells in (x,y)-plane were found in the image at mid-plane using the automatic approach for neuron detection in NeuN-stained sections described in Chapter 3.

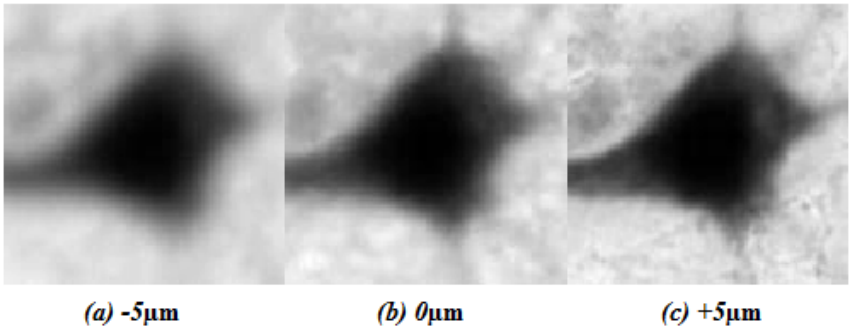

Figure 4.1: A neuron body at different focal planes. Shown here are planes at (a) -5μm, (b) 0μm and (c) $+5\mu$m offset. This neuron was found to have greatest measure of sharpness in the plane (c).

4.3.2 Segmentation of neuron bodies

For delineating neuron borders and separating closely located neurons in the tissue, we used a watershed algorithm to create basins each containing a single neuron. Since the nature of the staining used is such that it amplifies the contrast between the neurons and the rest of the tissue, neurons are clearly visible with distinguishably brighter background. We used Otsu's method [29] to separate neuron bodies from the background in each watershed basin and obtain image pixels that belong to individual neurons. Anisotropic diffusion from Chapter 3 was applied on images to prevent oversegmentation and watershed process was applied using pixel values of diffused image. The main advantage of this approach over morphological distance maps often developed in a step before applying the watershed is retention of true image valleys and peaks. For instance, as seen in section 3.3.1, these maps do not use information from variation of pixel intensities but rather rely only on segmented objects' shape. This often leads to undersegmentation or oversegmentation of neuron bodies and is very sensitive to staining artefacts, as a result of thresholding before the development of maps. After segmentation of image, pixels within the basins that contain a neurons were used for measuring the neuron sharpness at each z-level. Watershed basins as well as outlines of neurons are shown on Fig. 4.2.

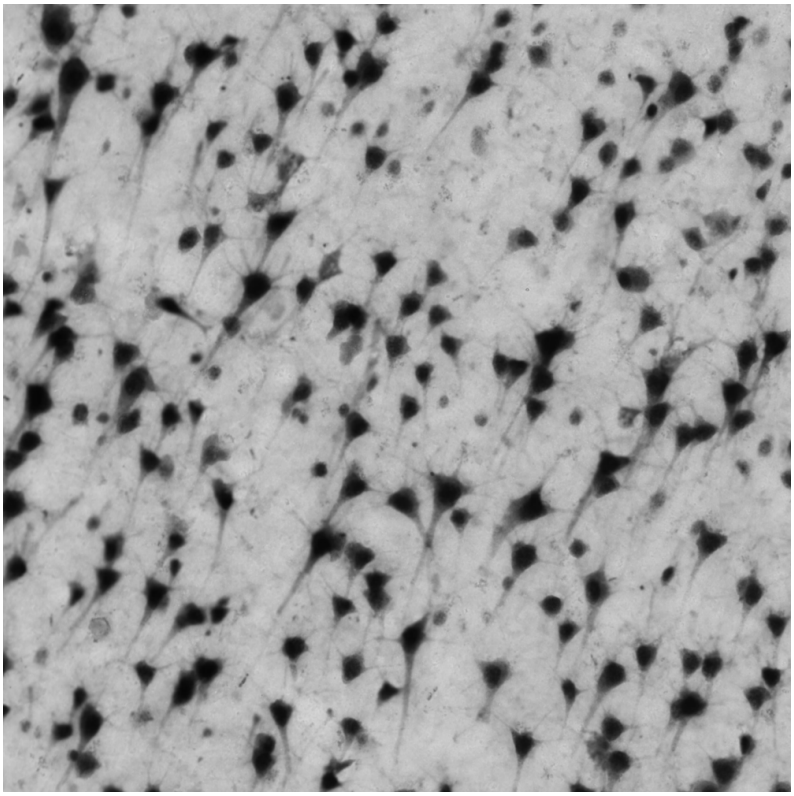

(a)

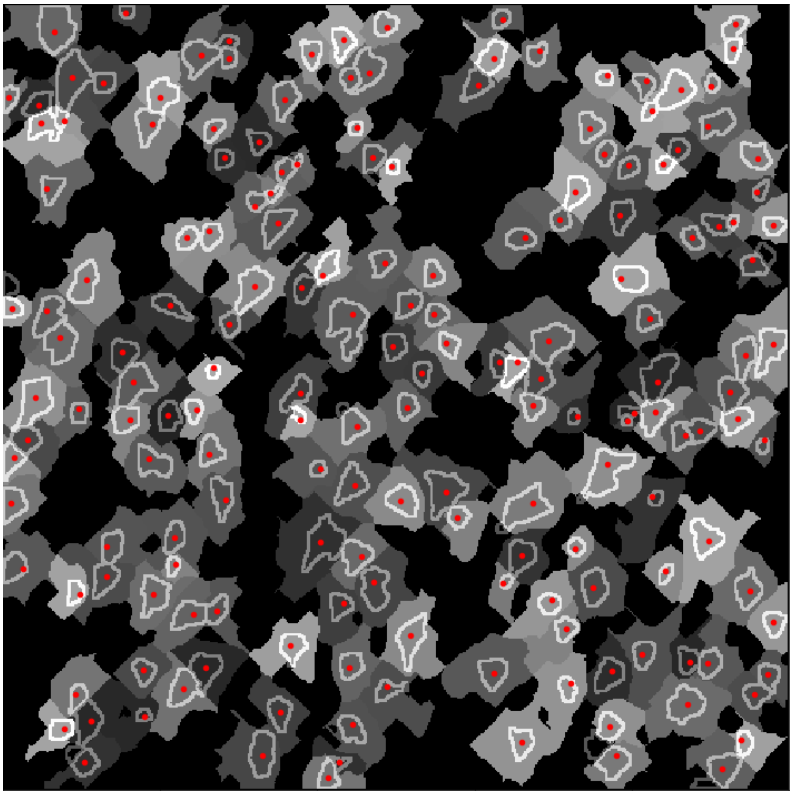

(b)

Figure 4.2: An example of digitized histological slide using bright-field imaging 4.2a and locations of neurons and watershed basins with outlined neuron borders 4.2b. Pixels within the basins are considered as *neuron domains* $\Omega_{n,l}$ and used for measuring the neuron sharpness at each z-level.

4.3.3 Image sharpness

To determine the central location of each neuron along the z-axis, we relied on the sharpness of the neuron body across all images in the stack to determine the level at which the maximum sharpness was obtained. After reviewing a comparison of several focusing measures [109], we used the Variance of Laplacian metric, applied to the intensity of those pixels belonging to a neuron body, as the measure of neuron sharpness. For a neuron n, at z-level l, we compute the focusing measure using the formula

$$\phi_{n,l} = \frac{1}{|\Omega_{n,l}|} \sum_{(x,y)\in\Omega_{n,l}} (\nabla^2(x,y) - \overline{\nabla^2 I})^2, \tag{4.1}$$

where $\Omega_{n,l}$ is (x,y)-domain of the neuron and $\overline{\nabla^2 I}$ is the mean value of the image Laplacian within $\Omega_{n,l}$. This measure was first proposed in [112] for the use of autofocusing in microscopy. It is inexpensive to compute, insensitive to image noise and produces scalar outputs that can be easily compared across the section stack. To obtain the Laplacian of the images, we convolved each image in the stack with the discrete Laplacian operator

$$L = \begin{bmatrix} 0 & 1 & 0 \\ 1 & -4 & 1 \\ 0 & 1 & 0 \end{bmatrix} \tag{4.2}$$

The rationale for choosing this measure is as follows. If a neuron in a level along z-axis is out of focus, its pixels, and especially pixels along the border of the neuron, will be blurred, resulting in low variation of the signal, less sharper edges and lower gradient magnitude. This will also be reflected on the Laplacian which will have less dispersed values in blurred image areas. The opposite will happen in the image at the correct z-axis for a neuron of interest. Therefore, to correctly place each neuron in the observed tissue patch, we identify the z-level that has the maximum $\phi_{n,l}$ variance of Laplacian of the pixels in the neuron body.

4.3.4 Spline interpolation

After obtaining the third spatial dimension from 2D data as described above, the resulting z-coordinates will still fall under the number of focal layers in which the slide was scanned. To make neuron locations more realistic in 3D, we interpolated the measurements of neuron sharpness across the section stack and, instead of choosing the layer in which the sharpness measure is largest, we used z-value where the maximum of the spline is achieved (Fig. 4.3). This allows for neurons to be located with continuous z-coordinate instead of having limited set

of possible values.

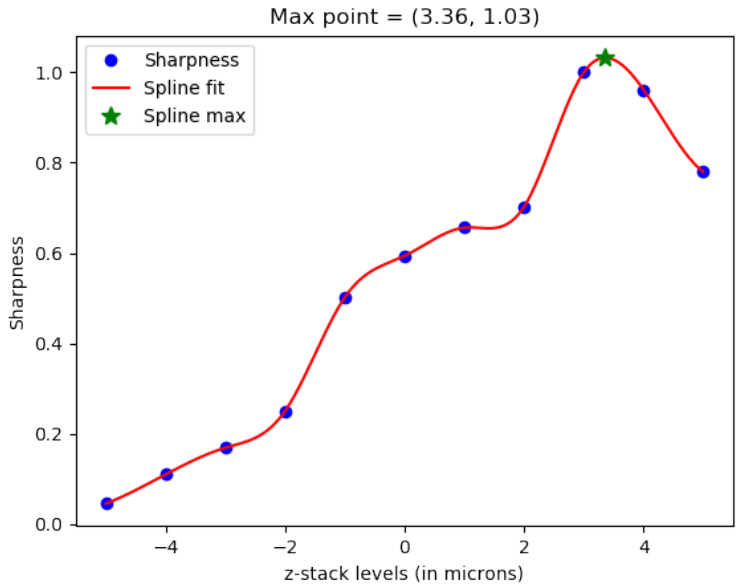

Figure 4.3: A cubic spline was interpolated through values of sharpness measure across z-layers. Instead of choosing the z-coordinate of a neuron from one of the z-levels, a continuous value where the spline achieves maximal value is chosen instead (green star).

4.4 Results

In this section we show results from processing a stack of 11 images, produced by scanning a chosen area of a histological section at z-levels in range from -5μm to $+5\mu$m, with a step of 1μm, at magnification of 40x 4.4. Images captured were of size 4096x4096 pixels corresponding to tissue area of approximately 0.86mm^2. Our neuronal localization algorithm was implemented using Python programming language. The time needed to process the whole stack and obtain 3D locations of neurons was under a minute using an average personal computer with Intel i5-4300U processor with 12Gb of memory. Most of the computation time was spent for performing the watershed algorithm and determining domains of neuron bodies.

4.5 Conclusion

In this chapter we presented a method for inferring a third spatial dimension for a given 2D neuron locations in a bright-field image of a histological slide of human brain scanned at multiple z-layers. A watershed algorithm was used to segment neuron bodies, which we tracked across all the images in the stack and measured the level of sharpness at each z-level. Variance of Laplacian was used as a sharpness measure, as a common measure in microscopy. Finally,

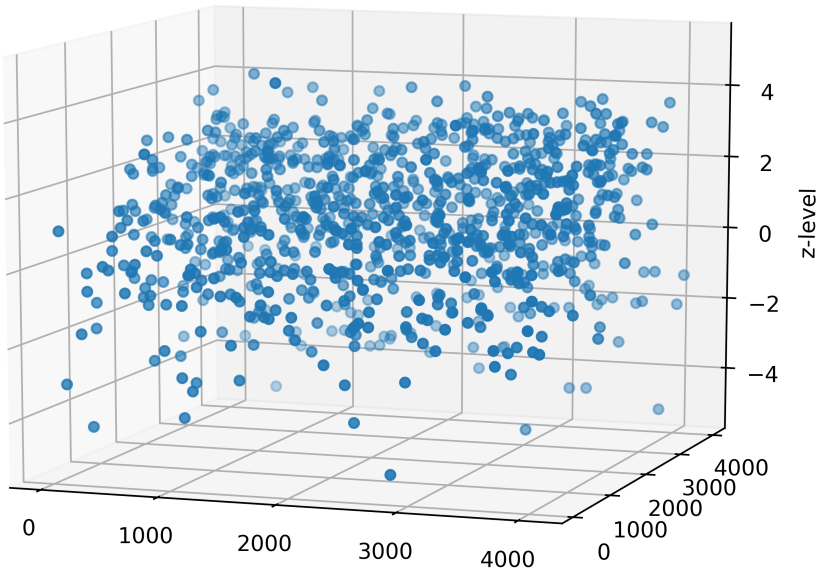

Figure 4.4: Visualization of 3D locations of all neurons found in the image stack. Values of z-coordinates are continuous instead of limited to the z-level offset due to the spline interpolation of measured sharpness values for each neuron.

to produce a more realistic values of z-coordinates, we interpolated a cubic spline through measured sharpness values for each neuron and instead of choosing a value from the z-level offsets, for the third spatial coordinate we chose the value for which the interpolated spline achieved a maximum.

Chapter 5

Computational Analysis of Laminar Structure of Cerebral Cortex

Interest in analysis of laminar structure is driven by evidence of relationship between features of cytoarchitectonics and cortical functions. It enables researchers to gain better understanding of anatomical and functional organization of the brain, as well as studying many neurological and psychiatric diseases that cause subtle changes in the brain structure. Automatic segmentation of cortical layers significantly improves speed and objectivity of such analysis and provides means to process large amount of histological data available today. Combining techniques and data sources from various fields, analysis of histological images of human brain allows for better understanding of brain structure and function.

Focus of this chapter, is the exploration of tissue features whose change across the gray matter facilitate distinction between layers in the cortex. A novel approach is presented, which uses features of individual neurons to investigate changes in architectonic differentiation and reveal changes in cellular distribution and types across cortical layers.

5.1 Quantitative analysis of laminar structure

Since the first methods for automated or semi-automated analysis of cortical layers were developed, central idea in almost all methods was the use of sampling along transverse lines drawn either manually or semi-automatically [69] across the cortex, perpendicular to the laminar structure and spanning the full width of the cortex [17], [18], [19]. At first, changes of optical density, or gray-level index (GLI) was measured by these profiles, which is a crude estimate of changes in neuronal density.

Recent methods for automated laminar analysis developed after the year 2000 have moved on from only using GLI in analysis of cortical profiles. In year 2002 [64], authors develop statistical features that characterize each GLI profile and its discreet derivative, like the first

four moments about the mean, treating the profile as a frequency distribution, for the total of 10 features for each profile. Authors also bring these features in relation to cytoarchitectonics and reflect on different distance measures used to compare profile vectors derived from different brain areas. An important step in development of profile features was made eight years later in [63] by the introduction of automatic methods for estimation of cell counts, thus providing realistic information about neuron density. Authors provide the number and distribution of neurons within several projection columns in rat cortex, reporting an estimate of neuron number per layers. This data is further used to derive the action potential output of projection columns specific for each layer, clearly showing direct link to analysis of the brain function through analysis of its cytoarchitecture.

The first article that uses features and statistics of individual neurons appeared in 2017. In [71], authors use automatic segmentation of cells in 7μm thick Nissl-stained sections of the mouse brain and develop 11 shape descriptor features for each cell. After manually setting the upper and lower bounds for thresholding, a binary image is produced, and blobs are classified as glial cells or neurons, which are further subdivided into pyramidal and non-pyramidal. Using profiles across the mouse cortex for each cell type, authors distinguish five cortical layers, merging layers II and III into single layer. However, only a few hundreds of cells are found on a small patch of tissue labeled by one expert. The method nevertheless offers a novel approach by using shape descriptors of individual cells for cell classification. A year after, use of GLI profiling on a large in 3D dataset was presented [65]. Authors develop automated analysis of the laminar structure of the BigBrain [21] by analysis of GLI peaks to distinguish between the layers. A relation between cytoarchitectonics an in vivo MRI imaging is discussed.

Most recently, in the year 2018, a first approach that does not use profiles across the cortex was proposed [72]. A combined approach of unsupervised and supervised machine learning was used on an extensive dataset of 2-photon microscopic images of the rat cortex. Neurons are automatically segmented and some neurobiologically sound statistics developed and combined with texture descriptors to produce several sets of features used in learning methods. Importance of neuron density is especially emphasized, and it is pointed out that it alone leads to revelation of laminar hierarchies by the proposed unsupervised method. Authors also address the issue of human bias in manual segmentation of cortical layers and use an unsupervised clustering approach to identify and represent the laminar structure. Supervised learning is used to transfer resulting layer segmentation on different brain regions.

Considerations from the review of concepts in historical and recent methods here and in Chapter 1 lead to following conclusions: (i) Over the years, the impact of human bias in brain parcellation has been increasingly recognized and many methods sought to overcome this issue by developing objective quantitative measures and usage of statistics to distinguish between different layers and brain areas. (ii) Recent advancements in technology yield massive amounts of

high-resolution and multimodal data which are far beyond the capabilities of any kind of manual analysis. (iii) Detailed anatomical and biologically meaningful information can be derived on a large-scale. This allows for the introduction of machine learning methods to the field that was until now dominated by the usage of exclusively image processing techniques. (iv) Neuron density seems to be the most important tissue descriptor, it alone facilitating the revealing of laminar structure, followed by neuronal size and shape. Derivation of higher-level descriptors, which may seem more or less neuroanatomically meaningful, can reveal currently neglected additional structuring principles and provide deeper understanding of laminar structure, leading to more reliable methods for layer segmentation. On the other hand, image texture features seem to have less discriminative power.

All this suggests that there is a trend to infer the laminar organization by studying its organization in ever more detail, going beyond limitations of the frameworks of manually created parcellation in conventional atlases. The research in the field should move away from human interpretation towards data-driven, unsupervised analysis with as little parameters as possible. However, the very recent methods are usually developed on rat or mouse cortex data, and the results for human cortex are lacking. To present a better insight in varying anatomy of the cortex as revealed by histological imaging, outline of some of its important properties follows.

5.2 Laminar organization of the cortex

In classical works of cytoarchitectonics, neurons are distributed in six horizontally superimposed layers that are distinguished in most areas of the cortex [2], [3], [5]. Some neurons may be also found in the white matter (WM). The layers are result of variations in cell density, size and shape which are specific for each cortical layer. These, and potential variation in other features specific to either each individual neuron or its surroundings are our main interest in this chapter.

As described in the literature [2], there are three main neuron types that are found in the cortex. Probably the most recognizable ones are *pyramidal* neurons. They are characterized by a large, triangular-shaped bodies, elongated in the vertical direction, with a prominent long dendrite extending from the upper pole. However, their sizes may vary substantially, from 12μm in the longest axis to 100μm. They are usually found in layers III and V of the cortex. *Granule cells* are mainly characterized by their small size, with diameter of their usually round-shaped bodies ranging from 4 to 9 μm. Their bodies may also have polygonal or triangular shape, with hardly giving off any dendrites. These are mainly found in layers II and IV. *Fusiform cells* are long and spindle shaped, with their body size spanning from 15 to 30μm in diameter, with both poles giving off noticeable dendrites. These neurons are usually found in layer VI of the cortex.

Layers in the cortex are numbered starting from the pial surface towards the white matter.

Layer I, or the *molecular layer* contains very small number of neurons and is mostly composed of arbors of dendrites and axons which are not revealed by cellular staining. Neurons in this layer are thus very sparse. They are also very small, with only few micrometers in diameter. Some of them have elongated, fusiform shape, and are disposed tangentially to the cortex. Layer II, the *external granular layer* is composed of numerous small granule neurons. These are densely packed and mostly round or polygonal in shape. Some small pyramidal neurons may also be found in this layer. Large pyramidal neurons characterize Layer III, which is also called *pyramidal cell layer*. Neurons of this layer are distributed less dense than in previous layer and are on average much larger. Layer IV, or internal granular layer is similar to the layer II, with numerous, densely packed small round cells. Layer V is called internal pyramidal layer resembles layer III in terms of neuron density. It is mostly composed of medium-sized pyramidal cells. Layer VI, or the *spindle (fusiform) neuron layer*, borders with the white matter. Neurons of this layer are somewhat densely distributed than in layer V, and are spindle-shaped, with axis oriented perpendicular to the cortical surface. Finally, it is worth mentioning that there is no clear border between layer VI and the white matter. Neurons gradually become sparsely distributed and smaller in size. Small fusiform neurons can be found even deeply in the white matter. This is perhaps why even the human experts do not agree on where the layer VI ends and white matter begins. This can be noticed for example on Fig. 2.11 or Fig. 2.10. in Chapter 2. Table 5.1 summarizes the considerations about classical characterization of neurons and cortical layers. As concluded in the previous section, density and size of neurons are the most

Table 5.1: Six horizontally superimposed layers are distinguished in most areas of the cortex. The layers are result of variations in neuron density, size and shape.

Layer number	Neuron density	Neuron size
Layer I	very sparse	small
Layer II	dense	small
Layer III	sparse	very large
Layer IV	dense	very small
Layer V	sparse	large
Layer VI	sparse	large
White matter	very sparse	small

important characterizations of the laminar structure. Table 5.1 shows that adjacent layers have different densities, with the exception at the border between layers V and VI. These layers are described as having similar density, although a minor difference still exists.

Location and area of neurons are fundamental properties of each neuron. Many other characteristics can be developed once when the location and border of a neuron are known, espe-

cially with regard to other neurons, for instance using distances to obtain neuronal density or measuring average size of neighboring neurons. Automatic detection of neurons in histological images developed in Ch. 3 provides the capacity to precisely and uniformly obtain locations of all neurons in the tissue section. Neuron segmentation method described in Ch. 4 gives the area for each neuron. These are the two central methods on whose results all further investigations in this dissertation are based, including derivation of other complex features and analysis of their changes within the cortical layers.

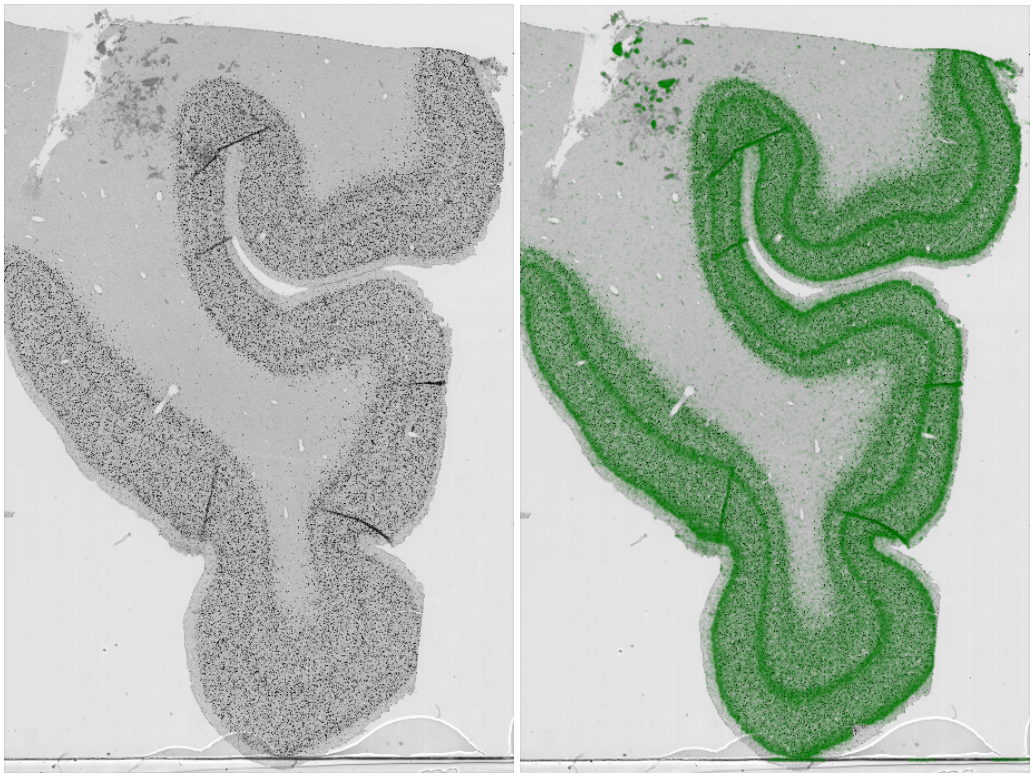

Figure 5.1: Left: An example of digitized histological preparation of human orbitofrontal cortex (gyrus rectus). Right: Locations of individual neurons which are result of automatic neuron detection are plotted over the original image. Variations in neuron densities follow the laminar structure.

5.3 Analysis of classical neuron features

Development of other neuron features based on neuron location and density is very natural. For instance, density as a number of neurons within some distance of a neuron, or by average distance to its k nearest neighbors. It is important to mention a distinction between two types of features: (i) those of each individual neuron, whether its own like location and area or derived as a statistic of features of neurons in some neighborhood, and (ii) image features obtained by conducting measurements in some chosen patch of an image, which more resembles to texture properties.

Values of the three features were measured for each of 229733 neurons found in the histological section 5.1. By plotting a histogram of their values one can observe that these features express a multimodal distribution. To separate the distributions, minimization of intraclass variance [29] was used. Based of anatomical description, Table 5.1 and visualized kernel density estimate in Fig. 5.2, three populations of similar densities are assumed (layers II and IV, layers III, V and VI, and Layer I and white matter), two populations of similar sizes and average neighbor sizes (layers III, V and VI, and layers I, II, IV and white matter). Neuron feature kernel density estimations with thresholds for minimization of intraclass variance are shown in Fig. 5.2. Fig. 5.3 shows visualization of separating the neurons by the thresholds across the cortical section.

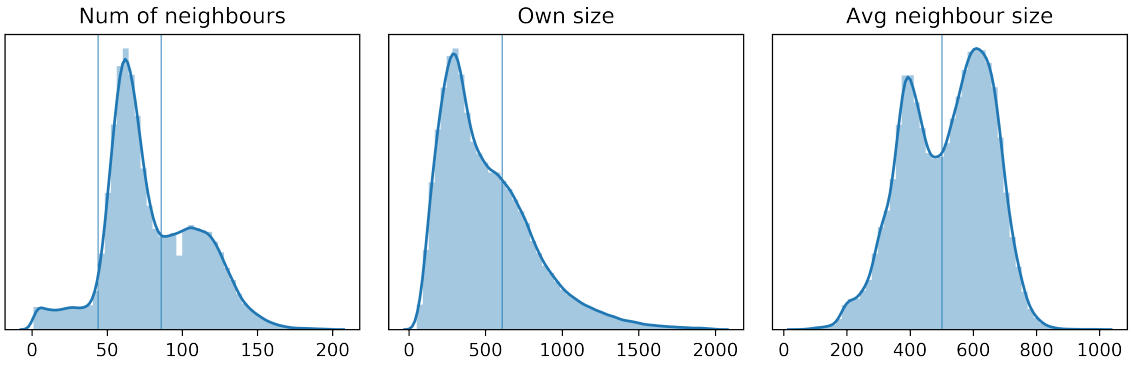

Figure 5.2: Cell features exhibit multimodal distribution. Thresholds that separate the distributions were obtained using minimization of intraclass variance [29]

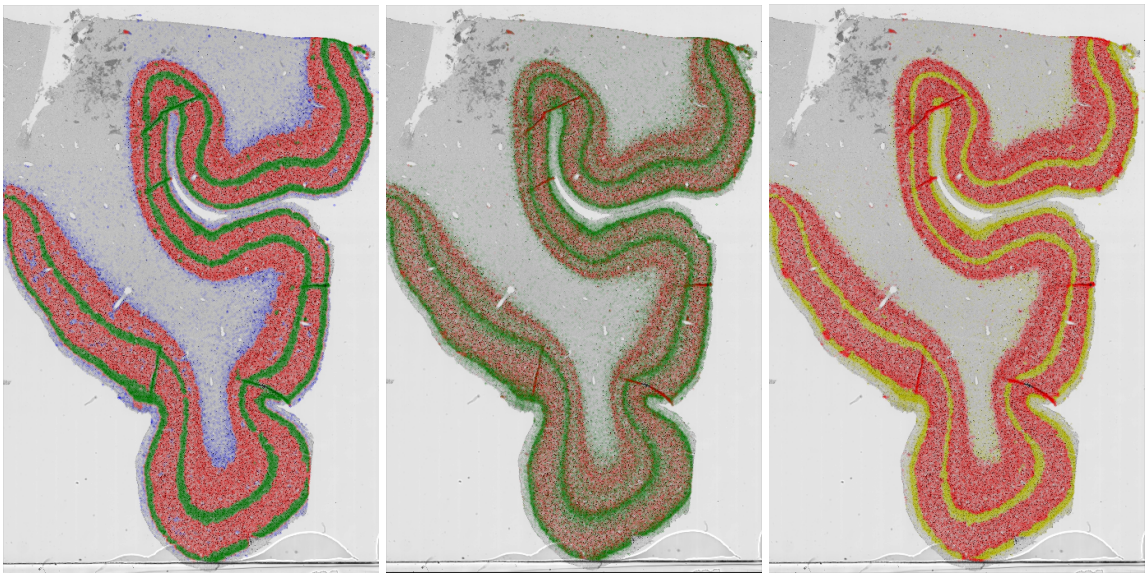

Figure 5.3: Characteristics of individual neurons reveal cortical layers. Left: Three types of neurons were distinguished by cell density in their surrounding area: very sparse (blue), sparse (red) and dense (green). Middle: Larger (red) and smaller (green) neurons. Right: Average size of neighboring neurons is also a feature that contributes to layer segmentation.

From the outlines, many other statistics can be developed using available software. For

instance, ImageJ's Particle analysis toolkit [73] provides a set of features for each individual neuron, such as statistics of pixel intensity, shape descriptors and even orientation based on parameters of the fitted ellipse.

5.4 Exploratory data analysis

Considerations in the previous section further confirm the importance of the spatial distribution of neurons in discriminating between cortical layers. Taking into account the conclusions about the importance of unsupervised approach to the analysis of laminar structure, clustering-based methods provide an important insight in spatial distribution of neurons. These algorithms often produce results based on some input parameters, whether they are manually set or chosen automatically. The goal of this section is to explore intrinsic structure of neuron distribution through analysis and application of different clustering algorithms, development of various neuron characterizations and analysis of their capacity to discriminate between the neurons of different layers. A portion of the section has been manually labeled and a dataset of over 17000 neurons from all layers including white matter has been obtained. This dataset is used throughout the section to visualize distribution of neurons in different layers and track their changes with regard to application of different methods and statistics.

5.4.1 Density-based clustering

In cluster analysis or *clustering*, the task is to group a set of objects using a defined similarity measure is such a way that similar objects are identified as members of the same group called a cluster. It widely used in many fields as a central task of exploratory data analysis, and various algorithms have been developed and studied, depending on the specifics of the application, especially the nature of the data being clustered [113], [114], [115].

Density-based clustering takes into account the spatial distance of the objects, thus defining clusters of higher or lower densities. Although there are many algorithms to choose from, not all are suitable for separation of neurons to appropriate layers, or even identification of potential sub-layers. Although the approach in this thesis strives to be data-driven with as little assumptions or parameters as possible, some aspects of the data need to be taken into account when choosing the appropriate clustering algorithm.

Algorithms like K-Means [116], K-Medioids [117], affinity propagation [118] and other similar algorithms assume globular shape of the data and cannot identify elongated clusters [119]. Such algorithms often require a predefined number of clusters or other parameters. Another undesirable property is non-determinism - different initialization setup may yield different results. Agglomerative clustering is a concept in which each object starts as its own cluster,

and clusters are merged by some similarity criterion repeatedly, until there is only one cluster remaining. This procedure produces a hierarchy, a binary tree, or a dendrogram in which the clustering can be tracked down to the single leaf. There are different strategies on how to merger and split the clusters. The subtrees can be ranked by distance to when clusters merged, or by using more complex criteria like mean distance between the clusters or some other measure. Based on this, the tree is cut at some level and subtrees, or clusters, are determined based on that cut. An important property of this approach is that the clusters can now take any shape, not only globular. However, it may sometimes not be straightforward to determine the level of cut for selecting the clusters. Concept of density-based spatial clustering in applications with noise (DBSCAN) [120] is similar to agglomerative clustering - it applies single linkage clustering to the results in dendrogram, which distinguishes clusters according to a distance parameter. Again, in practice this parameter may be difficult to choose. The method uses another parameter that determines the minimum density around a point and classifies all the points below the minimum density parameter as noise. Consequently, some points are not being assigned to any cluster. With significant improvement in performance that can be achieved using kd-trees for local region queries, the algorithm can tackle large datasets which can be impractical for algorithms other than simple ones, like for instance K-Means. This algorithm can also find non-linearly separable clusters like cortical layers but does not handle small variations in density very well. It often produces smaller clusters enclosed in larger ones, if the points have slightly lower or greater density than the rest of the cluster, which is often the case within cortical layers. Very sparse clusters are also often split into several smaller clusters. Nevertheless, this is the most suitable approach for neuron clustering so far and gives insight about specifics of clustering applied for that purpose, leading to some practical conclusions.

In the context of neuron distributions in the cortex, several important discriminative criteria of the clustering algorithms need to be considered. The algorithm should have low number or even no parameters that need to be tuned and selected. It should also have the ability to handle clusters of arbitrary shape since the cortex is gyrified and layers follow winding patters, allow clusters with slight variations in density due to the fact that neuron density is not absolutely uniform within each layer and finally, to be able to process large amounts of coordinates, since there may be hundreds of thousands or even millions of neurons found in the tissue section. A few algorithms found in the literature satisfy these criteria to different extent.

OPTICS

Ordering Points to Identify the Clustering Structure, or OPTICS [121], is a cluster analysis algorithm which does not produce explicit clusters, but instead creates an ordering of points representing their density-based clustering structure. The cluster-ordering obtained this way contains information equivalent to the density-based clustering corresponding to a broad range

of parameter settings. It addresses one of DBSCAN's major weaknesses, the problem of detecting meaningful clusters in data of varying density. The coordinates are (linearly) ordered such that points which are spatially closest become neighbors in the ordering. Additionally, a special distance is stored for each point that represents the density that needs to be accepted for a cluster in order to have both points belong to the same cluster. Similar to DBSCAN, the algorithm requires specifying two parameters: epsilon ε, which describes the maximum distance (radius) around the point to consider, and minimum number of points required to form a cluster, $MinPts$. A point i is considered as core point if at least $MinPts$ points are found within its ε-neighborhood.

The algorithm creates a two-dimensional *reachability plot*, which is used to obtain the hierarchical structure of the clusters. The ordering of the points as processed by OPTICS is represented on the x-axis and the reachability distance on the y-axis. Since points belonging to a cluster have a low reachability distance to their nearest neighbor, the clusters show up as valleys in the reachability plot. Deeper valleys in the plot are result of denser clusters.

By changing parameters of the algorithm, there are two similar types of result obtained: (i) only neurons from layers II and IV form clusters, with numbers of smaller clusters found within each of the two layers depending on ε values and all other layers are considered as noise, and (ii) layers II and IV form single cluster each, and many small-sized clusters are formed in other regions, surrounded mostly by noise. Such result is obtained if $MinPts$ is increased for the same ε value in case (i). To obtain meaningful clusters, kernels between 80μm and 200μm in radius can be chosen, with minimum number of points between 20 and over 150. Reducing the number of neurons identified as noise may be achieved by choosing maximum distance between the points as ε. However, this leads to increased computational complexity since every neighborhood query would return the full data set.

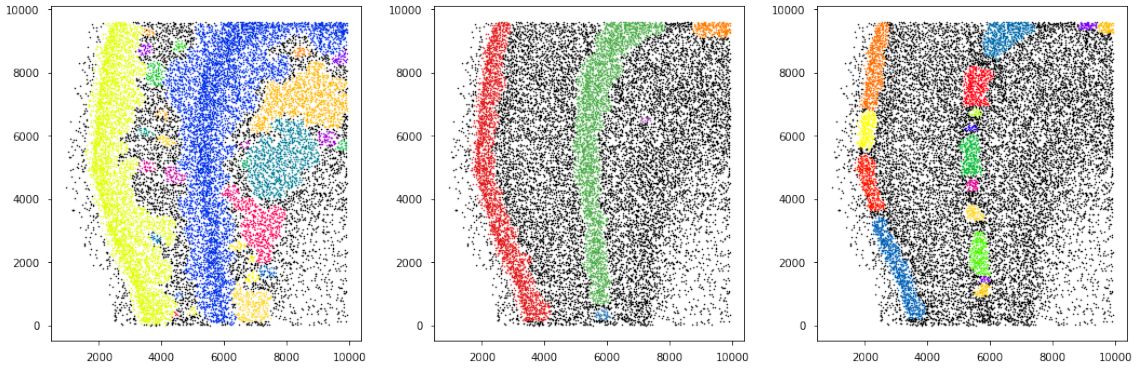

Figure 5.4: Left: $\varepsilon = 200$, $MinPts = 30$ Center: $\varepsilon = 200$, $MinPts = 45$ Center: $\varepsilon = 200$, $MinPts = 55$

HDBSCAN

An algorithm developed as an improvement of both the DBSCAN and OPTICS algorithms with the goal to allow varying density clusters is Hierarchical Density Estimates for Data Clustering, Visualization, and Outlier Detection (HDBSCAN) [122]. The algorithm starts by transforming the space according to density, exactly as DBSCAN does, and performs single linkage clustering on the transformed space. Instead of taking ε value as a cutoff level for the dendrogram, the dendrogram is condensed by viewing splits that result in a small number of points splitting off. This results in a smaller tree with fewer clusters and can then be used to select the most stable or persistent clusters. This process allows the tree to be cut at varying height, selecting the varying density clusters based on cluster stability. The immediate advantage of this are varying density clusters; the second benefit is elimination of the epsilon parameter as it is no longer needed for choosing a cut of the dendrogram. Instead, a new parameter is introduced. It determines minimum cluster size which is used to determine whether points are to be considered as a noise or splitting to form two new clusters. This parameter is much more interpretable and determines the minimum size of clusters to be considered. Nevertheless, by varying the minimum cluster size, the algorithm still cannot clearly separate neurons within the layer borders. Neurons of Layers II and IV usually grouped in two distinct clusters which, however, often protrude into other layers. Also, layers other than II and IV are identified as noise, with smaller clusters sometimes forming in layer VI, confirming the suggestions of neuroanatomy about layer VI having slightly denser distribution of neurons than layers III and V. Visually meaningful clustering was obtained using minimum cluster size in range between 50 and 300 neurons.

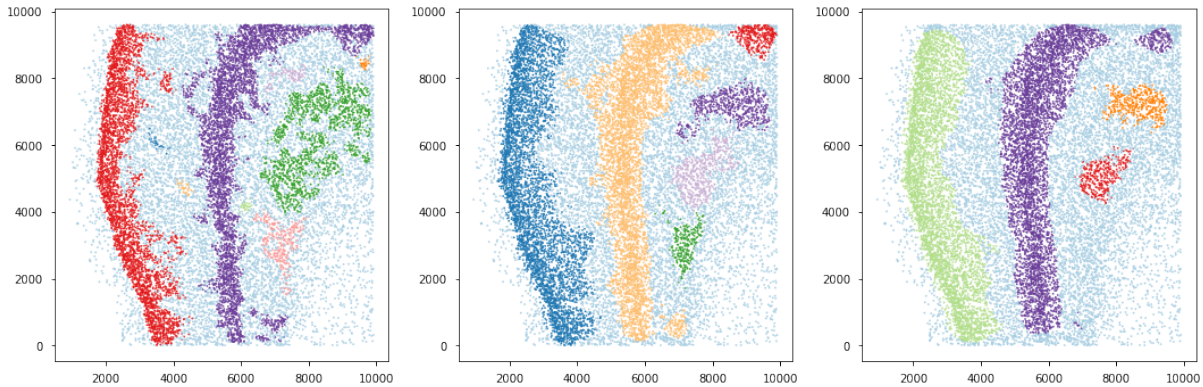

Figure 5.5: HDBSCAN clustering with minimum cluster size of 25, 100 and 250 neurons. Low minimum cluster size yields dispersed and granular clusters. Increasing this value results in clusters being consolidated, with dense clusters expanding into adjacent cortical layers and vanishing smaller clusters. Light blue represents neurons identified as noise.

FSDP

The basic assumption in clustering by fast search and find of density peaks (FSDP) [123], is that the cluster centers are surrounded by other data points which have lower local density. These centers are also assumed to be at relatively large distance from other similar points with large local densities. Therefore, two quantities are computed for each data point i, local density ρ_i,

$$\rho_i = \sum_j \chi(d_{ij} - d_c),$$

where $\chi(x) = 0$ if $x < 0$ and $\chi(x) = 1$ otherwise, with d_c being a cutoff distance, and δ_i

$$\delta_i = \min_{j:\rho_j > \rho_i} (d_{ij}).$$

In other words, ρ_i is the number of points whose distance to the point i is less than d_c, and δ_i is the minimum distance between a point i and the point which has higher local density. The points with high ρ_i and δ_i are then considered as cluster centers and other points are assigned to the same cluster as its nearest neighbor of higher density. Each point i is shown on a decision graph by using (ρ_i, δ_i) as its xy-coordinate, thus obtaining a *decision graph*. The density peaks can then be identified as outliers in the top right region. In our dataset, points with largest ρ values emerged, as expected, in layers II and IV. For smaller d_c distances, density peaks in other layers started to appear. The final clustering, however, cannot identify regions of similar density. Depending on d_c, cluster centers that emerge in areas of very high neuron density have large range of influence, due to the way points are assigned to the clusters, which results in clusters spanning across multiple layers. In other words, if d_c is large, cluster centers will be found mostly in layers II and IV, and neurons in all other layers will be assigned to clusters with centers in the two dense layers. Reasonable clusters started to emerge with the $d_c \approx 300\mu$m. Conversely, if chosen d_c is small, cluster centers will appear in all layers, with very granular clustering obtained with $d_c < 100\mu$m. Although some clusters may consist of neurons from single layer, influence of cluster centers of higher density prevents the formation of clusters with distinct border between the layers. Performance of FSDP algorithm with $d_c = 250\mu$m is shown in Fig. 5.6.

Since choosing the cutoff distance d_c is not straightforward, some algorithms that address this issue have been proposed [124], [125]. However, these algorithms often compute kernels over all data points, which is impractical for very large numbers of neurons. Also, it is questionable whether neurons at large distances should influence measurements of each other.

In conclusion, clustering algorithms were unable to provide satisfying results based only on neuron locations. It seems that the neuron distribution in the cortex is such that their intrinsic

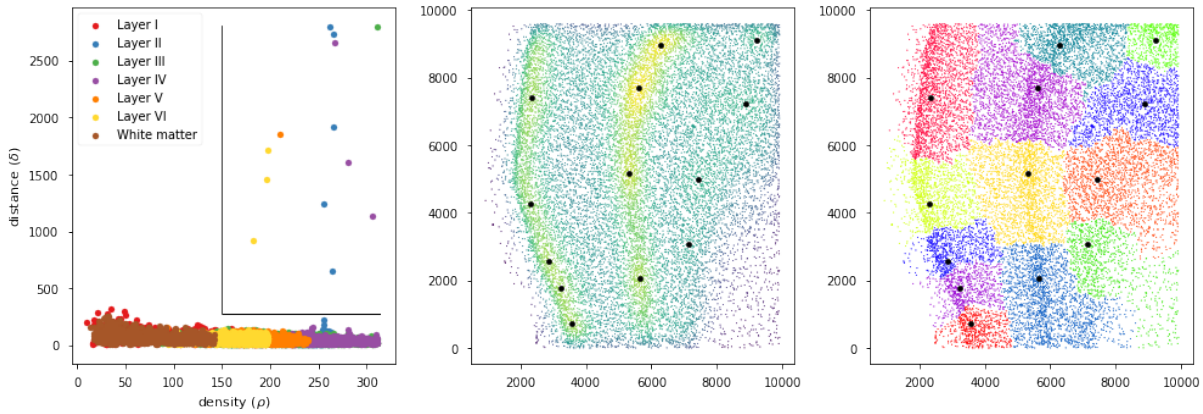

Figure 5.6: FSDP clustering. Left: points with high density (ρ) and large distance from another point with higher density (δ) emerge as outliers in top-right corner of the decision graph. Middle: Cluster centers are formed mostly in the areas of high neuron density. Right: final clustering output shows that the FSDP algorithm is unable to separate areas with different densities and create homogeneous clusters.

clustering structure may not be well characterized by a single set of global density parameters. However, the investigations performed have provided important insight into some of its properties. The algorithms were performing best when considering neurons within the radius between 100μm and 300μm. In terms of numbers of neurons, the algorithms used between 200 and 500 neurons to yield reasonable results. This leads to a conclusion that the changing nature of neuron distribution in the brain is best described when performing measurements in this range.

5.4.2 Individual and regional neuron features

The considerations from cluster analysis lead to conclusion that there are significant improvements to be made and that considering only the neuron locations is not enough for establishing clear delineation of cortical layers. Other characterizations are needed, such as the second fundamental property of neurons, its shape. In this section, other characteristics of neurons are derived from fundamental ones, such as density from neuron locations, or size from its shape. Characterizations are further developed based on either individual properties of neurons, or by using some statistics of properties of neurons in its neighborhood. The focus of this section is development and exploration of the properties that characterize individual neurons and their measurement in different layers.

One of the conclusions that may be derived from density-based cluster analysis is that fixed-size, predefined radius or kernel methods do not possess discriminative power strong enough to discover layers in laminar structure. There are other approaches to measuring variations in neuron density around an individual neuron, such as computing some statistics using a predefined number of its neighbors, rather than all neurons in predefined area. Although the two approaches may seem equivalent, analysis of nearest neighbors has some advantages. For instance, a predefined radius may be interpreted differently, depending on the image resolution.

Also, if it is known that a method is using fixed number of neighbors for each neuron, efficient data structures like kd-trees [126], [127] may be precomputed, enabling faster processing. Considering the large number of neurons found in a histological section, efficiency may be of critical importance.

Neuron measures and outliers detection

From its shape and location, several features were computed for each neuron, including it's area, perimeter, as well as shape descriptors like circularity and roundness. These features form the basis for automated investigations in brain microanatomy. Features like mean, mode and standard deviation of gray value, minimum and maximum gray level were measured but not used in the analysis as these may be heavily influenced by uneven staining across the section. Moreover, features based on gray level and staining, may exhibit different values in different sections, putting in question comparison of measurements made on these sections. However, they were proven very useful in detection of image elements misidentified as neurons. Neuron locations were obtained using the precise method developed in Ch. 3 and segmented using the method from 4, which uses grayscale-guided watershed to separate neurons, rather that distance maps obtained from gray-level thresholding. The two steps provided a binary image of segmented, non-overlapping neuron areas. Combined with the original histological image, the two were used as an input to ImageJ particle analysis pipeline [73] for computation of statistics and shape descriptors of individual blobs which represent neurons in the original image.

By examining the distribution of values obtained in measuring various statistics of neurons' shape, some important conclusions can be made about their distribution across the cortex, and especially with regard to identification of outliers, or image elements that were incorrectly identified as neurons. Values of all shape statistics were examined and neurons with limit values were examined visually in the histological image. Neurons with values at the tails of the distributions were plotted over the histological image to observe the distribution and occurrence of neurons with specific characteristics across the layers. For instance, neurons with largest **area** were found in layer III of the cortex, and were followed by neurons of layer V and layer VI. Out of 50 largest neurons, $42(84\%)$ were found in layer III, $5(10\%)$ in layer V and $2(4\%)$ in layer VI. Out of 500 largest neurons, $266(53\%)$ were found in layer III, $136(27\%)$ in layer V and $60(12\%)$ in layer VI. This comparison confirms that the procedure follows neuroanatomical observations from classical literature, as discussed in Section 5.3. Blobs with area standing out from the other largest values were visually examined and excluded as outliers.

Measurements of variations in grayscale intensity provided important characteristics for outliers detection, and their values were expressed differentially in the cortical layers. **Mean** grayscale value was found low for the neurons in layer IV, but after close visual examination most of them were neurons in group formations, thus creating larger contrast in the image. On

the other hand, neurons of layer VI had lowest individual neuron grayscale value. Neurons with highest mean grayscale values were mostly found in layer I. Measurements of **mode**, **minimum** and **maximum** grayscale values yielded similar results. Neurons with lowest **median** were predominantly found in layer VI, also in layer IV, and in the middle of layer III, sometimes referred to as layer IIIb. Those found in layer IV were usually overlapping neuron or small neuron clusters that grouped together appear darker in the image. No conclusion was made or the reason found for neurons of layer VI having such low individual grayscale intensities. **Standard deviation** of the values was not expressed differentially in layers, but neurons with very low standard deviation were usually found to be artefacts. **Skewness** and especially **kurtosis** had strong discriminative power in identification misidentified neurons. Neurons with values at the tails of the distribution for these two statistics were excluded as outliers.

Neurons with small values of contour descriptors like neuron **width** and **height** were excluded if their shape was less than 4μm in size across the neuron body, a measure determined by von Economo [3]. Values of **Feret diameter**, the longest distance between any two points along the neuron contour, were highest in the middle of layer III (IIIb), and the values of layers V and VI followed. Small Feret diameter is an slight indication to a possibly misidentified neuron. Neuron **circularity** and **roundness** were found the lowest in layer VI - which is known to be made of multipolar neurons with dendrites reaching in many directions. This in another case in which features of automatically segmented neurons reflect the descriptions from neuroanatomy and neuron morphology. **Aspect ratio**, or the ratio of axes of the ellipse fitted around the neuron has proven to be another way to detect outliers - blobs with high aspect ratio were predominantly elongated, deformed blobs, and discarded from the analysis.

Most of the neurons with values at the either tail of distributions for many basic neuron measures were found to be outliers, image elements misidentified as neurons. It is important to identify and exclude such outliers, as they may influence measurements taken on neurons in the area in close proximity of an outlier. The outliers were detected by different measures, usually having extreme values in several of them.

Dependence of nearest neighbors to distance and area

An informative measure that integrates number of neighbors and radius of its neighborhood is to observe the distance from a neuron to it's k-th neighbor. Fig. 5.7 shows how the distances are increasing in different layers. Maximum and minimum values, as well as mean and standard deviation are also shown. Distance to the k-th nearest neighbor increases in varying rates for neurons found in more or less dense layers. Due to the very low density, neurons of layer I and especially white matter have in average larger distances to the k-th nearest neighbor. Conversely, neurons in layers II and IV will find their neighbors in close vicinity, resulting in a curve with lower slope. A property also distinguished between the layers is the mean size of neighboring

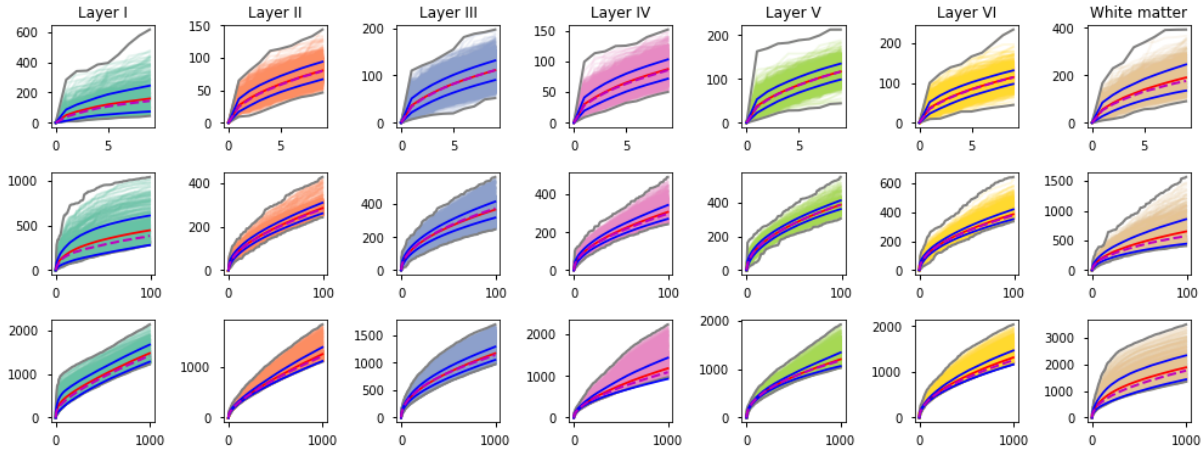

Figure 5.7: Distances to the k-th nearest neighbor for neurons in different layers. Mean (solid red line), median (dashed red line) and standard deviation around the mean (blue lines) exhibit different slope between the layers, depending on the neuron density in the neighborhoods around neurons. Top, middle and bottom row represent distances to 10, 100 and 1000 nearest neighbors, respectively.

neurons. The curves for each layer are shown with shared y-axis in Fig 5.8.

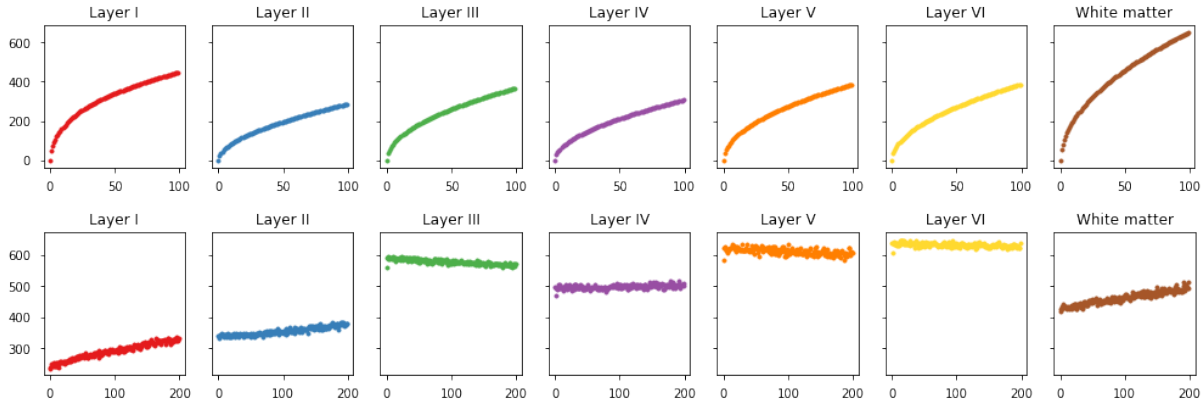

Figure 5.8: Top: mean distances to the 100th nearest neighbor. Curve slope is determined by neuron density - steeper slope indicates larger distances between the neurons. Bottom: mean area of the neurons up to the 200th nearest neighbor.

5.4.3 Measures of neighboring neurons

Observing properties of a defined number of nearest neighbors of a particular neurons has several advantages over observations made in fixed radius, both in interpretability and computational efficiency, as mentioned in the previous section. For the distances to a neurons' k-th nearest neighbor, mean, skewness, kurtosis, bin entropy and other statistics were computed for different values of $k \in [50, 100, 250, 500, 1000]$. To increase computation efficiency, a kd-tree [126] was computed which enabled fast queries on a chosen number of neighbors. For brevity, only some of the features whose changes between layers facilitate their segmentation are shown. Visualization of distribution of features according to layers and with respect to different number

of neighbors used to compute statistics is shown in 5.9.

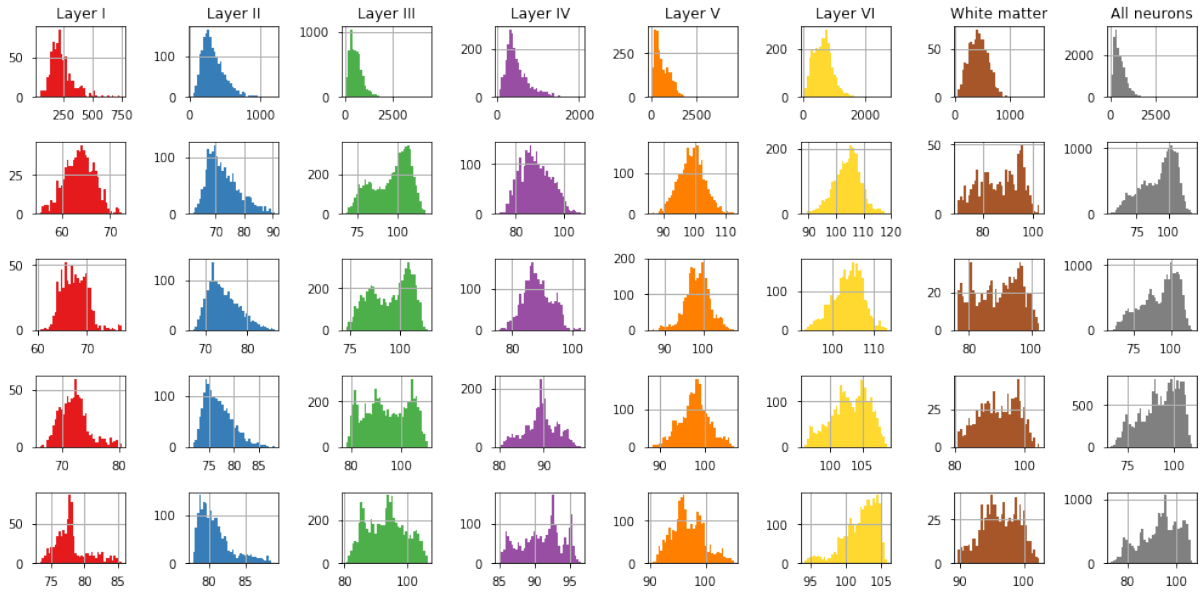

Figure 5.9: Average neuron area for neurons of each layer and for $k \in \{100, 250, 500, 1000\}$ nearest neighbors

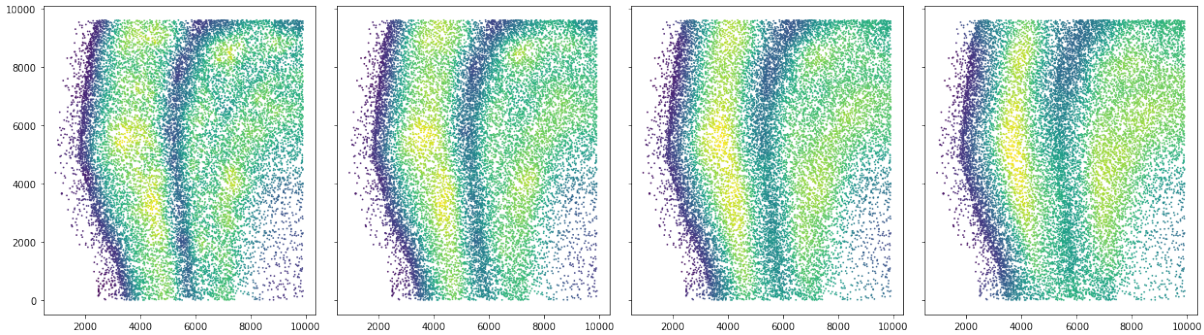

Figure 5.10: Average neuron area for k neighboring neurons, $k \in \{100, 250, 500, 1000\}$

Statistics of other measures were also computer. However, not all are useful for distinguishing neurons within the layers. For instance, neurons with measures related to pixel intensities such as standard deviation of grayscale values or their integrated density (sum of values) were not observed to be distributed with some particular trend but are rather dispersed across all layers. The exception to this is mean or median values, having lowest values mostly in layer VI. Still, the importance of this measure was not shown to be very high. Measures regarding neuron shape like area, circularity or perimeter provided more discriminative power. This is not unexpected, since the findings in classical neuroanatomical research relies to large extent on shape and size of the neurons. In conclusion, measures that were chosen for development of further features were neuron area, perimeter, circularity and median. Densities within a fixed radius dc of 25μm, 50μm, 125μm, 250μm and 500μm were also computed for each neuron and added to this set of features.

5.4.4 Convex hull

Another approach that combines area around a neuron and a number of its neighbors is obtaining a convex hull of its *k*-neighbors. Some simple statistics used to describe the hull of each neuron were used, like hull area, perimeter, average nearest distance for neurons found in the hull and standard deviation of nearest distances. The rationale behind this approach is the assumption that neuron density is reflected through the area contained within the hull, or hull's perimeter.

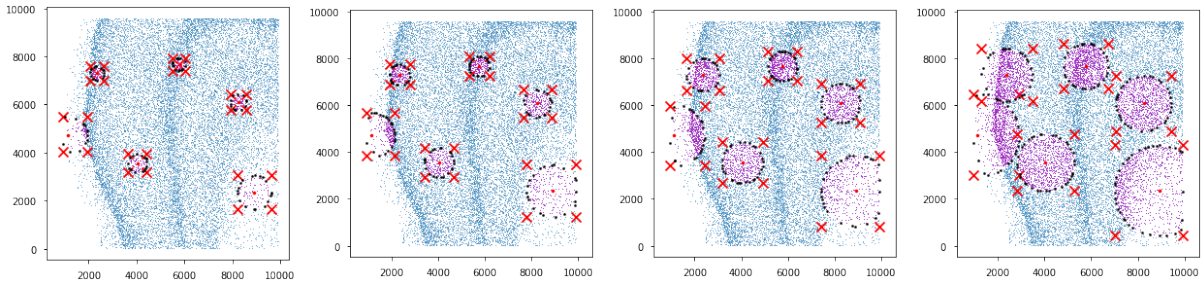

Figure 5.11: Convex hulls of 100, 250, 500 and 1000 nearest neighbors of neurons in different layers.

The spatial distribution of neurons may be quantitatively measured using *nearest neighbor index* (NNI). It is a measure of point distribution which quantitatively describes whether points follow usually subjective patterns of regular, clustered or random distribution. This measure is often used in geography and biology in studying dispersion of settlements or organization of trees in an area. For instance, NNI can be used to determine whether a forest has been planted by humans, in which case the pattern of distribution will be more regular, or has grown naturally, having a random spatial distribution. NNI measures the distance between each point and its nearest neighbor's location. All the nearest neighbor distances are averaged, and if the average distance is less than the average for a random distribution, the distribution of the features being analyzed is considered clustered. If the average distance is greater than a random distribution, the features are considered regularly dispersed. The index is expressed as the ratio of the mean observed distance divided by the expected distance, which is based on a random distribution with the same number of points covering the same total area,

$$NNI_i = \frac{\frac{1}{n}\sum_{j=1}^{n} d(i,j)}{0.5\sqrt{HullArea(i)/n}}. \tag{5.1}$$

The values of NNI are obtained in range of $0-2.15$, with the interpretation of observed values around 1 as randomly distributed points. Points with higher NNI are interpreted as more dispersed while points with lower NNI as more clustered. Fig. 5.12 shows values of NNI computed for convex hulls of neurons in different layers. Neurons in all layers with the exception of layer I and white matter express dispersed distribution, especially neurons of layer IV. NNI is computed for convex hulls containing 50, 100, 250 and 500 nearest neighbors.

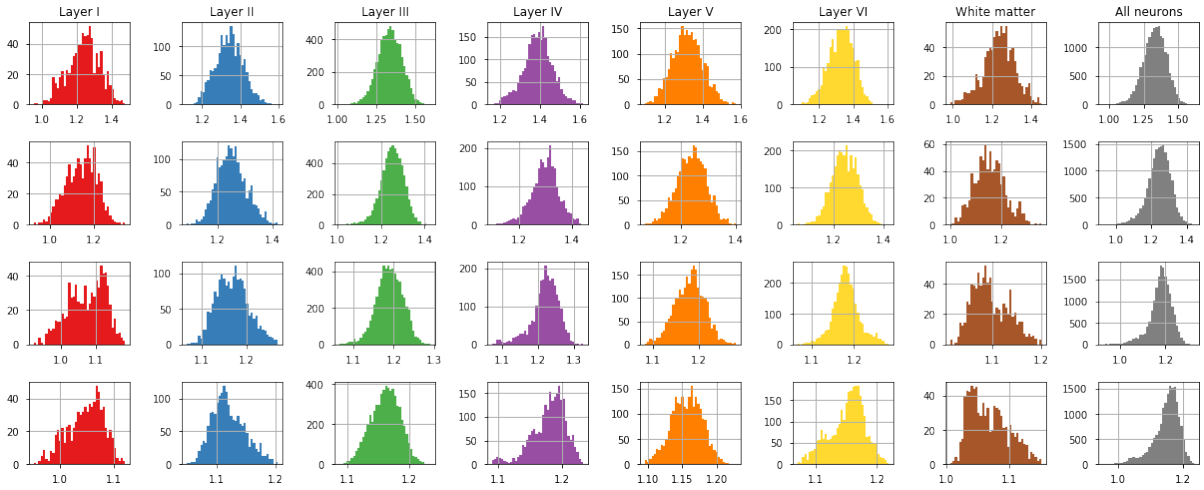

Figure 5.12: Nearest neighbor index (NNI) computed for convex hulls of 100, 250, 500 and 1000 nearest neighbors of each neuron. An estimate of type of organization of cells is given with respect to the NNI value. Neurons in most layers express dispersed to uniform distribution, as opposed to clustered distribution. Neurons of layer I seem to tend more towards random distribution. This is more expressed as larger number of nearest neighbors is considered, indicating that this result may be a consequence of using neighbors from adjacent layer II.

Second-order features

Statistics computed for neurons become neuron features themselves. All the statistics developed in the previous subsection can be used in the similar way as original neuron measures were used, as new descriptors of each neuron, and statistics of these may be computed. However, these *second-order* features did not bring significant advancements in discovery of features important for layer segmentation. The effect of taking a statistic of some other statistic often blurs the details created by original statistic. Also, these features may be hard to interpret from neuroanatomical perspective.

5.4.5 Oriented measurements

Depending on it's position in the cortex, a neuron may be placed more towards middle or more towards the edge of its layer. Features computed around a neuron, whether for a fixed number of its neighbors or in some specified range, may be confounded by reaching into adjacent layer and using neurons with different propertied for computation of statistics. To identify this case, measurements may be bounded and taken only from neurons found within the range of angle. Directing measurements at different angles around a neuron, it is possible to compare measurements made in these *slices*. Such features measured in several directions provide the capacity to identify border neurons and measure changes of neuronal properties. One of the simplest methods to compare measurements made in the slices is to compute their differences.

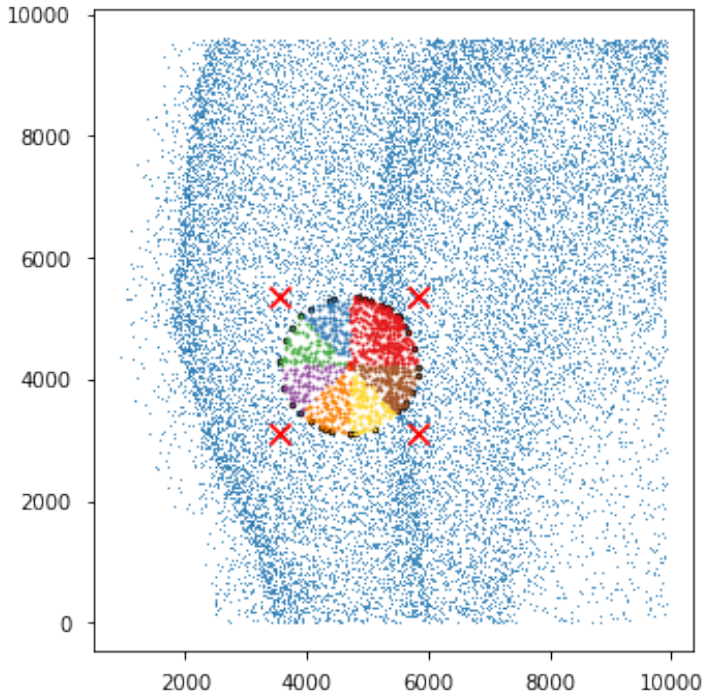

Figure 5.13: Measurements of a neuron's neighborhood may be taken at angle in different directions. These are especially important for neurons at the border of layers, whose neighborhood measurement may vary in different directions, resulting in local heterogeneity of neuron features.

Diversity measures

Slices may be further compared considering their number and the number of neurons found within each slice. They may be regarded as measurement units reaching from a single neuron, each unit representing a population of neighboring neurons found in a given direction from the central neuron. The relationship of different populations within an area has been extensively studied in the frame of biological diversity of species, landscapes and other [128], [129]. Considering the neurons in a slice as members of a single *species*, and the k neighbors of a neuron as the population of all species in their habitat, one may employ several biodiversity measures to evaluate the relationship between the species. In this context, the number of slices is the number of different species, or *richness*, and relative abundance of the different species in an area as *evenness*. These simple measures are commonly combined in order to utilize both aspects of diversity, which are often used and interpreted in association with other aspects of natural habitat [128]. The two most often used such measures are Shannon index [130] and Simpson index [131], who became popular through frequent use in quantitative studies of animal and plant species diversity.

The Shannon index was originally proposed in Information theory to quantify the entropy of appearance of characters in strings of text. In the context of biodiversity, it gives a quantitative measure of the uncertainty in predicting the species of an individual chosen randomly from the

population. The formula for calculating the index may be written in several ways

$$Shannon = -\sum_{i=1}^{R} p_i \ln p_i = -\sum_{i=1}^{R} \ln p_i^{p_i} = \ln\left(\frac{1}{\prod_{i=1}^{R} p_i^{p_i}}\right), \tag{5.2}$$

where R is the number of different species, or slices, and p_i is the proportion of species of the ith type in the population, or proportion of neurons in ith slice to the number of the neurons in k-neighborhood. If all slices have equal number of neurons, p_i values equal $1/R$, and the Shannon index takes the maximum value of $\ln R$. If the numbers are unequal, the weighted geometric mean of the p_i values is larger, which results in the index having smaller values. The index equals zero if the neurons from only one slice are present, since there is no uncertainty in predicting the slice they are in.

The Simpson index measures the probability that the two individuals randomly chosen (with replacement) from the total population will be of the same species. It is defined as

$$Simpson = \sum_{i=1}^{R} p_i^2, \tag{5.3}$$

where R and p_i are the same as in 5.2. This equation is equivalent to the weighted arithmetic mean of the proportional abundances p_i, with abundances used as the weights. The index gives information about the relation of number of types and the presence of the dominant type. Mean proportional abundance of the slices increases with decreasing number of slices and the increasing abundance of the slice with largest number of neurons, the index obtains small values in regions of high diversity like neurons on borders between the layers, thin layers, and especially layer I neurons. The index is large in homogeneous areas like the middle of layer III, where slices reaching from a neuron remain in the area of the layer. Values of the Simpson index are bound between $1/R$, which is reached when the number of neurons in all slices is equal, and unity, reached when only one slice is populated.

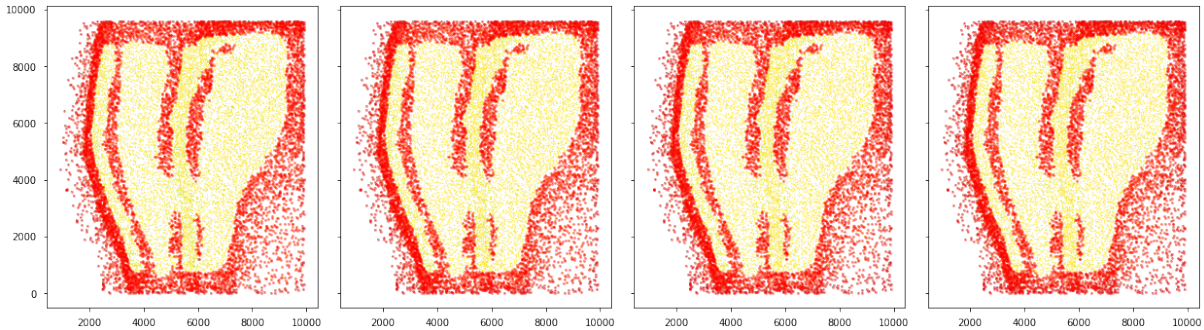

Figure 5.14: Diversity measures. Simpson measure computed for 250, 500, 1000 and 2000 nearest neighbors in 8 directions (slices).

5.4.6 Distance to areas with homogeneous density

Highest-level features of neurons, developed in this section, are related to measurements of distance from a neuron to closest neuron with certain values of previously developed features. For instance, as seen in Fig. 5.2 and Fig. 5.3, neurons of layer I and white matter can approximately be distinguished by having small neuron density in their vicinity. By this, *sparse regions* of the section are identified. In similar fashion are identified the *dense regions* containing layers II and IV. Moreover, the sparse region may further be split using the hull area feature developed in previous section - neurons in white matter will have large hull area, in contrast to the neurons of layer I, whose hull is bound between the border of the tissue and the layer II. By this, layer I and white matter are approximately identified. It is not a definitive and final classification of neurons in these layers. Some neurons may have been omitted, for it is important to be restrictive when identifying neurons in these regions, since misidentification of a single neuron of, for instance, layer III for neuron of layer I has a significant impact on the whole region of the digitized slice. Neurons of white matter may further be split by their distance to the sparse regions and hull area into sulcal and gyral neurons, since there is an apparent bimodal distribution of these features. Distances to these areas are used as high-level neuron features. Dense region may be split into layer II and layer for using the *distance to layer I* feature. Neurons of layer II will have smaller distance to layer I than those of layer IV, since there is the wide layer III separating the two dense layers. Finally, taking into account results from clustering analysis and the experience with the neuron features developed so far, standard deviation and mean of 250 nearest neighbors' distance to sparse and dense regions were added to the feature set for each neuron in the section. Some results from development of these features are shown in Fig. 5.15. An example of feature developed by computing statistics of distances is shown in Fig. 5.16.

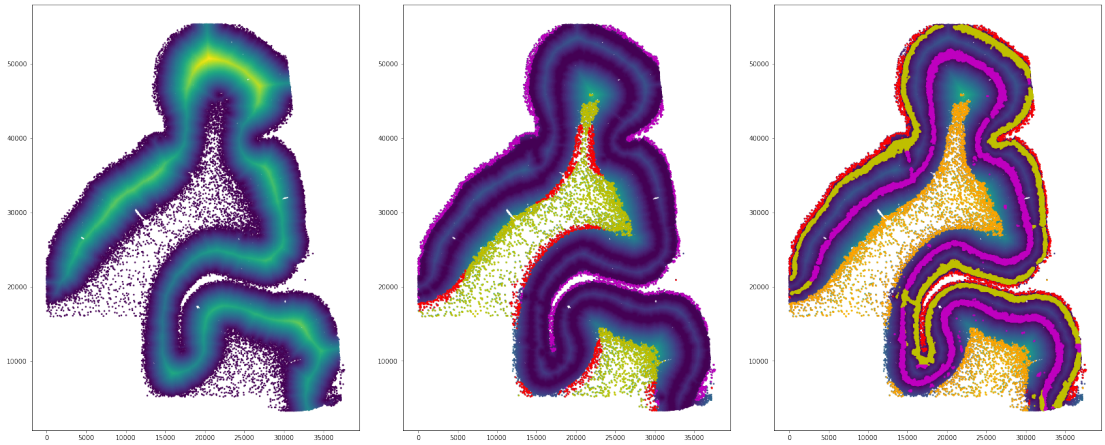

Figure 5.15: Developed high-level features based on several statistics are used for estimates of layer positions. Left: map of distances to sparse regions. Middle: Sparse regions are split into layer I and white matter regions, in which sulcal and gyral neurons are identified. Right: final output of the 4-region segmentation.

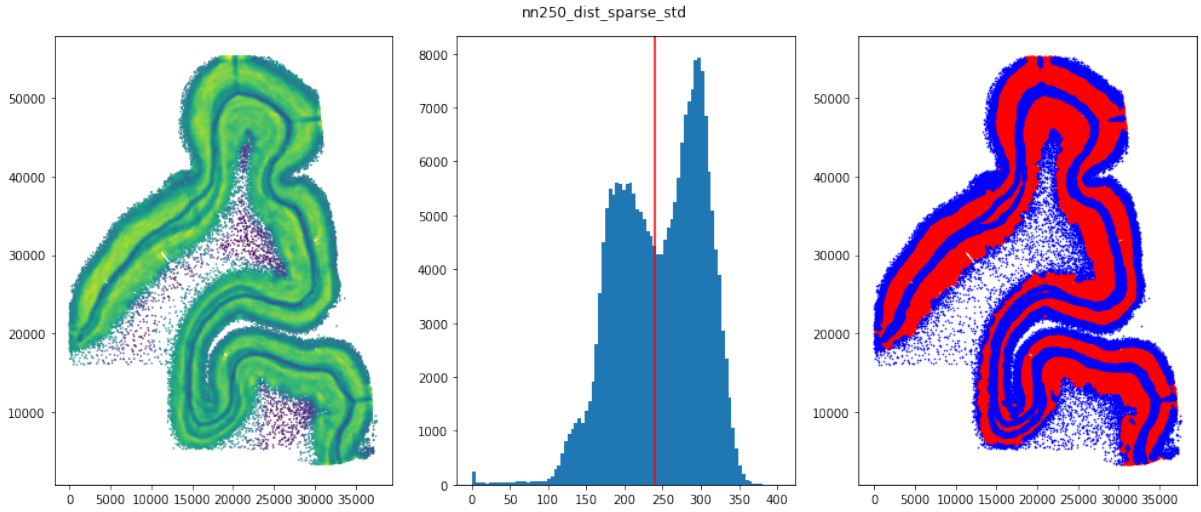

Figure 5.16: High-level features reveal cortical structure. Shown here are value map, histogram with interclass minimization value and according segmentation based on standard deviation of distance to the sparse regions for 250 nearest neighbors of each neuron.

5.5 Relating neuron features to cortical layers

The extensive feature set developed in the previous section provides informative descriptors of cortical organization. However, no single feature was found that would be able to provide clear segmentation of cortical layers. Although some features were clearly more expressed in certain layers than the others, it is not straightforward what exactly is changing between the layers as well as the impact and interconnection of different features. This leads to an assumption that there are information contained in the developed features that can be analyzed, combined and used to produce precise classification of neurons with regard to their location within the cortical layers.

The goal is to *learn* how to use the developed features to classify neurons and produce segmentation of cortical layers. In this section, supervised machine learning methods guided by manual segmentation of layers are used to investigate feature importance, create models that predict the neurons' layers and finally produce the segmentation of cortical layers on the whole histological section.

5.5.1 Dataset of manually labeled cortical layers

A portion of the histological preparation of human prefrontal cortex was given to three human experts who manually delineated borders between the layers in the cortex. The apparent inconsistencies and mutual disagreement between the experts on where to draw the boundaries shows the presence of experts' bias. As shown in detail in Fig. 2.10 and Table 2.1, the agreement of all three raters may be as low as 8.6%, for the thin layer IV. The experts' agreement on the neurons found in the layers is shown in Fig. 5.17.

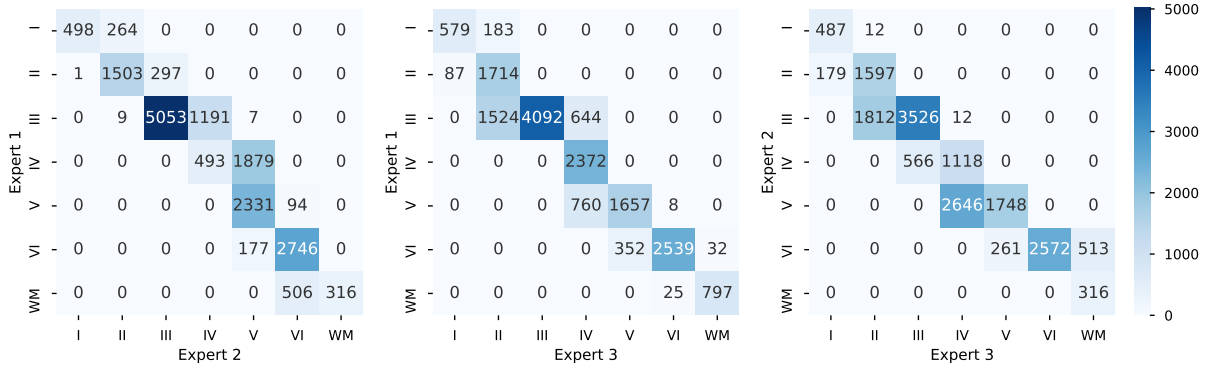

Figure 5.17: Agreement comparison for the three experts.

More detailed display of the underlying tissue properties that the experts were focused on is shown in Fig. A.4 and Fig. A.3 of Appendix A. The experts disagreed on the boundaries of all layers, with the exception of the very apparent layer I/layer II boundary. Cortical layers as delineated by the experts are shown in Fig. 5.18. As it is often the case with research in biological sciences, especially when dealing with human specimens, the amount of data available for use as baseline in this doctoral research was very limited, which is an important factor when choosing appropriate learning methods.

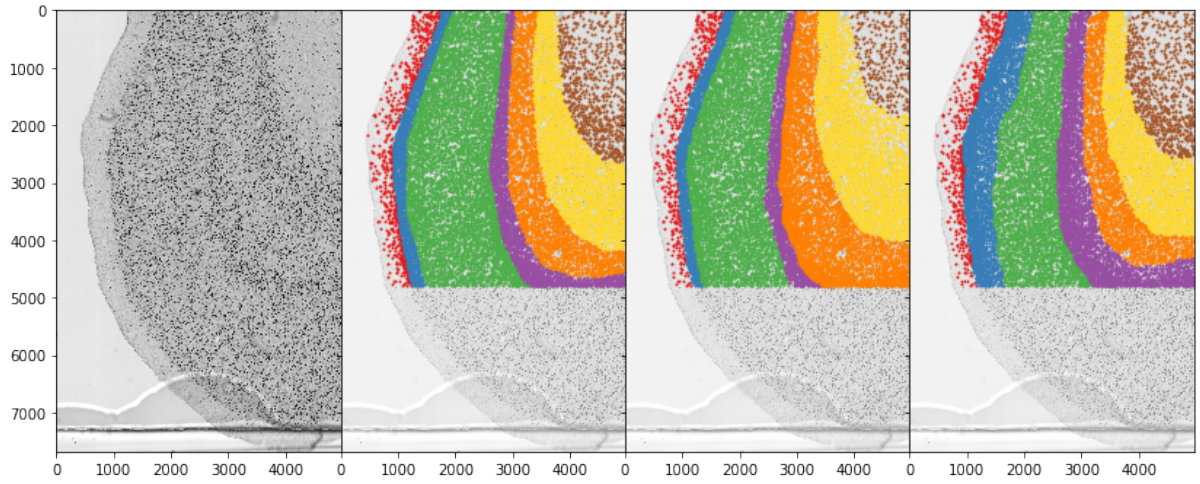

Figure 5.18: Cortical layers as delineated by the experts. Significant disagreement on the boundaries of the layers can be observed, as well as on the boundary between the cortex and the white matter.

5.5.2 Machine learning models

Reviewing the literature on machine learning [132], [133], decision trees were chosen as the method for prediction and interpretation of cortical lamination for its several advantages, being a state of the art for the prediction problems with tabular style input data such as neuron features. Decision trees require no data preparation and neuron features developed in previous section can be directly used as input for learning. They also need not be scaled or normalized, since

decision trees do not require data normalization, as is the case for many other methods such as clustering methods or neural networks. Another important characteristic is good performance without large training data and application on large datasets using standard computing resources performed in reasonable time.

Besides being a successful and widely-used, decision trees are simple to use, interpret and understand. They can easily be visualized, the rules used for splitting nodes can be examined, input features analyzed using built-in feature selection and importance measurements, and the results can easily be interpreted and communicated even to non-experts [134]. This was a desirable property, since this doctoral research is not only oriented towards parcellation of cortical layers but also to understanding what tissue features cause the parcellation.

Decision trees mirror human decision making more closely than other approaches [134], which is especially useful when modeling human activities, such as manual delineation of cortical layers, a straight example of decision-making process based on combination of several information about neurons' characteristics.

Tree classifiers

Learning method used for initial training and prediction of neurons' layers was decision tree classifier. Experiments were performed using scikit-learn [135], a Python library. Using stratified k-fold, the tree classifier was able to achieve 85% cross validation score. However, not all neuron features have proven useful and informative for the classifier, many of them having feature importance measure of 0. Moreover, reducing the number of features used has shown increase in model's performance, which was able to achieve cross validation score of approximately 90%. Validation curves for the two cases are shown in Fig. 5.19.

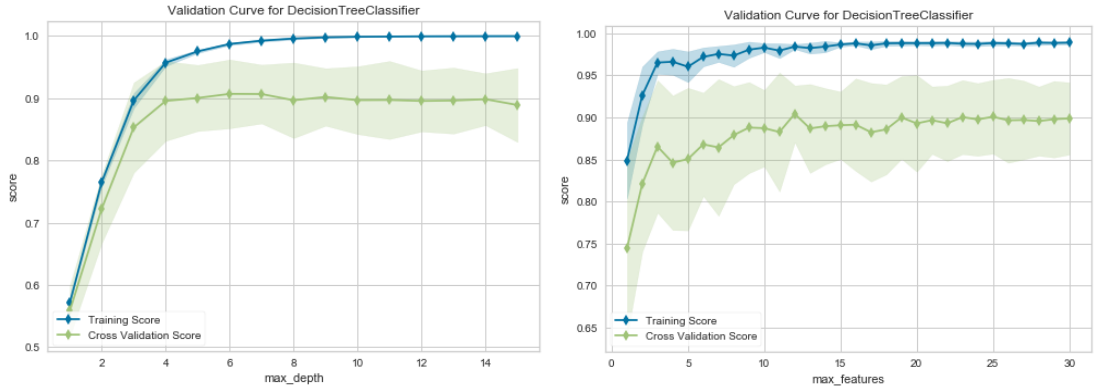

Figure 5.19: Validation curve for a single decision tree. The model was able to achieve better performance using a smaller number of selected high-level features.

Experiments with different sets of features have shown that although some combinations of features do achieve high accuracy on training data, that does not guarantee that the model will perform well on the whole histological section. The introduction of features based on distance

to sparse or dense regions has significantly improved model's ability to separate regions of the sections into parcels following the laminar layout of the cortex. However, a simple tree learner was not able to comprehend the variations of the neuronal features well enough to be able to generalize to the whole histological section.

Ensemble learning

A process by which multiple models are strategically generated and combined to produce a model with improved performance is known as *ensemble learning*. To obtain more accurate predictions, ensemble methods were used since they provide better predictive performance than could be obtained alone from any of the algorithms that constitute the ensemble. An ensemble-based system is obtained by combining several learning models to improve overall stability and predictive power. The assumption is that several weak classifiers may be combined into a single model which achieves much better performance. In other words, if each classifier makes different errors, then a combination of these classifiers can reduce the total error, which is a concept similar to low pass filtering of the noise. If decision boundaries of classifiers used in an ensemble are adequately diverse from each other, such a set is said to be diverse. Classifier diversity is most often achieved by training the members of the ensemble on different training datasets, which may be obtained from original dataset by re-sampling techniques such as bootstrapping or bagging. Data subsets are randomly chosen from the entire dataset, usually with replacements. Using weaker or more unstable classifiers ensure that individual decision boundaries are adequately different, even though data samples used for training originate from the same original dataset and are substantially similar. Small perturbations in the data or training parameters of such classifies yield sufficiently different decision boundaries [136].

One of the earliest publications on ensemble systems appeared in 1970s, when an ensemble of two linear models were presented, one fitted to the original data and the other to the residuals [137]. Authors in [138] proposed a partitioning of the feature space using several classifiers. In the year 1990, it was shown that generalization error of neural networks may be reduced by using an ensemble of neural networks [139]. During the same year it was proved in [140] that a strong classifier in probably approximately correct (PAC) sense[141], can be created by a combination of weak classifiers through a boosting procedure. Since, the use and research in ensemble systems have rapidly expanded, showing the improvement in predictive performance over single predictor models [142], [143].

According to [144], there are three primary reasons for using ensemble methods: statistical, computational and representational. The statistical reason stems from the fact that very often the amount of data available is too small compared with the size of hypothesis space. Therefore, the algorithm can converge to many different hypotheses that achieve similar accuracy on the test data. By combining them into an ensemble, the risk of choosing the wrong hypothesis is

reduced. The computational reason is related to the problem of model selection. An ensemble constructed by models that are run from different starting points may provide a better approximation of the unknown distribution of the data. The third, representational reason is the ability of an ensemble to expand the space of representable functions, if the true function cannot be represented by any function in hypotheses space.

To produce more precise segmentation of cortical layers through accurate prediction of neurons' layers, decision trees were combined using gradient boosting method, a well-known and widely used approach [145], [146]. Specifically, XGBoost (extreme gradient boosting) [147], a popular and efficient open-source implementation of the gradient-boosted trees algorithm in Python was used. This method was able to achieve accuracy of 1 on training data, with different subsets of features which, again, not all provided good generalization to the whole sections. The best results were obtained when combining the output of all three raters. Gradient boosting model was trained for each rater using `softmax` objective. The output probabilities were then summed, and the final prediction was made. Results of this approach are shown in 5.20, together with the probability map of the model's output. Classes of neurons are predicted, and neurons grouped in a way that follows laminar pattern of the cortex. This was achieved using only high-level features like oriented measurements, distances from areas of homogeneous densities, and also deviation and mean of these distances. Investigation of the impact of features on prediction of class was performed on both global (whole model) and local (individual neuron) level.

5.5.3 Analysis of individual feature attribution

For deeper understanding of both the model and the data that is being used for making predictions, interpretation of the results beyond accuracy and overall performance is needed. To that end, of great importance is to understand the impact of each feature that is used for making predictions in models such as ensembles by evaluating the importance values that are attributed to each input feature. These importances can be computed for the entire dataset explaining the overall behavior of the model (global), or for a single instance (individual). Global interpretability gives insight into the the relationship between features and the predicted values for the entire dataset, providing a sense of the magnitude and direction of the impact of each feature on the predicted value. On the other hand, interpreting features locally enables evaluation of the impact of each feature on the predicted value for a single specific observation.

There are four typical global feature importance measures used for most tree-based systems: (i) weight, or the number of times a feature is used to split the data across all trees [147], (ii) cover, or the number of times a feature is used to split the data across all trees weighted by the volume of training data that goes through these splits, (iii) gain, or the average improvement of the model in sense of reduction of training loss when the particular feature is used, introduced in

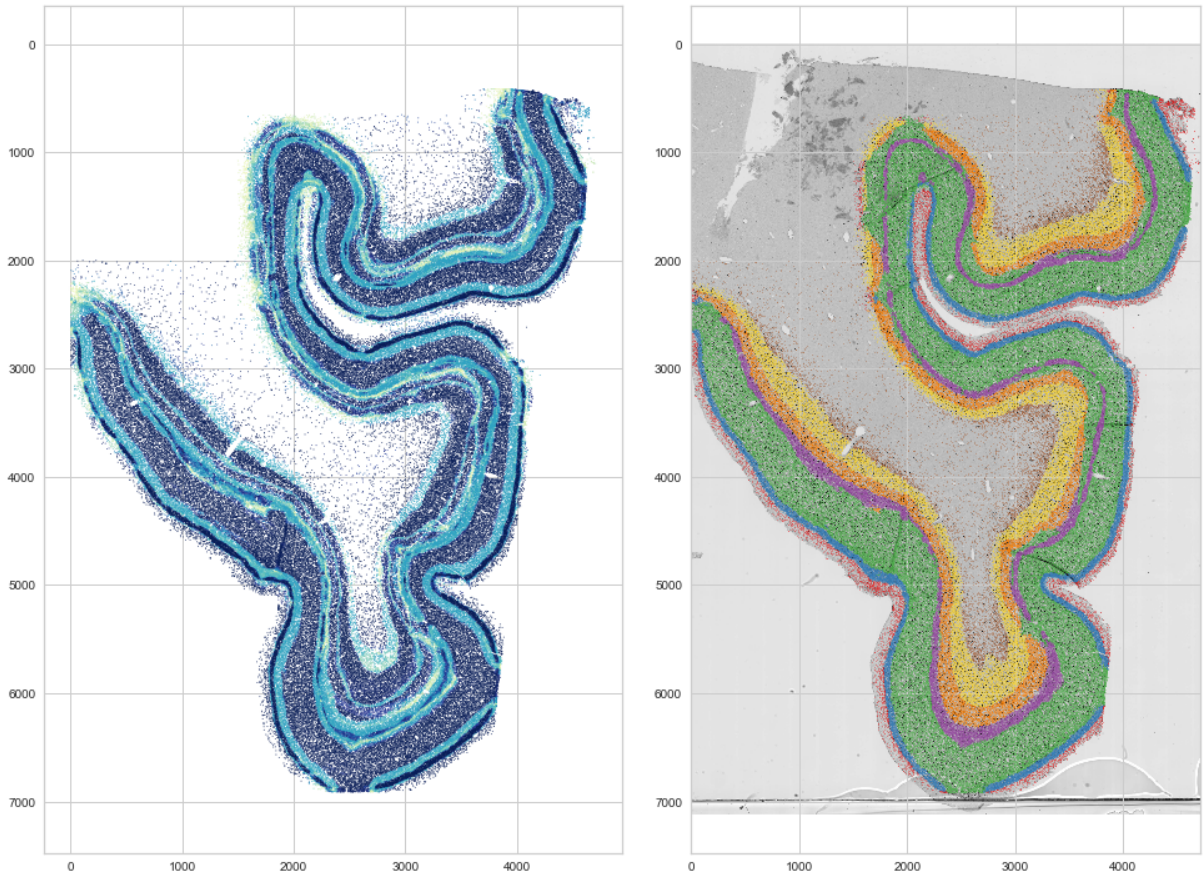

Figure 5.20: Final output of gradient boosting learner with confidence map.

[148], and (iv) permutation, which is measured by introducing small perturbations in the feature values which will, according to the importance of the particular feature, reflect on the model's error [149]. However, methods for computing feature importances for individual predictions are less established for trees. Although individualized model-agnostic methods exist [150], [151], [152], and can be applied to trees [153], they are much slower than specific methods. It seems that the only currently available methods are by Sabaas [154] and the SHAP method [155].

It is not straightforward to determine which of these importance measures to use when interpreting a learning model. However, two properties that are reasonable to expect from a model explanation method are *consistency* and *accuracy*. A method is said to be consistent if the importance estimate of a feature cannot decrease if there is a change of the model such that the model relies more on that feature. The accuracy property states that the sum of all the feature importances should equal the total importance of the model. By analyzing the measures i-iv, and the Saabas and SHAP measures, it can be concluded that SHAP, Saabas and gain satisfy the second property. Furthermore, all the measures considered are proven to be inconsistent, with the exception of the SHAP method [155]. It means that it is the only reliable method for measuring feature importances, which is an important observation to make.

Therefore, the SHAP approach proves optimal for estimation of neuron features that fa-

cilitate neuron classification and cortical segmentation. Importances of the features used for training the ensemble model in the previous section are shown in Fig. 5.21.

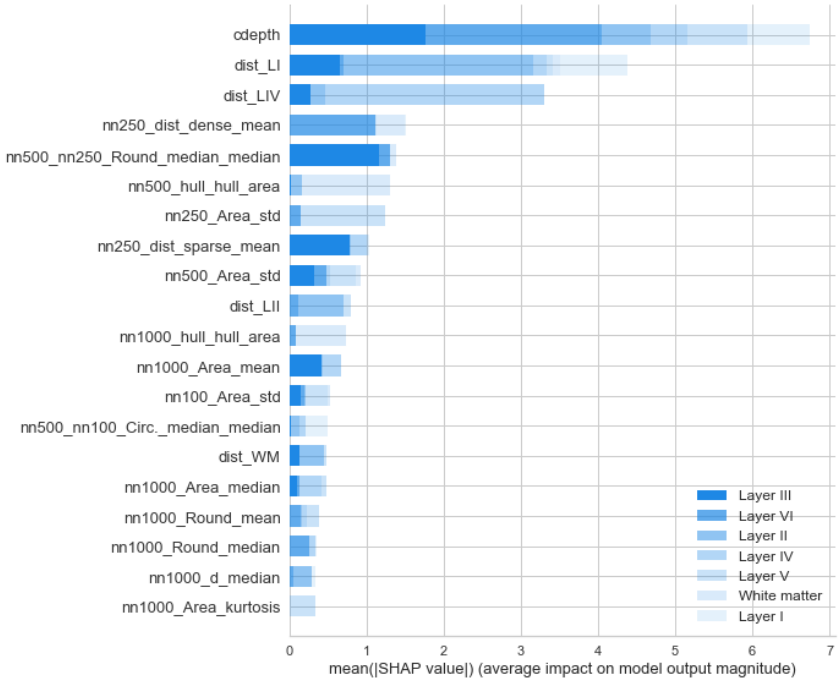

Figure 5.21: Importance of neuron features in SHAP analysis.

Important aspect of this approach is the measurement and visualization of features that contributed to making a prediction on a single instance of the data. Fig. 5.22 shows which neuron features of a single neuron of layer VI contributed to increase from the base SHAP value and making the prediction. The image also shows the importance of features that decreased the output value for prediction of the same neuron as a white matter neuron.

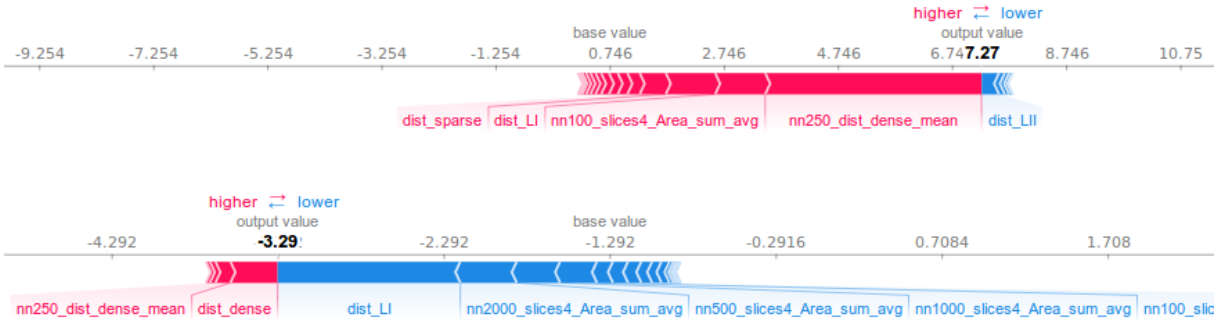

Figure 5.22: Contribution of different features for making a prediction of a neuron's layer. Top: neuron features of a single neuron of layer VI that contributed to increase from the base SHAP value and making the prediction. Bottom: the importance of features that decreased the output value for prediction of the same neuron as a white matter neuron

5.5.4 Comparison with human experts

On labeled data, single tree model was able to achieve accuracy of over 0.90, and ensemble methods achieved accuracy of 1. However, it is important to consider ability of the learning models to classify neurons in context of inter-rater variability. Average agreement between two experts on labeling neuron classes was 0.7549 ± 0.0485 for sparse 2.10 training dataset and 0.8090 ± 0.0487 for dense 2.11 dataset. A comparison was made with single-tree classifier and XGBoost ensemble method trained on dataset made by combining data from three experts into one and then gave predictions for each individual expert. Data was split in 75% training and 25% test subsets. Both models offered better average agreement than human experts, with single decision tree achieving 0.8683 ± 0.0397 accuracy for thin section and 0.8941 ± 0.0486 for thick section. Accuracy of XGBoost was 0.8712 ± 0.0420 for thin and 0.8937 ± 0.0420 for thick section. The two models were also trained separately on datasets provided by the experts with probability of each class as the output. Predictions were then combined and by this provided and ensemble-like prediction for test data. Again, learning models offered better average agreement than human experts. Combination of three single decision trees achieved 0.8228 ± 0.1081 accuracy for thin section and 0.8388 ± 0.0943 for thick section. Accuracy of XGBoost was 0.8724 ± 0.0419 for thin and 0.8967 ± 0.0465 for thick section. It is noticeable that XGBoost offers better classification accuracy than single tree methods, and creating another ensemble from three different dataset achieves slightly better accuracy than a single model trained on the dataset created as a combination of three dataset provided by the experts.

5.6 Conclusion

This chapter presented a novel framework for analysis of laminar structure of the cortex. From the location and basic measures of neurons, more complex features were developed for use in machine learning models. Tree ensembles, as today's one of the most powerful and interpretable models were used on data manually labeled by three human experts. The most accurate classification results were obtained by training three XGBoost models separately on three datasets provided by the experts and creating another ensemble from the three, combining their probability outputs for final neuron class prediction.

Measurement of importances of developed features for on both global model level and individual prediction level was performed using SHAP values, an only possible consistent and accurate method for assessment of individual feature attribution. Features of the highest level were proven to have the largest importance. This is because they integrate low level feature with anatomical observations, and have a wide reach across the histological section. Features based on oriented measurements, or slices, had considerable feature importance, being able to identify neurons on the border of layers and help towards more accurate classification. It was

shown that building on lower-level features by computing some statistics or combining them in some other way yields features that have greater discriminative power and thus greater measured importance. This is probably because of their capacity to overcome local variations in neuron features and taking, for instance, mean of those features. In contrast, using very local features or measures of a neuron like, for instance, its area, there is no increase in accuracy of prediction of the neuron layer, this features often having importance of 0. This is probably why different methods for local pattern analysis and classical image feature extraction methods are not very successful in cortical layer analysis. In this chapter, an event radius was established, giving an estimate of the size of the neuron's neighborhood in which measurements should be made in order for it to be large enough to avoid local variations in neuron distribution and recognize its location within the cortical structure on one hand, and narrow enough so that measurements made are not confounded by reaching too far into adjacent layers.

During experiments with different models and combinations of datasets, it was noticed that parts of layer III and layer VI are sometimes divided into sublayers that follow the direction of laminar structure, although being very short and not extending through a significant portion of the slice. Further investigations using the developed methodology may provide more detailed insight into sublayering of cortical structure.

Chapter 6

Conclusion

In modern neuroscience, investigations in brain cytoarchitectonics and functional neuroanatomy are still based on histological results from century ago, which were obtained using microscope, manual drawings and crude apparatus available at that time. Significant technological and methodological advancements have been made since, and much more data is available today through digitalization and computerization of investigations in histology which enables high-resolution scanning and sharing of histological data. However, in light microscopy, neuron counting, and especially cortical layer segmentation and cellular-level analysis are still in domain of manual work of researchers.

The objective of this research was development of computational methods for automatic and objective analysis of histological images of human brain suitable for advanced and fast analysis of brain cytoarchitecture and laminar structure. An integrated approach was developed, which combines quantitative analysis of neuronal distributions with exploration of underlying principles of variation that facilitate parcellation of cortical layers. The methods were developed aiming for a completely data-driven approach, with as little assumptions about the data as possible. Focus in development of the methods was to recreate the human performance as close as possible, given the natural inconsistencies in manual labels provided by the experts. Through analysis and comparison of experts' performance we have addressed the question of correctness and existence of true baseline in such tasks.

Most of the nowadays automatic methods for analysis of histological sections of the brain are focused on fluorescent imaging, as it provides better three-dimensional insight in cellular structure. However, analysis on a large scale is not possible with fluorescent imaging because of its narrow field of view in observation of histological specimens. There is a lack of methods for precise, detailed and fast analysis of brain cytoarchitectonics for bright-field microscopy imaging. Recently published bioRxiv paper [72] shows results of inferring laminar hierarchical structure by analysis of cellular features obtained from fluorescent histological preparation of mouse cortex which suggests the demand for development of new methods and increasing

interest towards research in this area.

6.1 Scientific contributions of doctoral research

Computational method for detection and classification of neurons in histological images of human brain.

This doctoral research presented a new, precise and fast method automatic detection of neurons in histological sections digitized in high resolution. The method is based on edge-preserving anisotropic diffusion, and the two are the cornerstone for scientific contributions developed through this doctoral research. The method is developed using the dataset obtained from three experts in neuroanatomy and was proven to produce results of high precision, indistinguishable from the performance of the experts. However, the method is consistent, providing the same results on repeated data and uses the same criteria for identification of neurons on all available specimens, thus removing otherwise significant bias present in manual labeling. The automatic method was used to provide seed points for the watershed algorithm which used anisotropically diffused images, providing better results than watershed using original images or using morphological distance maps. Neuron bodies had significantly less local grayscale intensity variations which resulted in smoother boundaries and precise neuron segmentation. This segmentation was used for estimation of neuron location in three-dimensional context, within stack of images produced by scanning the histological section in multiple optical planes. Neuron segmentation was used to compute the initial measures of neurons like their shape and intensity measures.

The method was used on BigBrain data as an example of extending its use to other staining methods and application on large-scale data. During the experiments, it was noticed that out-of-focus scans influence its performance. The important image elements like edges may be heavily degraded and information about delineation of neurons, especially overlapping, is already lost beyond recovery, and it is recommended to repeat the scanning process. This scanning artefact was reported to the group that performed the digitization of histological sections.

Computational method for segmentation of cortical layers in histological images of human brain.

The goal in development of this novel method was not only to produce parcels of brain areas and label them according to their layer, but also development, investigation and interpretation of neuron features that have the most impact in facilitating the automatic segmentation. Moreover, to my best knowledge, this is the first *bottom-up* approach in analysis of brain cytoarchitecture, one that builds from the cellular level and infers about larger structures based on features of individual neurons, thus creating a new methodology for brain research.

Initial research in parcellation of the cortex using neuron density and body area presented

how the two features, unevenly distributed among the neurons in different layers, reveal laminar structure. They alone were not enough for precise delineation of the layers, or for more detailed investigations in distribution of neurons. Density-based clustering methods were also unable to provide satisfying results. However, they provided an intuition for further investigation, by identifying the radius of $100-300\mu$m around the neuron which is significant for estimation of its features, establishing a radius of measurements sufficient for capturing subtle changes in the brain. It usually included 200-600 nearest neurons.

More than 300 features of neurons were developed and analyzed in several feature classes. The most successful were those based on density and area of the neurons, but also those derived from them by computing different statistics and performing oriented measurement taken in different directions from a neuron. Very high-level features proved the most important for prediction of neuron's position within the cortical layers. Area of the hull of k closest neighbors was shown to help discriminating between the neurons of layer I and white matter, since the former are located between the edge of preparation and layer II, which prevents areal expansion of the hull. These were used for obtaining information about the cortical depth each neuron was at, and yielded an important feature that significantly improved the final classification. It is also an example of how traditional neuron descriptors can be combined with new, engineered features to facilitate distinction between the neurons contained in different layers. Through measurements of nearest neighbor index, it was concluded that neurons in our data tend more towards regularity and uniform spatial distribution than formation of small clusters.

The developed features were used in an ensemble learning model which was able to learn the underlying structure of neuron distribution in the layers and create accurate predictions of neuron classes. The most accurate classification results were obtained by combining tree ensemble methods. Three XGBoost models were trained separately on three datasets provided by the experts and combined into an ensemble, combining their probability outputs for final neuron class prediction. Through analysis of feature importance it is possible to obtain more detailed insight into laminar structure and what neuron descriptors contribute to classification within six cortical layers and white matter.

Publicly available database of original and expert-annotated histological images and procedure for evaluation of neuron detection and cortical layer segmentation methods.

One of the steps towards unification of automatic methods is a database of manually labeled neurons and cortical layers. Using such a database, the existing methods can be tested and compared and new ones developed faster, making them more visible and available in the scientific community. A database, endowed with procedures for evaluation of method performance makes a platform for development of methods for histological image processing, the third contribution of this research. Neurons and layers were manually labeled by three experts, and an evaluation procedure that combines labeled data was developed, providing the capacity of the database to

inform about the inter-rater variability. The database will be continually expanded with more samples and various methods through continued work on this research.

The developed library for analysis of histological features provides a broad range of functions for computing hundreds of different measures of neurons in a histological section. The methods are easily expandable for further investigations and development of new tissue features. Particular emphasis was placed on data visualization functions for better insight into details of feature development and selection.

6.2 Guidelines for future research

The scenario of using the developed methods was described on a particular brain region and a limited set of manually labeled neurons and cortical layers. Future investigations will be based on further expansion and utilization of the developed methods in different brain regions, cell populations and histological sections prepared using different staining methods, with the goal of better understanding the laminar structure of the cortex.

The presented methodology for modeling the brain cytoarchitecture provides good framework within which further research should be conducted, one that considers the specificity of different brain regions and stainings and which enables the emergence of new, better description and understanding of the brain structure in different areas and stages of development through processing of ever larger amount of histological data available today in global research centers.

Appendix A

Visualization of neuron features

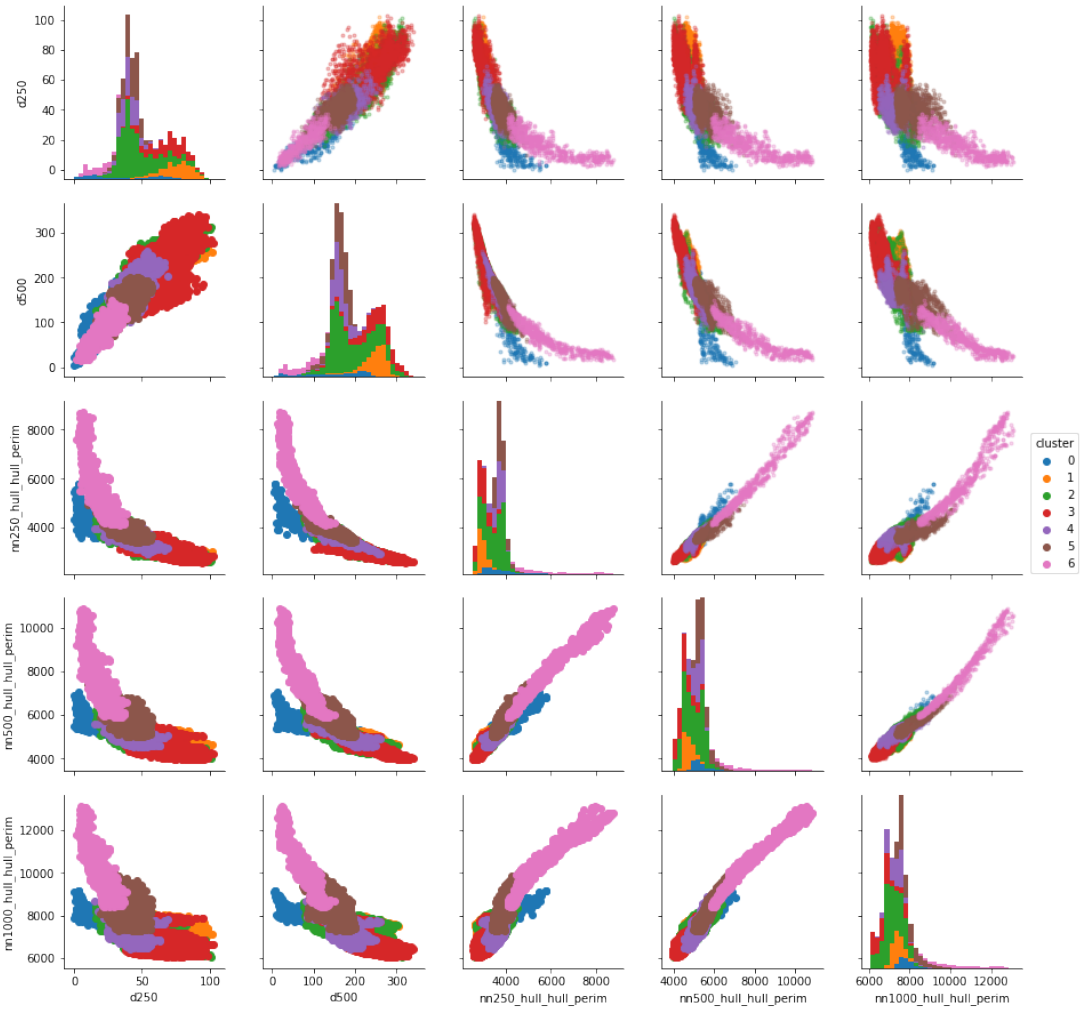

Figure A.1: Pairgrid of neuron features related to local density and size of the convex hull. Cluster numbers represent layers from layer I (0) to white matter (6).

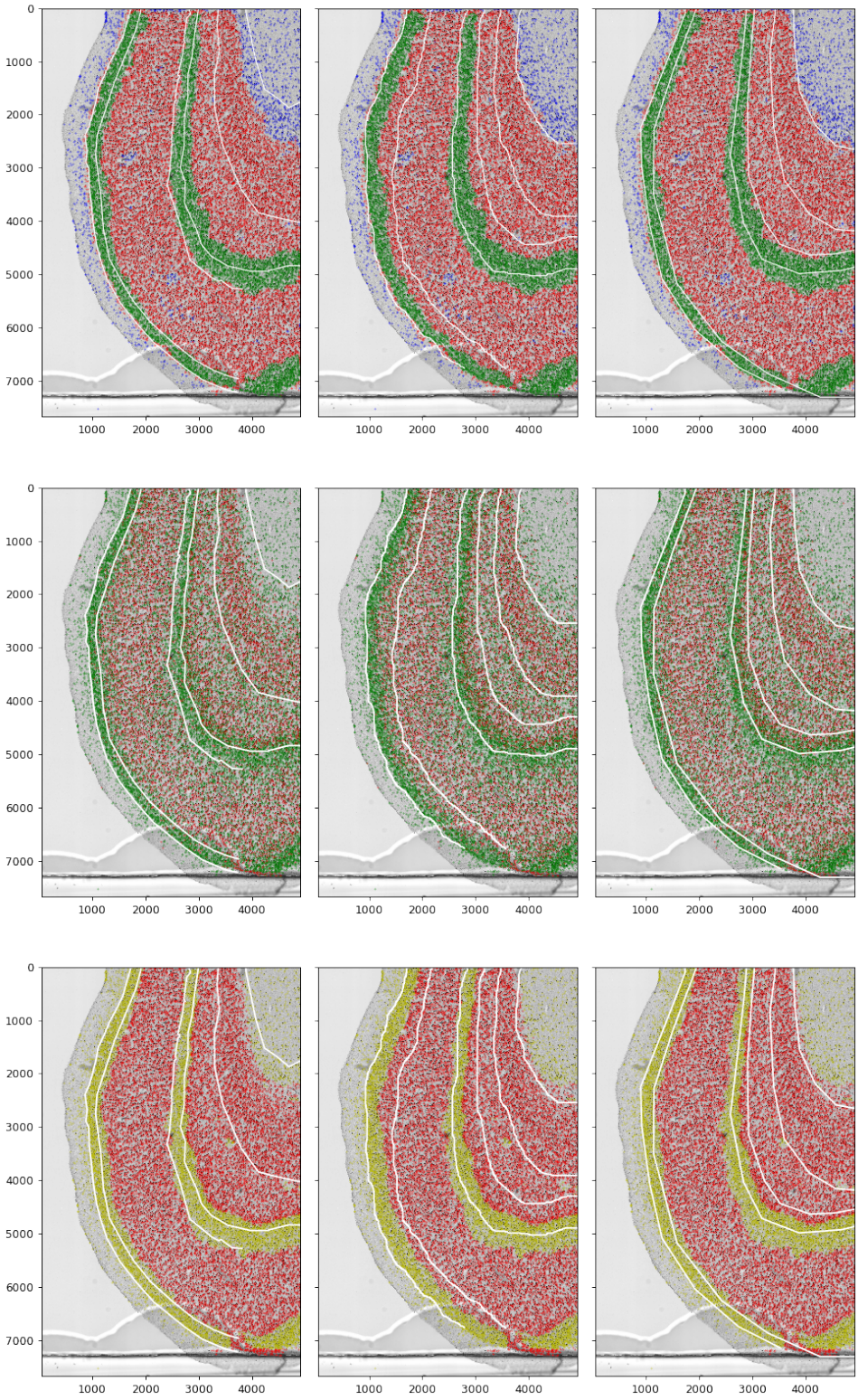

Figure A.2: Ability of experts to capture changes in density and size of neurons in cortical layers on thin tissue dataset with sparse neuron population revealed by minimization of intraclass variance for neuron density (top), size (middle) and average neuron neighbor size (bottom).

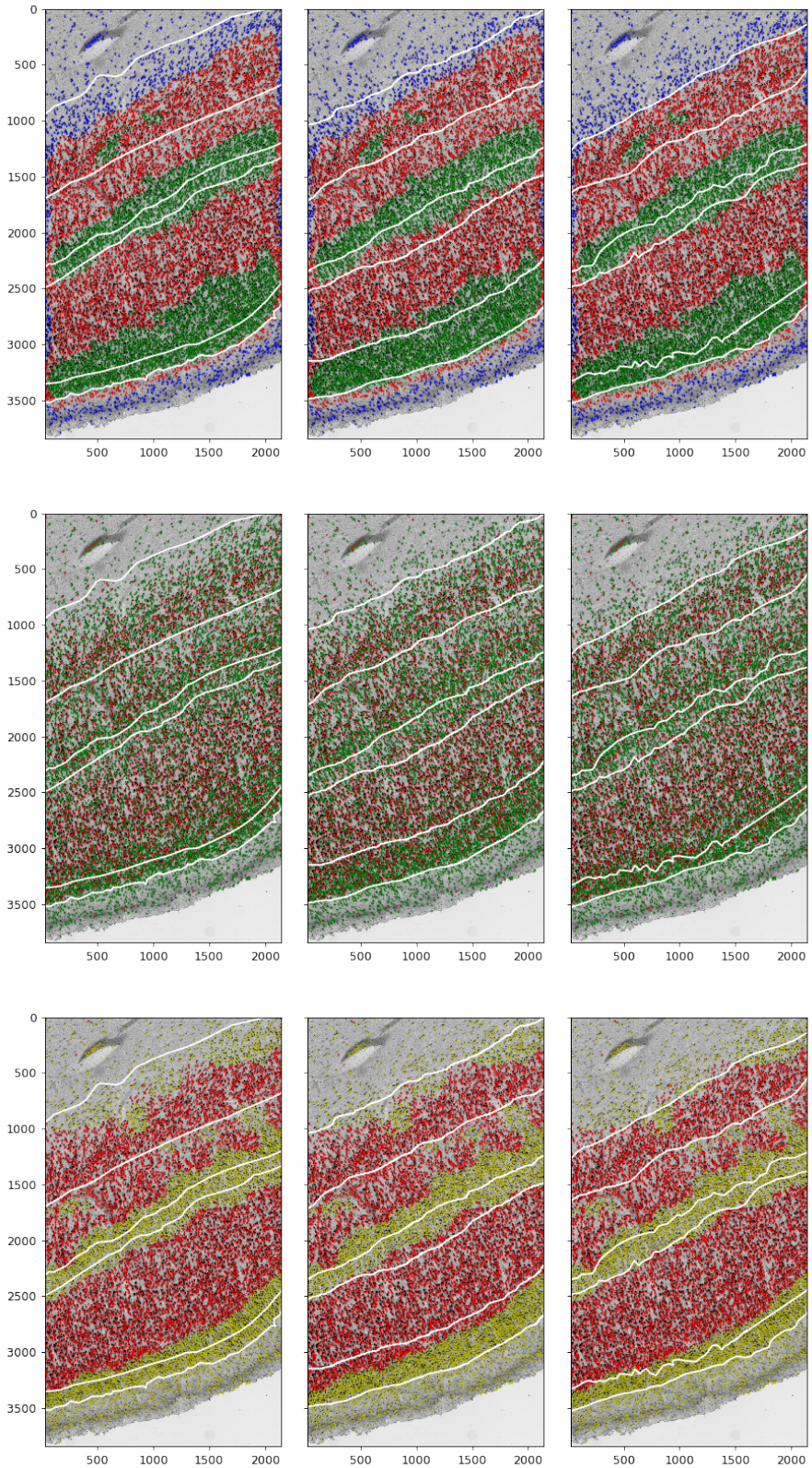

Figure A.3: Ability of experts to capture changes in density and size of neurons in cortical layers on thick tissue dataset with dense neuron population revealed by minimization of intraclass variance for neuron density (top), size (middle) and average neuron neighbor size (bottom).

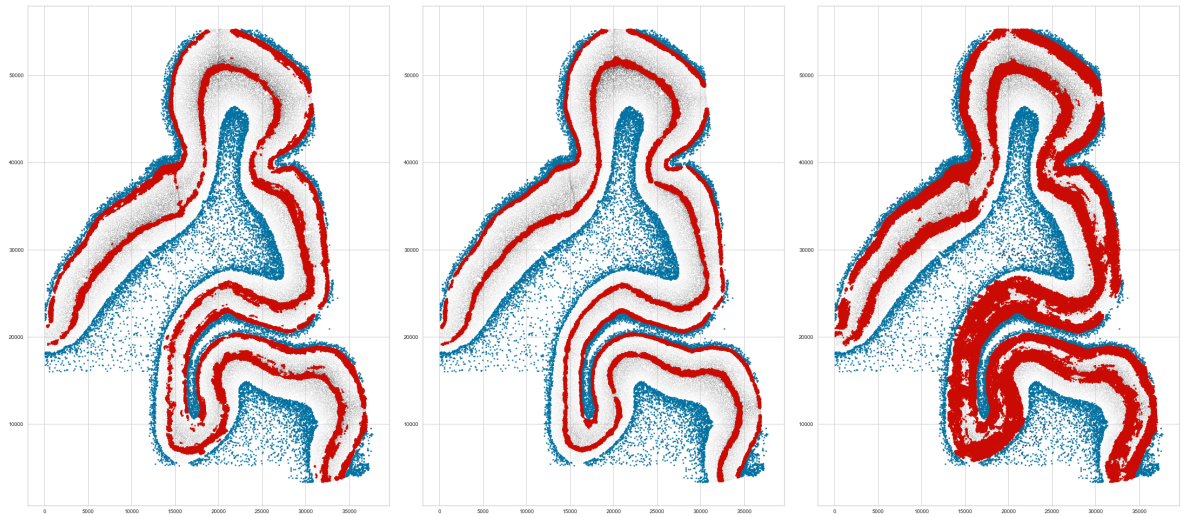

Figure A.4: Since experts delineate different tissue inhomogeneities, resulting in high inter-rater variability, it is not possible to achieve single ground truth and establish clear border between the layers, indicating the quality of performance of a single expert. However, results from this research suggest that the ability of the machine learning model to generalize from labeled data may be indicator that the borders manually drawn between the layers were made in a sensible way, dividing the laminar structure in homogeneous layers, with low intra-layer variations. In the figure above, each image represents a model train on manual labels of one of three experts. It is noticeable how predictions of dense regions (layers II and IV, shown in red) are more clear for the model in the middle than for the other two models.

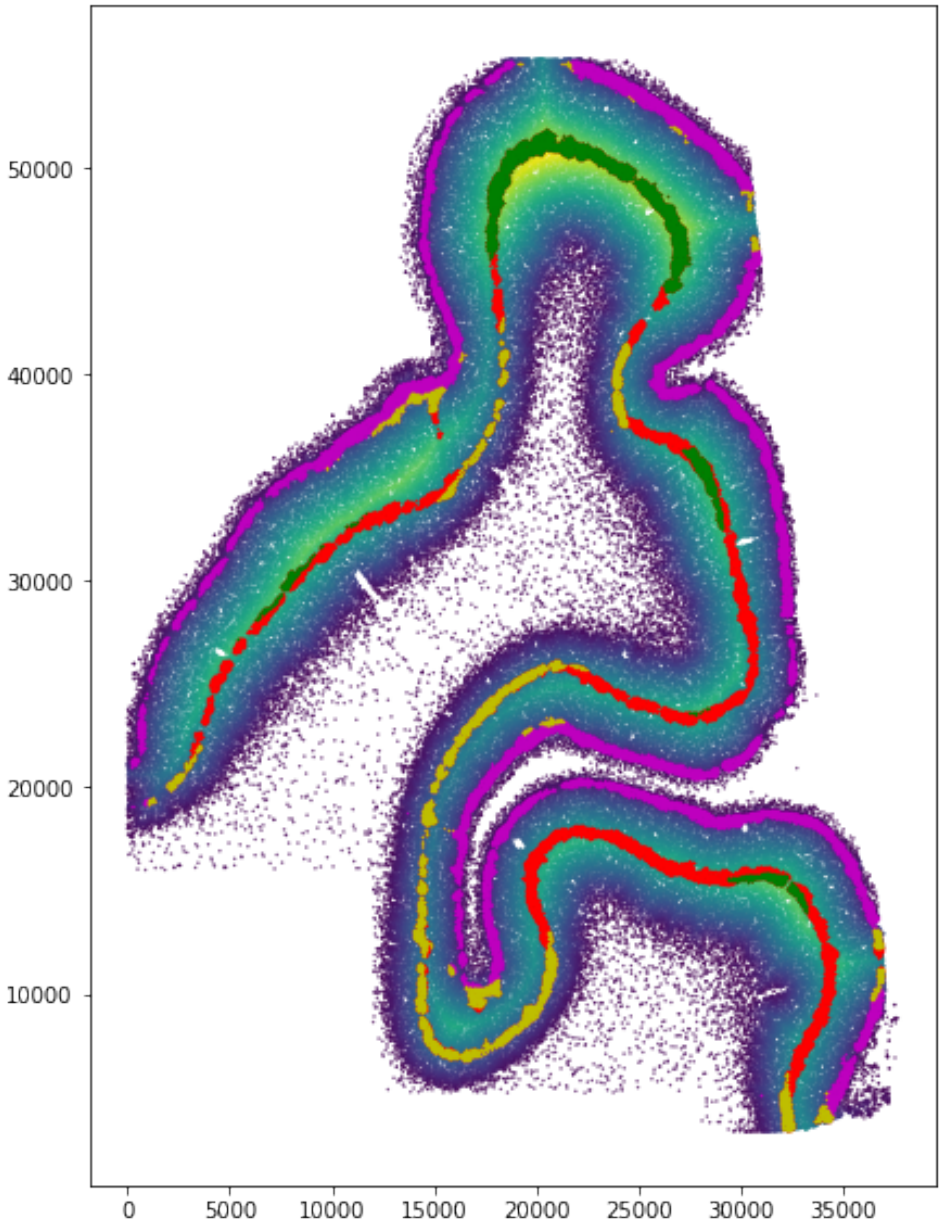

Figure A.5: Visualization of distance to sparse regions overlayed with layer II and layer IV neurons. Populations of neurons in layer IV are split according to their distance to sparse areas, as a result of cortical gyrification.

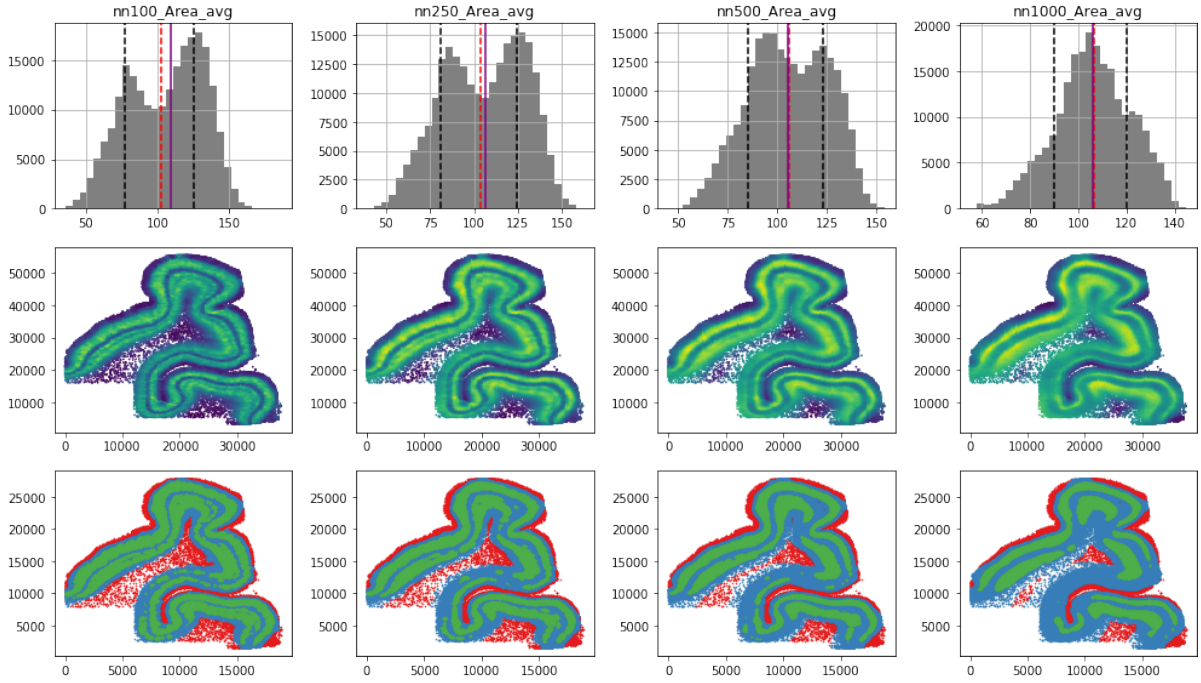

Figure A.6: Area average for different number of nearest neuron neighbors. In the range of number of neighbors which should be used to identify local variations in cytoarchitectonics, lower number of neighbors better reveals changes in low-level features such as neuron measures like area or local density, while more neighbors are needed for more complex features like oriented measurements or hull measurements.

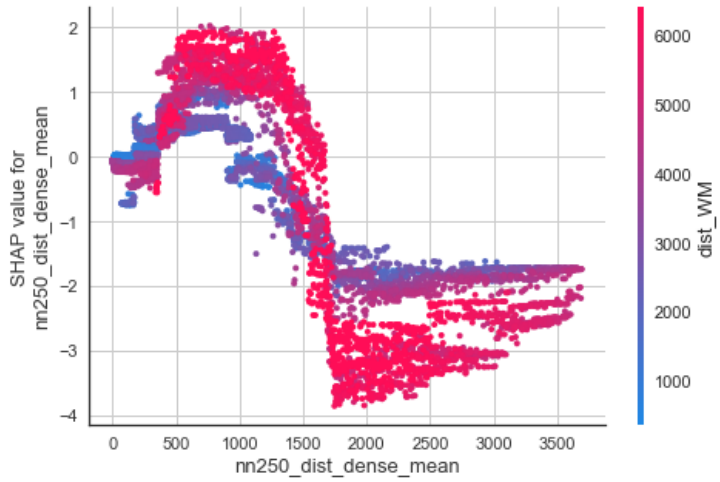

Figure A.7: SHAP interaction values provide insight into mutual influence of different neuron features in prediction of their layer.

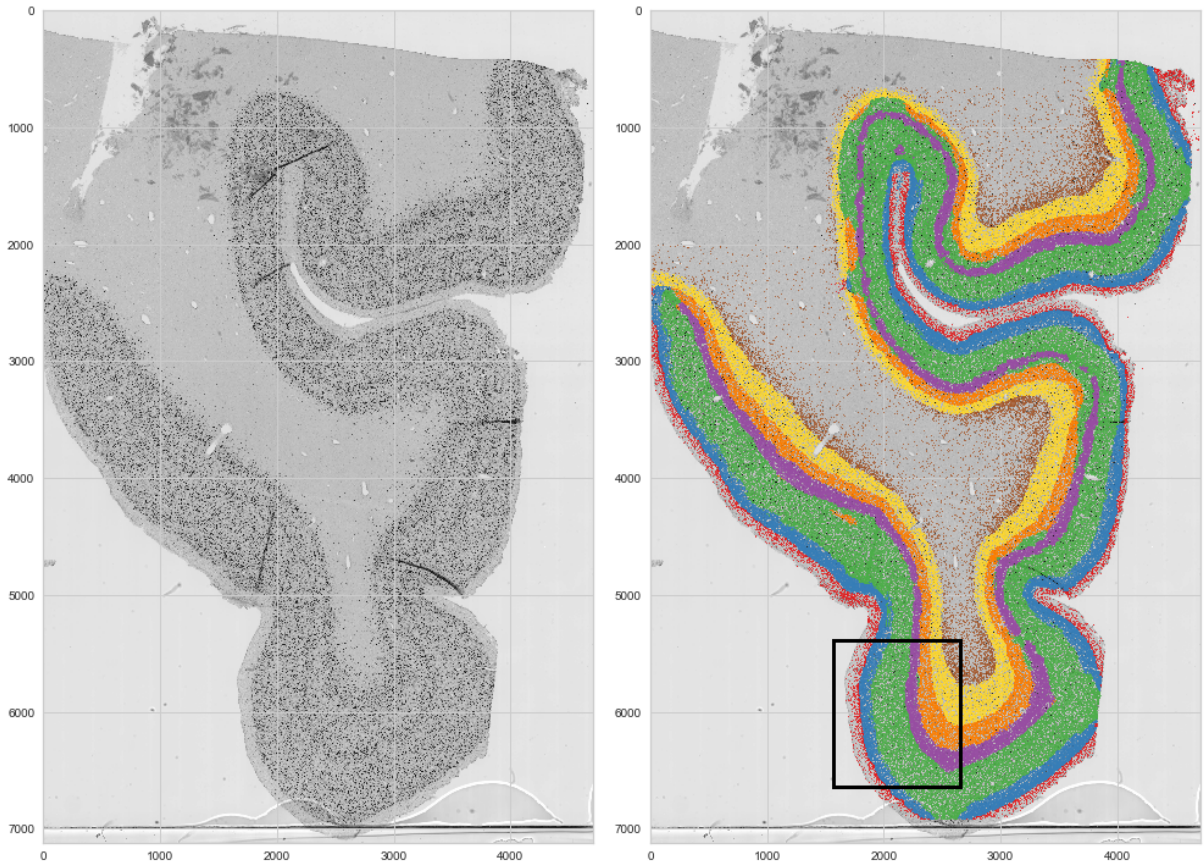

Figure A.8: CATboost, one of the latest tree ensemble methods was applied to the training data, showing results in generalization to the whole section similar to that of XGBoost method. Black rectangle indicates manually labeled portion used for training the model.

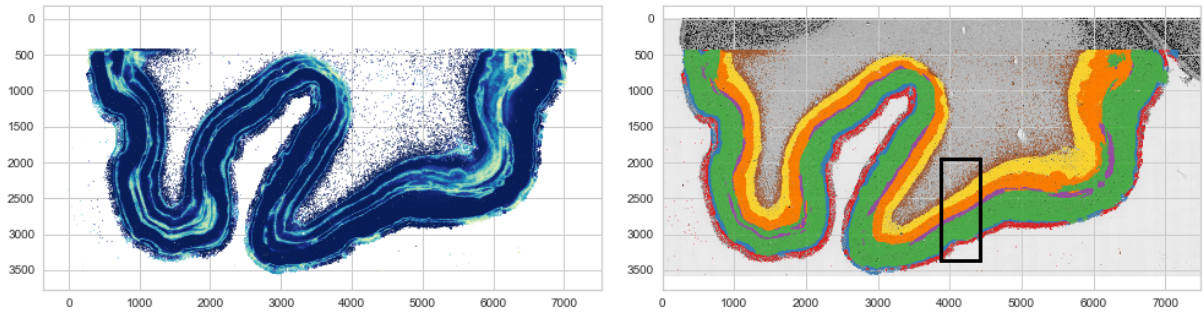

Figure A.9: Performance of the model depends on quality of the data. If elements of the digitized histological section are blurred or other artefacts are present, it may influence automatic detection of neurons and their correct delineation, resulting in incorrect segmentation. To obtain better results, more labeled data should be acquired and histological image possibly rescanned. Black rectangle indicates manually labeled portion used for training the model.

Bibliography

[1] Ramon, Y., Cajal, S., Textura del Sistema Nervioso del Hombre y de los Vertebrados. Madrid Nicolas Moya, 1904, Vol. 2.

[2] Brodmann, K., Vergleichende Lokalisationslehre der Grosshirnrinde in ihren Prinzipien dargestellt auf Grund des Zellenbaues. Barth, 1909.

[3] von Economo, C. F., Koskinas, G. N., Die cytoarchitektonik der hirnrinde des erwachsenen menschen. J. Springer, 1925.

[4] Rizzolatti, G., Luppino, G., Matelli, M., "The organization of the cortical motor system: new concepts", Electroencephalography and clinical neurophysiology, Vol. 106, No. 4, 1998, str. 283–296.

[5] Kaas, J. H., "The functional organization of somatosensory cortex in primates", Annals of Anatomy-Anatomischer Anzeiger, Vol. 175, No. 6, 1993, str. 509–518.

[6] Lashley, K. S., Clark, G., "The cytoarchitecture of the cerebral cortex of ateles: A critical examination of architectonic studies", Journal of Comparative Neurology, Vol. 85, No. 2, 1946, str. 223–305.

[7] Devlin, J. T., Poldrack, R. A., "In praise of tedious anatomy", Neuroimage, Vol. 37, No. 4, 2007, str. 1033–1041.

[8] von Bonin, G., "A first study of the size of the cells in the cerebral cortex", Journal of Comparative Neurology, Vol. 66, No. 1, 1937, str. 103–111.

[9] Abercrombie, M., "Estimation of nuclear population from microtome sections", The anatomical record, Vol. 94, No. 2, 1946, str. 239–247.

[10] Shariff, G. A., "Cell counts in the primate cerebral cortex", Journal of Comparative Neurology, Vol. 98, No. 3, 1953, str. 381–400.

[11] Cragg, B., "The density of synapses and neurones in the motor and visual areas of the cerebral cortex.", Journal of Anatomy, Vol. 101, No. Pt 4, 1967, str. 639.

[12] Rockel, A., Hiorns, R. W., Powell, T., "The basic uniformity in structure of the neocortex.", Brain: a journal of neurology, Vol. 103, No. 2, 1980, str. 221–244.

[13] Rajkowska, G., Goldman-Rakic, P. S., "Cytoarchitectonic definition of prefrontal areas in the normal human cortex: Ii. variability in locations of areas 9 and 46 and relationship to the talairach coordinate system", Cerebral cortex, Vol. 5, No. 4, 1995, str. 323–337.

[14] Pelvig, D., Pakkenberg, H., Stark, A., Pakkenberg, B., "Neocortical glial cell numbers in human brains", Neurobiology of aging, Vol. 29, No. 11, 2008, str. 1754–1762.

[15] Pakkenberg, B., Gundersen, H., "Total number of neurons and glial cells in human brain nuclei estimated by the disector and the fractionator", Journal of microscopy, Vol. 150, No. 1, 1988, str. 1–20.

[16] Pakkenberg, B., "Total nerve cell number in neocortex in chronic schizophrenics and controls estimated using optical disectors", Biological psychiatry, Vol. 34, No. 11, 1993, str. 768–772.

[17] Hudspeth, A., Ruark, J., Kelly, J., "Cytoarchitectonic mapping by microdensitometry", Proceedings of the National Academy of Sciences, Vol. 73, No. 8, 1976, str. 2928–2931.

[18] Ryzen, M., "A microphotometric method of cell enumeration within the cerebral cortex of man", Journal of Comparative Neurology, Vol. 104, No. 2, 1956, str. 233–245.

[19] Hopf, A., "Registration of the myeloarchitecture of the human frontal lobe with an extinction method.", Journal fur Hirnforschung, Vol. 10, No. 3, 1968, str. 259.

[20] Schmitt, O., Hömke, L., Dümbgen, L., "Detection of cortical transition regions utilizing statistical analyses of excess masses", Neuroimage, Vol. 19, No. 1, 2003, str. 42–63.

[21] Amunts, K., Lepage, C., Borgeat, L., Mohlberg, H., Dickscheid, T., Rousseau, M.-É., Bludau, S., Bazin, P.-L., Lewis, L. B., Oros-Peusquens, A.-M. *et al.*, "Bigbrain: an ultrahigh-resolution 3d human brain model", Science, Vol. 340, No. 6139, 2013, str. 1472–1475.

[22] LeCun, Y., Bengio, Y., Hinton, G., "Deep learning", nature, Vol. 521, No. 7553, 2015, str. 436.

[23] He, K., Zhang, X., Ren, S., Sun, J., "Deep residual learning for image recognition", in Proceedings of the IEEE conference on computer vision and pattern recognition, 2016, str. 770–778.

[24] Danuser, G., "Computer vision in cell biology", Cell, Vol. 147, No. 5, 2011, str. 973–978.

[25] Tolles, W., "Section of biology: The cytoanalyzer—an example of physics in medical research", Transactions of the New York Academy of Sciences, Vol. 17, No. 3 Series II, 1955, str. 250–256.

[26] Prewitt, J. M., Mendelsohn, M. L., "The analysis of cell images", Annals of the New York Academy of Sciences, Vol. 128, No. 3, 1966, str. 1035–1053.

[27] Meijering, E., "Neuron tracing in perspective", Cytometry Part A, Vol. 77, No. 7, 2010, str. 693–704.

[28] Xing, F., Yang, L., "Robust nucleus/cell detection and segmentation in digital pathology and microscopy images: a comprehensive review", IEEE reviews in biomedical engineering, Vol. 9, 2016, str. 234–263.

[29] Otsu, N., "A threshold selection method from gray-level histograms", IEEE transactions on systems, man, and cybernetics, Vol. 9, No. 1, 1979, str. 62–66.

[30] Pham, D. L., Xu, C., Prince, J. L., "Current methods in medical image segmentation", Annual review of biomedical engineering, Vol. 2, No. 1, 2000, str. 315–337.

[31] Gunn, S. R., "On the discrete representation of the laplacian of gaussian", Pattern Recognition, Vol. 32, No. 8, 1999, str. 1463–1472.

[32] Vincent, O. R., Folorunso, O., "A descriptive algorithm for sobel image edge detection", in Proceedings of Informing Science & IT Education Conference (InSITE), Vol. 40. Informing Science Institute California, 2009, str. 97–107.

[33] Ding, L., Goshtasby, A., "On the canny edge detector", Pattern Recognition, Vol. 34, No. 3, 2001, str. 721–725.

[34] Soille, P., Morphological image analysis: principles and applications. Springer Science & Business Media, 2013.

[35] Hodneland, E., Bukoreshtliev, N. V., Eichler, T. W., Tai, X.-C., Gurke, S., Lundervold, A., Gerdes, H.-H., "A unified framework for automated 3-d segmentation of surface-stained living cells and a comprehensive segmentation evaluation", IEEE transactions on medical imaging, Vol. 28, No. 5, 2009, str. 720–738.

[36] Salembier, P., Serra, J., "Mathematical morphology and its applications to signal processing", Signal Processing, Vol. 29, 1992, str. 231–235.

[37] Plissiti, M. E., Nikou, C., Charchanti, A., "Automated detection of cell nuclei in pap smear images using morphological reconstruction and clustering", IEEE Transactions on information technology in biomedicine, Vol. 15, No. 2, 2011, str. 233–241.

[38] Lu, C., Mandal, M., "Toward automatic mitotic cell detection and segmentation in multispectral histopathological images", IEEE journal of biomedical and health informatics, Vol. 18, No. 2, 2014, str. 594–605.

[39] Shitong, W., Min, W., "A new detection algorithm (nda) based on fuzzy cellular neural networks for white blood cell detection", IEEE Transactions on information technology in biomedicine, Vol. 10, No. 1, 2006, str. 5–10.

[40] Lin, Z., Jin, J., Talbot, H., "Unseeded region growing for 3d image segmentation", in Selected papers from the Pan-Sydney workshop on Visualisation-Volume 2. Australian Computer Society, Inc., 2000, str. 31–37.

[41] Duong, T. H., Hoberock, L. L., "Duho image segmentation based on unseeded region growing on superpixels", in Computing and Communication Workshop and Conference (CCWC), 2018 IEEE 8th Annual. IEEE, 2018, str. 558–563.

[42] Roerdink, J. B., Meijster, A., "The watershed transform: Definitions, algorithms and parallelization strategies", Fundamenta informaticae, Vol. 41, No. 1, 2, 2000, str. 187–228.

[43] Veta, M., Huisman, A., Viergever, M. A., van Diest, P. J., Pluim, J. P., "Marker-controlled watershed segmentation of nuclei in h&e stained breast cancer biopsy images", in Biomedical Imaging: From Nano to Macro, 2011 IEEE International Symposium on. IEEE, 2011, str. 618–621.

[44] Cloppet, F., Boucher, A., "Segmentation of overlapping aggregating nuclei cells in biological images", ICPR (Pattern Recognition, 2008), 2008, str. 1–4.

[45] McInerney, T., Terzopoulos, D., "Deformable models in medical image analysis: a survey", Medical image analysis, Vol. 1, No. 2, 1996, str. 91–108.

[46] Delgado-Gonzalo, R., Uhlmann, V., Schmitter, D., Unser, M., "Snakes on a plane: A perfect snap for bioimage analysis", IEEE Signal Processing Magazine, Vol. 32, No. 1, 2015, str. 41–48.

[47] Sciarabba, M., Serrao, G., Bauer, D., Arnaboldi, F., Borghese, N., "Automatic detection of neurons in large cortical slices", Journal of neuroscience methods, Vol. 182, No. 1, 2009, str. 123–140.

[48] Kong, H., Gurcan, M., Belkacem-Boussaid, K., "Partitioning histopathological images: an integrated framework for supervised color-texture segmentation and cell splitting", IEEE transactions on medical imaging, Vol. 30, No. 9, 2011, str. 1661–1677.

[49] Yin, Z., Bise, R., Chen, M., Kanade, T., "Cell segmentation in microscopy imagery using a bag of local bayesian classifiers", in Biomedical Imaging: From Nano to Macro, 2010 IEEE International Symposium on. IEEE, 2010, str. 125–128.

[50] Janssens, T., Antanas, L., Derde, S., Vanhorebeek, I., Van den Berghe, G., Grandas, F. G., "Charisma: An integrated approach to automatic h&e-stained skeletal muscle cell segmentation using supervised learning and novel robust clump splitting", Medical image analysis, Vol. 17, No. 8, 2013, str. 1206–1219.

[51] Kumar, S., Ong, S. H., Ranganath, S., Ong, T. C., Chew, F. T., "A rule-based approach for robust clump splitting", Pattern Recognition, Vol. 39, No. 6, 2006, str. 1088–1098.

[52] Beaver, W., Kosman, D., Tedeschi, G., Bier, E., McGinnis, W., Freund, Y., "Segmentation of nuclei in confocal image stacks using performance based thresholding", in Biomedical Imaging: From Nano to Macro, 2007. ISBI 2007. 4th IEEE International Symposium on. IEEE, 2007, str. 53–56.

[53] Freund, Y., Mason, L., "The alternating decision tree learning algorithm", in icml, Vol. 99, 1999, str. 124–133.

[54] Das, S. L., Keyser, J., Choe, Y., "Random-forest-based automated cell detection in knife-edge scanning microscope rat nissl data.", in IJCNN, 2015, str. 1–8.

[55] Mayerich, D., Kwon, J., Panchal, A., Keyser, J., Choe, Y., "Fast cell detection in high-throughput imagery using gpu-accelerated machine learning", in Biomedical Imaging: From Nano to Macro, 2011 IEEE International Symposium on. IEEE, 2011, str. 719–723.

[56] Xie, W., Noble, J. A., Zisserman, A., "Microscopy cell counting and detection with fully convolutional regression networks", Computer methods in biomechanics and biomedical engineering: Imaging & Visualization, Vol. 6, No. 3, 2018, str. 283–292.

[57] Akram, S. U., Kannala, J., Eklund, L., Heikkilä, J., "Cell segmentation proposal network for microscopy image analysis", in Deep Learning and Data Labeling for Medical Applications. Springer, 2016, str. 21–29.

[58] Dong, B., Shao, L., Da Costa, M., Bandmann, O., Frangi, A. F., "Deep learning for automatic cell detection in wide-field microscopy zebrafish images", in Biomedical Imaging (ISBI), 2015 IEEE 12th International Symposium on. IEEE, 2015, str. 772–776.

[59] Fuchs, T. J., Buhmann, J. M., "Computational pathology: Challenges and promises for tissue analysis", Computerized Medical Imaging and Graphics, Vol. 35, No. 7-8, 2011, str. 515–530.

[60] Meijering, E., Carpenter, A. E., Peng, H., Hamprecht, F. A., Olivo-Marin, J.-C., "Imagining the future of bioimage analysis", Nature biotechnology, Vol. 34, No. 12, 2016, str. 1250.

[61] Schleicher, A., Palomero-Gallagher, N., Morosan, P., Eickhoff, S., Kowalski, T., De Vos, K., Amunts, K., Zilles, K., "Quantitative architectural analysis: a new approach to cortical mapping", Anatomy and embryology, Vol. 210, No. 5-6, 2005, str. 373–386.

[62] Wimmer, V. C., Bruno, R. M., De Kock, C. P., Kuner, T., Sakmann, B., "Dimensions of a projection column and architecture of vpm and pom axons in rat vibrissal cortex", Cerebral cortex, Vol. 20, No. 10, 2010, str. 2265–2276.

[63] Meyer, H. S., Wimmer, V. C., Oberlaender, M., De Kock, C. P., Sakmann, B., Helmstaedter, M., "Number and laminar distribution of neurons in a thalamocortical projection column of rat vibrissal cortex", Cerebral cortex, Vol. 20, No. 10, 2010, str. 2277–2286.

[64] Zilles, K., Schleicher, A., Palomero-Gallagher, N., Amunts, K., "Quantitative analysis of cyto-and receptor architecture of the human brain", in Brain Mapping: The Methods (Second Edition). Elsevier, 2002, str. 573–602.

[65] Wagstyl, K., Lepage, C., Bludau, S., Zilles, K., Fletcher, P. C., Amunts, K., Evans, A. C., "Mapping cortical laminar structure in the 3d bigbrain", Cerebral Cortex, Vol. 28, No. 7, 2018, str. 2551–2562.

[66] Schleicher, A., Amunts, K., Geyer, S., Kowalski, T., Schormann, T., Palomero-Gallagher, N., Zilles, K., "A stereological approach to human cortical architecture: identification and delineation of cortical areas", Journal of chemical neuroanatomy, Vol. 20, No. 1, 2000, str. 31–47.

[67] Amunts, K., Zilles, K., "Architectonic mapping of the human brain beyond brodmann", Neuron, Vol. 88, No. 6, 2015, str. 1086–1107.

[68] Toga, A. W., Thompson, P. M., Mori, S., Amunts, K., Zilles, K., "Towards multimodal atlases of the human brain", Nature Reviews Neuroscience, Vol. 7, Dec. 2006, str. 952, dostupno na: http://dx.doi.org/10.1038/nrn2012

[69] Schleicher, A., Amunts, K., Geyer, S., Morosan, P., Zilles, K., "Observer-independent method for microstructural parcellation of cerebral cortex: A quantitative approach to cytoarchitectonics", NeuroImage, Vol. 9, No. 1, 1999, str. 165 - 177, dostupno na: http://www.sciencedirect.com/science/article/pii/S1053811998903858

[70] Nosova, S., Turlapov, V., “Parallel 2d ray casting algorithm for brain cell registration with brodmann’s layer decomposition from nissl-stained mouse cortex images”, Procedia Computer Science, Vol. 119, 2017, str. 215–223.

[71] Nosova, S., Snopova, L., Turlapov, V., “Automatic detection of neurons, astrocytes, and layers for nissl-stained mouse cortex”, 2017.

[72] Li, D., Zavaglia, M., Wang, G., Hu, Y., Xie, H., Werner, R., Guan, J.-S., Hilgetag, C. C., “Discrimination of the hierarchical structure of cortical layers in 2-photon microscopy data by combined unsupervised and supervised machine learning”, bioRxiv, 2018, str. 427955.

[73] Rueden, C. T., Schindelin, J., Hiner, M. C., DeZonia, B. E., Walter, A. E., Arena, E. T., Eliceiri, K. W., “Imagej2: Imagej for the next generation of scientific image data”, BMC bioinformatics, Vol. 18, No. 1, 2017, str. 529.

[74] Wanner, A., Kirschmann, M., Genoud, C., “Challenges of microtome-based serial block-face scanning electron microscopy in neuroscience”, Journal of microscopy, Vol. 259, No. 2, 2015, str. 137–142.

[75] Matenaers, C., Popper, B., Rieger, A., Wanke, R., Blutke, A., “Practicable methods for histological section thickness measurement in quantitative stereological analyses”, PloS one, Vol. 13, No. 2, 2018, str. e0192879.

[76] Kim, K. K., Adelstein, R. S., Kawamoto, S., “Identification of neuronal nuclei (neun) as fox-3, a new member of the fox-1 gene family of splicing factors”, Journal of Biological Chemistry, 2009, str. jbc–M109.

[77] Mullen, R. J., Buck, C. R., Smith, A. M., “Neun, a neuronal specific nuclear protein in vertebrates”, Development, Vol. 116, No. 1, 1992, str. 201–211.

[78] Sarnat, H. B., Nochlin, D., Born, D. E., “Neuronal nuclear antigen (neun): a marker of neuronal maturation in the early human fetal nervous system1”, Brain and Development, Vol. 20, No. 2, 1998, str. 88–94.

[79] Parekh, R., Ascoli, G., “Neuronal Morphology Goes Digital: A Research Hub for Cellular and System Neuroscience”, Neuron, Vol. 77, No. 6, Mar. 2013, str. 1017–1038, dostupno na: http://linkinghub.elsevier.com/retrieve/pii/S0896627313002328

[80] Wilson, M., “Introduction to widefield microscopy”, https://www.leica-microsystems.com/science-lab/introduction-to-widefield-microscopy/, 2017.

[81] Ross, J. D., Cullen, D. K., Harris, J. P., LaPlaca, M. C., DeWeerth, S. P., "A three-dimensional image processing program for accurate, rapid, and semi-automated segmentation of neuronal somata with dense neurite outgrowth", Frontiers in Neuroanatomy, Vol. 9, Jul. 2015, dostupno na: http://journal.frontiersin.org/Article/10.3389/fnana.2015.00087/abstract

[82] Mathew, B., Schmitz, A., Muñoz-Descalzo, S., Ansari, N., Pampaloni, F., Stelzer, E., Fischer, S., "Robust and automated three-dimensional segmentation of densely packed cell nuclei in different biological specimens with Lines-of-Sight decomposition", BMC Bioinformatics, Vol. 16, No. 1, Dec. 2015, dostupno na: http://bmcbioinformatics.biomedcentral.com/articles/10.1186/s12859-015-0617-x

[83] Oberlaender, M., Dercksen, V. J., Egger, R., Gensel, M., Sakmann, B., Hege, H.-C., "Automated three-dimensional detection and counting of neuron somata", Journal of neuroscience methods, Vol. 180, No. 1, 2009, str. 147–160.

[84] Judaš, M., Šimić, G., Petanjek, Z., Jovanov-Milošević, N., Pletikos, M., Vasung, L., Vukšić, M., Kostović, I., "The zagreb collection of human brains: a unique, versatile, but underexploited resource for the neuroscience community", Annals of the New York Academy of Sciences, Vol. 1225, No. 1, 2011.

[85] Goode, A., Gilbert, B., Harkes, J., Jukic, D., Satyanarayanan, M., "Openslide: A vendor-neutral software foundation for digital pathology", Journal of pathology informatics, Vol. 4, 2013.

[86] OpenSlide, Hamamatsu format, dostupno na: https://openslide.org/formats/hamamatsu/

[87] Deroulers, C., Ameisen, D., Badoual, M., Gerin, C., Granier, A., Lartaud, M., "Analyzing huge pathology images with open source software", Diagnostic pathology, Vol. 8, No. 1, 2013, str. 92.

[88] Štajduhar, A., Džaja, D., Judaš, M., Lončarić, S., "Automatic detection of neurons in neun-stained histological images of human brain", Physica A: Statistical Mechanics and its Applications, Vol. 519, 2019, str. 237–246.

[89] Russ, J. C., Dehoff, R. T., Practical stereology. Springer Science & Business Media, 2012.

[90] Altunkaynak, B. Z., Onger, M. E., Altunkaynak, M. E., Ayrancı, E., Canan, S., "A brief introduction to stereology and sampling strategies: basic concepts of stereology", NeuroQuantology, Vol. 10, No. 1, 2011.

[91] Schmitz, C., Hof, P., "Design-based stereology in neuroscience", Neuroscience, Vol. 130, No. 4, 2005, str. 813–831.

[92] Beaulieu, C., "Numerical data on neocortical neurons in adult rat, with special reference to the gaba population", Brain research, Vol. 609, No. 1-2, 1993, str. 284–292.

[93] Gittins, R., Harrison, P. J., "Neuronal density, size and shape in the human anterior cingulate cortex: a comparison of nissl and neun staining", Brain research bulletin, Vol. 63, No. 2, 2004, str. 155–160.

[94] Meijering, E., "Cell segmentation: 50 years down the road [life sciences]", IEEE Signal Processing Magazine, Vol. 29, No. 5, 2012, str. 140–145.

[95] Liu, T., Li, G., Nie, J., Tarokh, A., Zhou, X., Guo, L., Malicki, J., Xia, W., Wong, S. T., "An automated method for cell detection in zebrafish", Neuroinformatics, Vol. 6, No. 1, 2008, str. 5–21.

[96] Inglis, A., Cruz, L., Roe, D. L., Stanley, H., Rosene, D. L., Urbanc, B., "Automated identification of neurons and their locations", Journal of microscopy, Vol. 230, No. 3, 2008, str. 339–352.

[97] Gilboa, G., Sochen, N. A., Zeevi, Y. Y., "Regularized shock filters and complex diffusion", in European Conference on Computer Vision. Springer, 2002, str. 399–413.

[98] Xu, L., Lu, C., Xu, Y., Jia, J., "Image smoothing via l 0 gradient minimization", in ACM Transactions on Graphics (TOG), Vol. 30, No. 6. ACM, 2011, str. 174.

[99] Min, D., Choi, S., Lu, J., Ham, B., Sohn, K., Do, M. N., "Fast global image smoothing based on weighted least squares", IEEE Transactions on Image Processing, Vol. 23, No. 12, 2014, str. 5638–5653.

[100] Paris, S., Durand, F., "A fast approximation of the bilateral filter using a signal processing approach", Computer Vision–ECCV 2006, 2006, str. 568–580.

[101] Evans, L. C., "Partial differential equations (providence, ri: American mathematical society)", Lecture Notes at UC Berkeley, 1998.

[102] Perona, P., Malik, J., "Scale-space and edge detection using anisotropic diffusion", IEEE Transactions on pattern analysis and machine intelligence, Vol. 12, No. 7, 1990, str. 629–639.

[103] Guidotti, P., "Anisotropic diffusions of image processing from perona-malik on", Advanced Studies in Pure Mathematics, Vol. 99, 2015, str. 20XX.

[104] Gerig, G., Kubler, O., Kikinis, R., Jolesz, F. A., "Nonlinear anisotropic filtering of mri data", IEEE Transactions on medical imaging, Vol. 11, No. 2, 1992, str. 221–232.

[105] Sewell, G., The numerical solution of ordinary and partial differential equations. John Wiley & Sons, 2005, Vol. 75.

[106] Weickert, J., Benhamouda, B., Why the Perona-Malik filter works. Datalogisk Institut, Københavns Universitet, 1997.

[107] Kichenassamy, S., "The perona–malik paradox", SIAM Journal on Applied Mathematics, Vol. 57, No. 5, 1997, str. 1328–1342.

[108] Vincent, R. D., Janke, A., Sled, J. G., Baghdadi, L., Neelin, P., Evans, A. C., "Minc 2.0: a modality independent format for multidimensional medical images", in 10th Annual Meeting of the Organization for Human Brain Mapping, Vol. 2003, 2004, str. 2003.

[109] Pertuz, S., Puig, D., Garcia, M. A., "Analysis of focus measure operators for shape-from-focus", Pattern Recognition, Vol. 46, No. 5, May 2013, str. 1415–1432, dostupno na: http://linkinghub.elsevier.com/retrieve/pii/S0031320312004736

[110] Štajduhar, A., Lepage, C., Judaš, M., Lončarić, S., Evans, A. C., "3d localization of neurons in bright-field histological images", in ELMAR (ELMAR), 2018 60th International Symposium. IEEE, 2018, str. 75–78.

[111] Pantanowitz, L., Farahani, N., Parwani, A., "Whole slide imaging in pathology: advantages, limitations, and emerging perspectives", Pathology and Laboratory Medicine International, Jun. 2015, str. 23.

[112] Pech-Pacheco, J. L., Cristóbal, G., Chamorro-Martinez, J., Fernández-Valdivia, J., "Diatom autofocusing in brightfield microscopy: a comparative study", in Pattern Recognition, 2000. Proceedings. 15th International Conference on, Vol. 3. IEEE, 2000, str. 314–317.

[113] Xu, R., Wunsch, D., "Survey of clustering algorithms", IEEE Transactions on neural networks, Vol. 16, No. 3, 2005, str. 645–678.

[114] Fahad, A., Alshatri, N., Tari, Z., Alamri, A., Khalil, I., Zomaya, A. Y., Foufou, S., Bouras, A., "A survey of clustering algorithms for big data: Taxonomy and empirical analysis", IEEE transactions on emerging topics in computing, Vol. 2, No. 3, 2014, str. 267–279.

[115] Sajana, T., Rani, C. S., Narayana, K., "A survey on clustering techniques for big data mining", Indian Journal of Science and Technology, Vol. 9, No. 3, 2016.

[116] MacQueen, J. *et al.*, "Some methods for classification and analysis of multivariate observations", in Proceedings of the fifth Berkeley symposium on mathematical statistics and probability, Vol. 1, No. 14. Oakland, CA, USA, 1967, str. 281–297.

[117] Kaufman, L., Rousseeuw, P. J., Finding groups in data: an introduction to cluster analysis. John Wiley & Sons, 2009, Vol. 344.

[118] Frey, B. J., Dueck, D., "Clustering by passing messages between data points", science, Vol. 315, No. 5814, 2007, str. 972–976.

[119] Jain, A. K., "Data clustering: 50 years beyond k-means", Pattern recognition letters, Vol. 31, No. 8, 2010, str. 651–666.

[120] Ester, M., Kriegel, H.-P., Sander, J., Xu, X. *et al.*, "A density-based algorithm for discovering clusters in large spatial databases with noise.", in Kdd, Vol. 96, No. 34, 1996, str. 226–231.

[121] Ankerst, M., Breunig, M. M., Kriegel, H.-P., Sander, J., "Optics: ordering points to identify the clustering structure", in ACM Sigmod record, Vol. 28, No. 2. ACM, 1999, str. 49–60.

[122] Campello, R. J., Moulavi, D., Zimek, A., Sander, J., "Hierarchical density estimates for data clustering, visualization, and outlier detection", ACM Transactions on Knowledge Discovery from Data (TKDD), Vol. 10, No. 1, 2015, str. 5.

[123] Rodriguez, A., Laio, A., "Clustering by fast search and find of density peaks", Science, Vol. 344, No. 6191, 2014, str. 1492–1496.

[124] Wang, S., Wang, D., Li, C., Li, Y., "Comment on "clustering by fast search and find of density peaks"", arXiv preprint arXiv:1501.04267, 2015.

[125] Mehmood, R., Zhang, G., Bie, R., Dawood, H., Ahmad, H., "Clustering by fast search and find of density peaks via heat diffusion", Neurocomputing, Vol. 208, 2016, str. 210–217.

[126] Bentley, J. L., "Multidimensional binary search trees used for associative searching", Communications of the ACM, Vol. 18, No. 9, 1975, str. 509–517.

[127] Maneewongvatana, S., Mount, D. M., "It's okay to be skinny, if your friends are fat", in Center for Geometric Computing 4th Annual Workshop on Computational Geometry, Vol. 2, 1999, str. 1–8.

[128] Magurran, A. E., Measuring biological diversity. John Wiley & Sons, 2013.

[129] Nagendra, H., "Opposite trends in response for the shannon and simpson indices of landscape diversity", Applied geography, Vol. 22, No. 2, 2002, str. 175–186.

[130] Shannon, C. E., "A mathematical theory of communication", Bell system technical journal, Vol. 27, No. 3, 1948, str. 379–423.

[131] Simpson, E. H., "Measurement of diversity.", Nature, 1949.

[132] Bramer, M., Principles of data mining. Springer, 2007, Vol. 180.

[133] Liu, S., Wang, X., Liu, M., Zhu, J., "Towards better analysis of machine learning models: A visual analytics perspective", Visual Informatics, Vol. 1, No. 1, 2017, str. 48–56.

[134] James, G., Witten, D., Hastie, T., Tibshirani, R., An introduction to statistical learning. Springer, 2013, Vol. 112.

[135] Pedregosa, F., Varoquaux, G., Gramfort, A., Michel, V., Thirion, B., Grisel, O., Blondel, M., Prettenhofer, P., Weiss, R., Dubourg, V., Vanderplas, J., Passos, A., Cournapeau, D., Brucher, M., Perrot, M., Duchesnay, E., "Scikit-learn: Machine learning in Python", Journal of Machine Learning Research, Vol. 12, 2011, str. 2825–2830.

[136] Brown, G., Wyatt, J., Harris, R., Yao, X., "Diversity creation methods: a survey and categorisation", Information Fusion, Vol. 6, No. 1, 2005, str. 5–20.

[137] Tukey, J. W., Exploratory data analysis. Reading, Mass., 1977, Vol. 2.

[138] Dasarathy, B. V., Sheela, B. V., "A composite classifier system design: Concepts and methodology", Proceedings of the IEEE, Vol. 67, No. 5, 1979, str. 708–713.

[139] Hansen, L. K., Salamon, P., "Neural network ensembles", IEEE transactions on pattern analysis and machine intelligence, Vol. 12, No. 10, 1990, str. 993–1001.

[140] Schapire, R. E., "The strength of weak learnability", Machine learning, Vol. 5, No. 2, 1990, str. 197–227.

[141] Valiant, L. G., "A theory of the learnable", Communications of the ACM, Vol. 27, No. 11, 1984, str. 1134–1142.

[142] Oza, N. C., Tumer, K., "Classifier ensembles: Select real-world applications", Information Fusion, Vol. 9, No. 1, 2008, str. 4–20.

[143] Sagi, O., Rokach, L., "Ensemble learning: A survey", Wiley Interdisciplinary Reviews: Data Mining and Knowledge Discovery, Vol. 8, No. 4, 2018, str. e1249.

[144] Dietterich, T. G., "Ensemble methods in machine learning", in International workshop on multiple classifier systems. Springer, 2000, str. 1–15.

[145] Breiman, L., "Arcing the edge", Technical Report 486, Statistics Department, University of California at Berkeley, Tech. Rep., 1997.

[146] Mason, L., Baxter, J., Bartlett, P. L., Frean, M. R., "Boosting algorithms as gradient descent", in Advances in neural information processing systems, 2000, str. 512–518.

[147] Chen, T., Guestrin, C., "Xgboost: A scalable tree boosting system", in Proceedings of the 22nd acm sigkdd international conference on knowledge discovery and data mining. ACM, 2016, str. 785–794.

[148] Breiman, L., Classification and regression trees. Routledge, 2017.

[149] Auret, L., Aldrich, C., "Empirical comparison of tree ensemble variable importance measures", Chemometrics and Intelligent Laboratory Systems, Vol. 105, No. 2, 2011, str. 157–170.

[150] Baehrens, D., Schroeter, T., Harmeling, S., Kawanabe, M., Hansen, K., MÃžller, K.-R., "How to explain individual classification decisions", Journal of Machine Learning Research, Vol. 11, No. Jun, 2010, str. 1803–1831.

[151] Ribeiro, M. T., Singh, S., Guestrin, C., "Why should i trust you?: Explaining the predictions of any classifier", in Proceedings of the 22nd ACM SIGKDD international conference on knowledge discovery and data mining. ACM, 2016, str. 1135–1144.

[152] Štrumbelj, E., Kononenko, I., "Explaining prediction models and individual predictions with feature contributions", Knowledge and information systems, Vol. 41, No. 3, 2014, str. 647–665.

[153] Lundberg, S. M., Nair, B., Vavilala, M. S., Horibe, M., Eisses, M. J., Adams, T., Liston, D. E., Low, D. K.-W., Newman, S.-F., Kim, J. *et al.*, "Explainable machine learning predictions to help anesthesiologists prevent hypoxemia during surgery", bioRxiv, 2017, str. 206540.

[154] Saabas, A., "Interpreting random forests", dostupno na: https://github.com/andosa/treeinterpreter 2014.

[155] Lundberg, S. M., Erion, G. G., Lee, S.-I., "Consistent individualized feature attribution for tree ensembles", arXiv preprint arXiv:1802.03888, 2018.

List of Figures

List of Tables

Biography

Andrija Štajduhar was born on 13th of June 1990 in Zagreb. He graduated in 2013 at Department of Mathematics, Faculty of Science, University of Zagreb. Since January of 2015, Andrija is employed as a research assistant in Croatian Institute for Brain Research (CIBR), School of Medicine, University of Zagreb. In the same year he enrolled in Computer Science Ph.D. program at Faculty of Electrical Engineering and Computing, University of Zagreb. In winter of 2017 he spend 10 weeks as visiting researcher at Montreal Neurological Institute (MNI), MgGill University in Montreal, Canada. Later that year, Healthy Brains for Healthy Lives initiative from McGill University awarded him with a Talent program award which brought him back to MNI as a graduate research trainee in the period of 10 months during 2017 and 2018. During his work at the CIBR, he collaborated on different national and international research projects and initiatives in diverse topic areas including medical imaging and image processing, statistics, data analysis and neuroscience. In spring 2018 he was a program chair of BrainHack 2018 Zagreb.

List of Publications

Journal papers

[1] Štajduhar, A., Džaja, D., Judaš, M., Lončarić, S., "Automatic Detection of Neurons in NeuN-stained Histological Images of Human Brain", Physica A: Statistical Mechanics and its Applications, Vol. 519, April 2019, pp. 237-246

[2] Knezović V., Kasprian G., Štajduhar A., Schwartz E., Weber M., Gruber, G. M., Brugger, P. C., Prayer D., Vukšić M., "Underdevelopment of the human hippocampus in callosal agenesis – an in vivo fetal MRI study", American Journal of Neuroradiology, Vol. 40(3), March 2019, pp. 576-581

[3] Mladinov, M., Sedmak, G., Fuller, H. R., Leko, M. B., Mayer, D., Kirincich, J., Štajduhar, A., Borovečki, F., Hof, P. R., Šimić, G., "Gene expression profiling of the dorsolateral and medial orbitofrontal cortex in schizophrenia", Translational Neuroscience Vol. 7(1), November 2016, pp. 139-150

[4] Štajduhar, A. and Lipovac, A., "On Fluid Dynamics of Freshwater and Seawater in Marine Systems", Our Sea, International Journal of Maritime Science and Technology, Vol. 63(1), pp. 1-4, March 2016

[5] Novak, A. and Štajduhar, A., "Application of linear and nonlinear heat equation in digital image processing", KoG Magazine, Vol 18(18), pp. 45-52, January 2015

Conference proceedings and abstracts

[1] Štajduhar, A., Lepage, C., Judaš, M., Lončarić, S., Evans, A. C., "3D Localization of Neurons in Bright-Field Histological Images", ELMAR, September 2018., Zadar, Croatia

[2] Štajduhar, A., Judaš, M., Lončarić, S., "Automatic segmentation of cortical layers in histological images of human brain", FENSforum 2018, Berlin, Germany

[3] Štajduhar, A., Sedmak, G., Judaš, M., "Identification of new GABA receptors using computational approach", FENSforum 2016, Copenhagen, Denmark

Textbooks

[4] Novak, A., Štajduhar, A., "Logic, Set Theory and Discrete Mathematics", University of Dubrovnik, June 2014.

Životopis

Andrija Štajduhar rođen je 13. lipnja 1990. godine u Zagrebu. Diplomirao je 2013. godine na Matematičkom odsjeku Prirodoslovno-matematičkog fakulteta Sveučilišta u Zagrebu. Od siječnja 2015. zaposlen je kao asistent na Hrvatskom institutu za istraživanje mozga (HIIM) Medicinskog fakulteta Sveučilišta u Zagrebu. Iste godine upisuje doktorski studij Računarstvo na Fakultetu elektrotehnike i računarstva Sveučilišta u Zagrebu. U zimi 2017. proveo je 10 tjedana kao gostujući istraživač na Montreal Neurological Institute (MNI) Sveučilišta McGill u Montrealu, Kanada. Kasnije te godine, Talent program inicijative Healthy Brains for Healthy Lives Sveučilišta McGill dodjeljuje mu nagradu koja ga ponovo dovodi na MNI kao znanstvenog novaka na poslijediplomskom usavršavanju u trajanju od 10 mjeseci tijekom 2017. i 2018. godine. Tijekom rada na HIIM-u surađivao je na nekoliko domaćih i međunarodnih istraživačkih projekata i inicijativa u različitim područjima uključujući obradu i analizu medicinskih slika, statistiku, analizu medicinskih podataka i neuroznanost. U proljeće 2018. bio je voditelj skupa BrainHack 2018. u Zagrebu.